Bidigital Teletaction System Design and Performance

by

Gabriel Moy

B.S. (Northwestern University) 1994
B.S. (Northwestern University) 1994
M.S. (University of California at Berkeley) 1998

A dissertation submitted in partial satisfaction of the
requirements for the degree of
Doctor of Philosophy

in

Engineering-Electrical Engineering and Computer Sciences

in the

GRADUATE DIVISION
of the
UNIVERSITY of CALIFORNIA at BERKELEY

Committee in charge:

Professor Ronald S. Fearing, Chair
Professor Frank Tendick
Professor Steven L. Lehman

Fall 2002

The dissertation of Gabriel Moy is approved:

Chair Date

Date

Date

University of California at Berkeley

Fall 2002

Bidigital Teletaction System Design and Performance

by

Gabriel Moy

Abstract

Bidigital Teletaction System Design and Performance

by

Gabriel Moy

Doctor of Philosophy in Engineering-Electrical Engineering and Computer Sciences

University of California at Berkeley

Professor Ronald S. Fearing, Chair

This dissertation explores the design and performance of a bidigital teletaction, a two-fingered tactile sensing and feedback, system. This tactile recording and playback device is a basic step towards developing another sensory transmission device, such as radio for audio transmission and television for video transmission.

Starting with human mechanoreceptor responses and perception, a linear elastic model of teletaction, and current sensor and actuator technologies, we design and build a tactile feedback device which can display a wide range of pressure profiles. Our feedback devices present tactile information to the user by changing the pressure inside sealed, expandable air chambers placed next to the finger. Element to element spacing is 2 mm. We use capacitive tactile sensors to collect real-time touch data for presentation to the user.

Our human psychophysics experiments show that the tactile feedback device can display simulated 5 mm period gratings. We also show that the full bidigital teletaction system successfully senses, transmits, and displays tactile information from a mock 2 mm diameter blood vessel embedded in a soft silicone gel pulsing at approximately 1 Hz.

Professor Ronald S. Fearing
Dissertation Committee Chair

To my family and friends...

Contents

List of Figures

List of Tables

Acknowledgements

It's been a long trip and I have met many people along the way. First off, I'd like to thank my advisor, Professor Ron Fearing for his guidance, flexibility, and patience during my research and dissertation writing. He taught me not to be afraid of failure, but to embrace it as a learning tool and a necessary step towards success. He gave me the freedom to explore wild ideas not only in group meetings, but also in my own research. Most importantly, his patience allowed me to proceed at my own pace and to develop my ideas thoroughly before implementing them. With careful guidance, I was able to successfully put together a complex electro-mechanical device. He never told me how difficult my research topic was until I had achieved partial success. It was only then that he told me how almost all other research groups had given up on the problem. I sincerely thank him for his confidence in my ability and never giving up on me.

Many thanks to my research group – Ken Chiang, Ujjwal Singh, Joe Yan, Jeff Thompson, Rob Wood, Srinath Avadhanula, Ranjana Sahai, Wolfgang Zesch, Eiji Shimada, Hiro Shinoda, Metin Sitti, Mimmo Campolo, Kiwoon Kim, John Lin, Chris Wagner, and Melinda Ler – and my committee – Professor Frank Tendick, Professor Steven Lehman, and Professor Jitendra Malik – for their invaluable insights and help.

I would also like to thank my family for their support throughout my life and especially the bad times. My Mom, Dad, and brother Barratt showed me that with enough persistence and a bit of luck, anything is possible.

I thank all my friends, but especially George Chiou, Jeff Shih, Chris Chang, James Yeh, Matt Thomas, and Audrey Maher for all their support, distractions, and late night food excursions. Without them, I would not have been able to survive the long trek through graduate school. Last, but not least, I would like to thank the Cal Cycling members from 1994 to 2002 for all the fun, mayhem, and miles we enjoyed together.

Many thanks to NSF for supporting this project.

Chapter 1

Introduction

Tactile feedback, like visual and aural feedback, is an essential part of the human sensory system. Information about texture, local compliance, and local shape is important in applications such as telesurgery or handling of fragile objects in telerobotics. Tactile feedback adds another dimension to virtual reality simulations after visual and aural feedback. Unlike the visual and aural systems, we do not know the necessary spatial, temporal, or amplitude resolution necessary for near perfect feedback.

In the visual realm, a video camera records images in real-time for playback on a monitor. In the audio realm, a microphone records sound waves in real-time for playback through speakers. Both realms can also have their information stored for future playback. In the tactile realm, there are no standards for high quality recording or playback. Work on tactile feedback devices started as sensory substitution for the

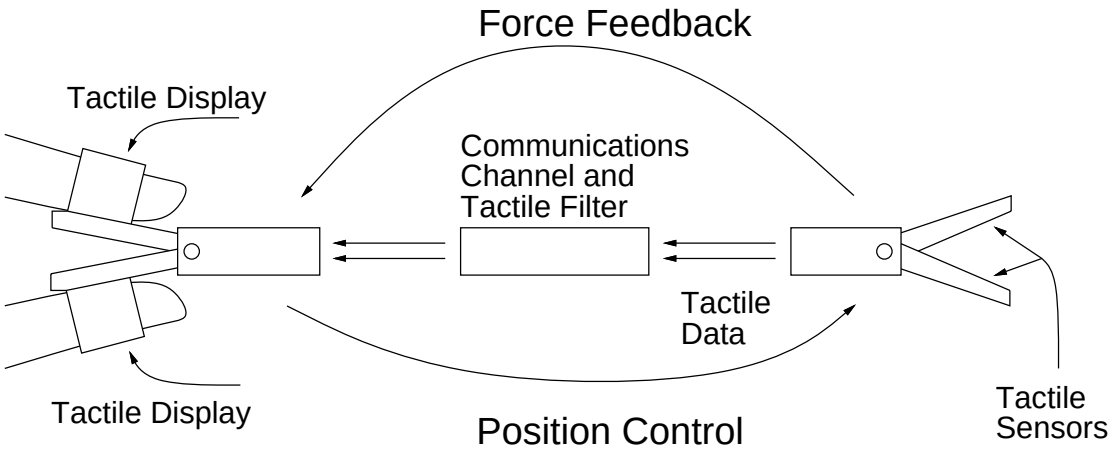

Figure 1.1: A teletaction system integrated on a laparoscopic instrument.

blind [Bliss, 1969]. Braille devices are one of the most basic tactile feedback devices with 8 actuators and only 1 bit of information per actuator. While it is not possible to build an ideal tactile feedback system, we explore the necessary parameters and build a tactile feedback system with the chosen technologies and tradeoffs.

Teletaction is the sensing of a remote object. A teletaction system is a combination of a tactile sensor and tactile display system where the sensors interact with the environment and the displays interact with the user. With an ideal teletaction system, the patterns felt by the user would be indistinguishable from direct contact with the environment. The interest in a teletaction system in this dissertation follows from the need for tactile feedback in laparoscopic surgery. Figure 1.1 shows a teletaction system on a laparoscopic instrument.

1.1 Applications for tactile feedback

Some of the applications for tactile feedback and teletaction are:

- Sensory substitution for blind computer users [Hardwick, 1998, Way, 1997a, Way, 1997b]
- Sensing of hazardous environments, such as space or underwater
- Virtual reality applications [Hardwick, 1998]
- Laparoscopic surgery [Dargahi, 1999]
- Telerobotic surgery [Howe, 1995]
- Breast lump detection [Wellman, 1999]
- Sensing of clothing materials for on-line commerce [Konyo, 2000]
- Functional MRI tests

We concentrate our focus on the application of laparoscopic surgery.

1.2 Teletaction and laparoscopic surgery

In laparoscopic surgery, surgeons use cameras and instruments through a few small incisions in the abdomen instead of using conventional surgical instruments through a large incision. The major advantage of laparoscopic procedures is the reduced damage

to muscle from a major incision, which in turn reduces recovery time. Conventional surgery has the advantage of direct visual and tactile feedback as well as unrestricted workspace access. Major drawbacks to laparoscopic surgery include a limited vision field, limited workspace access, and lack of tactile feedback. Currently, laparoscopic instruments have no tactile sensing or display capabilities.

The lack of tactile feedback can cause problems when visual feedback is not adequate. Surgeons can accidentally cut a blood vessel hidden underneath a layer of fat. In open surgery, tumors and other abnormalities might be detected and localized by tactile cues instead of visual cues. Integration of a teletaction system onto laparoscopic instruments will give surgeons more information at their disposal during minimally invasive procedures.

1.3 Research questions and thesis outline

In order to develop an effective teletaction system for laparoscopic surgery, we start by surveying the human tactile system and current tactile sensor and display technologies in Chapter 2. In Chapter 3, we discuss the design and fabrication of the teletaction system. We test the teletaction system performance by experiments in blood vessel detection with unidigital or bidigital tactile feedback. Results are discussed in Chapter 4. In Chapter 5, we draw conclusions from the experiments, discuss future improvements to the teletaction system, and specific applications suited to the teletaction system.

1.4 Contributions of this thesis

The purpose of this thesis is to enable readers to design and build a teletaction system consisting of capacitive tactile sensors and compliant tactile displays. Concepts behind the tactile sensor and tactile display design make them disposable and allow for a wide range of scaling.

One set of human psychophysics experiments determine the teletaction system performance in a spatial orientation task. A second set of human psychophysics experiments test the effectiveness of having tactile feedback in two fingers versus only having tactile feedback in one finger. Measurements show the linearity and uniformity of the compliant tactile display.

Chapter 2

Background

In this chapter, we review the human tactile system and the components of a teletaction system. We discuss the human tactile system at the mechanoreceptor level and at the perception level. We use these results to formulate the ideal parameters for a teletaction system. A teletaction system consists of tactile sensors to interact with the environment, tactile displays to present collected sensor data to the user, and a communications channel to transmit and transform the data to specific sensor and display geometries. In this chapter, we also survey the current tactile sensor and display technologies.

2.1 Human tactile sensing

The human tactile sensing system can be broken down into mechanoreceptor responses and perception. Mechanoreceptors convert the mechanical deformations of

the skin into electrical nerve impulses. Perception is the interpretation of these signals in the brain.

2.1.1 Mechanoreceptors

In glabrous skin, there are four types of mechanoreceptors responsible for converting the mechanical deformations of the skin to electrical signals sent to the nerves. The mechanoreceptors are named Merkel disks, Meissner's corpuscles, Pacinian corpuscles, and Ruffini endings, or SA I, FA I, FA II, and SA II, respectively. The four mechanoreceptors are compared in Table 2.1. The SA units are more sensitive to static skin indentation [Westling, 1987], while the FA units are more sensitive to moving stimuli. The SA I and FA I units have small and well defined receptive fields of 11 mm^2 and 13 mm^2, respectively. The SA I units have the greatest edge sensitivity [Johansson, 1982b]. The SA II and FA II units have large receptive fields of 59 mm^2 and 101 mm^2, respectively.

Some tactile displays are designed to stimulate the mechanoreceptors by providing a display of shape. This shape representation typically excites the SA I units due to good spatial resolution, sensitivity to maintained skin indentation, and low frequency. It may also excite the FA I units if the tactile display is running at a high frequency (>8 Hz). The fastest tactile displays are running at less than 50 Hz, which encompasses the SA I unit's easily excitable range, and at the middle of the FA I unit's easily excitable range.

	FA I	FA II	SA I	SA II
Rate of adaptation	fast	fast	slow	slow
Mean Receptive Area	13 mm^2	101 mm^2	11 mm^2	59 mm^2
Spatial Resolution	poor	very poor	good	fair
Sensory Units	43%	13%	25%	19%
Frequency range of response	10-200 Hz	70-1000 Hz	1-200 Hz	1-200 Hz
Most easily excited frequency range	8-64 Hz	>64 Hz	2-32 Hz	< 8 Hz

Table 2.1: Comparison of the slowly adapting (SA I and SA II) and fast adapting (FA I and FA II) mechanoreceptors (adapted from [Shimoga, 1992] and [Johansson, 1982a]).

The SA I units, are predicted to be about 0.7 to 1.0 mm below the skin surface. This depth is based on finite element models [Maeno, 1998c] and data collected on macaque monkeys [Phillips, 1981b]. The spatial density of the SA units is determined to be approximately 0.7 sensors per mm^3 in the fingertips [Valbo, 1979].

2.1.2 Perception

Along with the human sensing system, we look at perception, human tactile sensing sensitivity, sensor density, spatial frequency response, and temporal frequency response [Loomis, 1986, Srinivasan, 1987, Johnson, 1981a]. Spatial resolution tests show that the 75% thresholds for gap detection and grating detection are 0.87 mm and 0.5 mm, respectively [Johnson, 1981a, VanBoven, 1994]. Other studies show the enhanced detection of surface roughness by reducing shear stress information [Lederman, 1978], the effects of grating resolution perception due to amplitude variations [Weisenberger, 1998], and the relationship between skin hardness, pressure perception, and two-point discrimination [Dellon, 1995]. Small dots of 40 μm di-

ameter and 8 μm height can be detected 75% of the time with active scanning [Johansson, 1983]. The dynamic response of the human finger to objects with and without surface roughness is analyzed with finite element modeling [Maeno, 1998b]. The limits of perceptual tasks when tactile information is eliminated shows the need for tactile feedback in teleoperator and virtual environment systems [Lederman, 1999].

2.2 Tactile sensors

Tactile sensors are used to collect local contact information, such as contact location, contact force, contact area, local shape, texture, and thermal properties. Important sensor technology considerations are size, cost, scalability, ease of production, sensitivity, robustness. [Howe, 1994] and [Lee, 2000] present an overview of tactile sensing technology. Tactile sensors can sense either strain [Fearing, 1985, Maeno, 1998b] or stress [Biagiotti, 2002].

2.2.1 Capacitive sensors

A capacitive sensor array consists of two intersecting layers of copper strips separated by a dielectric layer as shown in Figure 2.1. One of the layers consists of the drive lines and the other consists of the sense lines. When a force profile is applied over the sensing area, the dielectric layer compresses and decreases the distance between the drive and sense strips, which increases the capacitance. We measure the

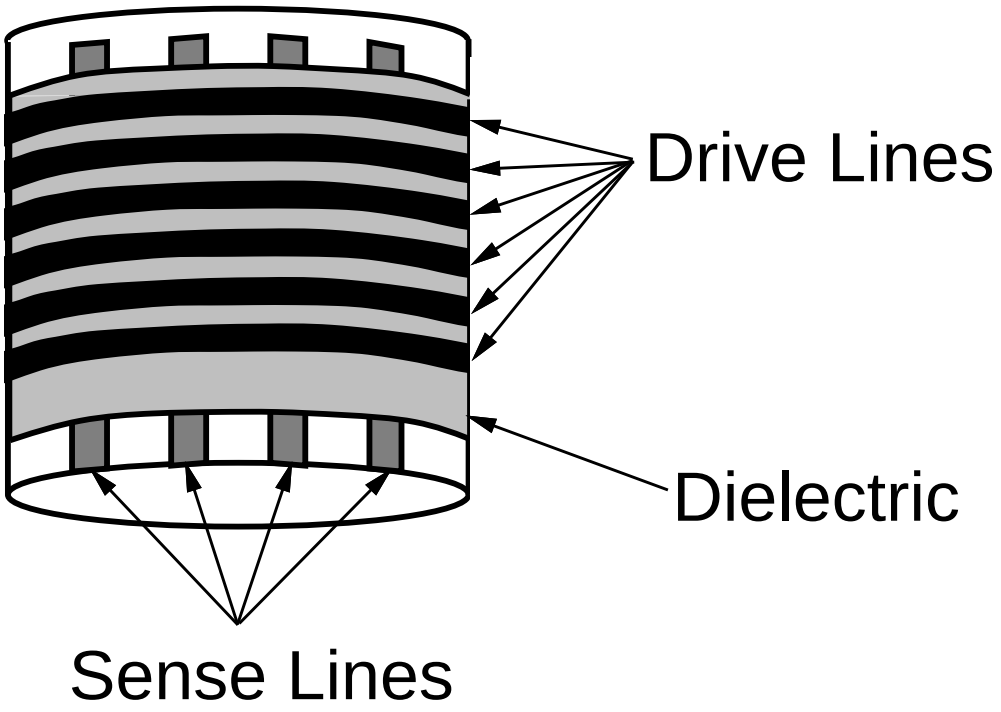

Figure 2.1: Drive lines, sense lines, and dielectric layers of a capacitive tactile sensor.

capacitance change over the whole array to obtain a snapshot of the applied force profile. The dielectric configuration is important in determining sensitivity. One of the problems with capacitive sensor technology is the wiring and packaging. Wires can be eliminated by using sensor elements embedded in conductive rubber [Hakozaki, 2002]. Since the sensor array elements consist of thin copper strips and a compressible dielectric layer, capacitive tactile sensors can be adapted to cylindrical and hemispherical configurations.

Typical capacitive tactile sensors range in size from 1 mm^2 with 8×8 elements [Gray, 1996] to 16 mm^2 with 8×8 elements [Howe, 1995] to a 25 mm diameter cylinder with 3×16 elements [Nicolson, 1993] to a 25 mm diameter cylinder with 8×8 elements

[Fearing, 1990]. Some advantages of capacitive sensor technology include ease of fabrication, low cost, and scalability.

2.2.2 Piezoelectric sensors

A piezoelectric tactile sensor array using polyvinylidene fluoride film has high force sensitivity, large bandwidth, and good linearity [Dargahi, 1999]. The sensor consists of the following layers: silicon, upper polyvinylidene fluoride (PVDF) electrode, connection electrode, PVDF film, lower PVDF electrode connection electrode, and a plexiglass substrate. The PVDF sensing elements detect a change in stress on the surface of the sensor. Dargahi builds a 15 mm long, 4 element piezoelectric tactile sensor for a laparoscopic instrument that has a linear response from 0 to 2.0 N.

2.3 Tactile displays

Tactile displays convey touch information to the user. Touch information consists of mechanical and thermal properties. We are more interested in transmitting the mechanical properties of touch to the fingertips. A wearable tactile display is described in [Gemperle, 2001].

Tactile displays originated with tactile reading aids for the blind using piezoelectric driven pins and direct pneumatic actuation [Bliss, 1969]. An ideal tactile display requires an actuator density of 1 per mm^2 [Asamura, 2001], with up to 2 mm in-

dentation and 1 N of force per tactor, and a bandwidth > 50 Hz; that is, a power density of 10 W/cm^2. The performance requirements are a result of the 70 SA I mechanoreceptors per cm^2 [Valbo, 1979] and force and displacement for compression of the finger [Serina, 1997]. Typically, tactile displays control either displacements or forces. The limiting factor for tactile displays is actuator size.

2.3.1 Pneumatically actuated displays

Pneumatically actuated displays use actuators to control the flow or pressure of air to drive pins [Bliss, 1969, Cohn, 1992, Caldwell, 1999] or inflate air chambers [Moy, 2000]. Pneumatics gives good power density and uses simple components but has difficult and nonlinear control of either pressure or flow, low power efficiency, and large valves [Chiang, 2000].

2.3.2 Mechanically actuated displays

Tactile display designs have used solenoids [Frisken-Gibson, 1987, Fischer, 1995], shape memory alloy [Kontarinis, 1995, Hasser, 1996, Wellman, 1997, Taylor, 1998b], RC servomotors [Wagner, 2002], piezoelectric beams [VanDoren, 1987, Debus, 2002] and voice coils [Murray, 1998, Pawluk, 1998]. Mechanical actuation typically gives fast and stiff responses and has good control characteristics, but is very bulky.

2.3.3 Electrical and electrostatic stimulation

A polyimide-on-silicon electrostatic fingertip tactile display creates an electrostatic attraction between the skin and electrode surface which presents a "sticky" or "buzzing" sensation [Beebe, 1995]. An electrostatic tactile display for the tongue was designed and fabricated [Bach-y-Rita, 1998]. Electrocutaneous stimulation creates tactile sensations by passing electric current through the skin [Ostrom, 1999, Kaczmarek, 1991, Kajimoto, 2001]. A reason not to use electrostatic displays or electrocutaneous stimulation is the chance of electrochemical or thermal burns.

2.3.4 Other

A couple of other technologies used for tactile displays are electrorheology and soft gel actuators. In electrorheological displays, the user touches a rubber surface which changes stiffness through electrochemical reactions [Taylor, 1998a]. Another configuration is to use electrolysis to increase or decrease the pressure of the resulting hydrogen and oxygen mixture inside a tactile display element [Kowalik, 1994]. Ionic Conducting Polymer Gel Film (ICPF) actuators pressing against the fingertip are used to present fine texture, such as in cloth [Konyo, 2000]. A passive tactile display with variable pin density is made using an array of capped rods [Shimojo, 1999].

2.4 Teletaction mechanics

The teletaction system needs to provide the operator with the sensation that his or her own finger is touching the remote surface. The key problem is to find a set of forces which most closely approximates the actual contact. We define two types of teletaction systems: *Strain Matching* and *Stress Matching* [Fearing, 1997]. Consider a finger touching an object through an elastic layer which ideally has the same modulus, E, and Poisson's ratio, ν, as the idealized finger. For ideal *Strain Matching*, we need a tactile display which generates identical strain in the finger mechanoreceptors as in the real contact. For ideal *Stress Matching*, we need a tactile display which generates identical stresses (to within the spatial sampling limit) on the finger surface.

Why is the elastic layer needed in the teletaction system? Consider the spatial impulse response of the teletaction system, i.e. the response to a pin prick. If the tactile sensor does not have a spatial low-pass filter, it is impossible to localize the pin to better than one tactel, no matter how dense the sensors, and the pin may be between sensors and not sensed. Since it is very difficult to achieve display density comparable to human mechanoreceptor density (on the order of $200cm^{-2}$), an elastic layer, which acts as a spatial low-pass filter, is essential. Otherwise, the user would feel an array of pins instead of a smooth contact. If high-density high-stress actuators were available for a display, a low-pass filter would then be necessary to prevent skin damage when touching sharp objects. Thus, the best teletaction system feels like touching the real world through an elastic layer, or glove. The higher the sensor and

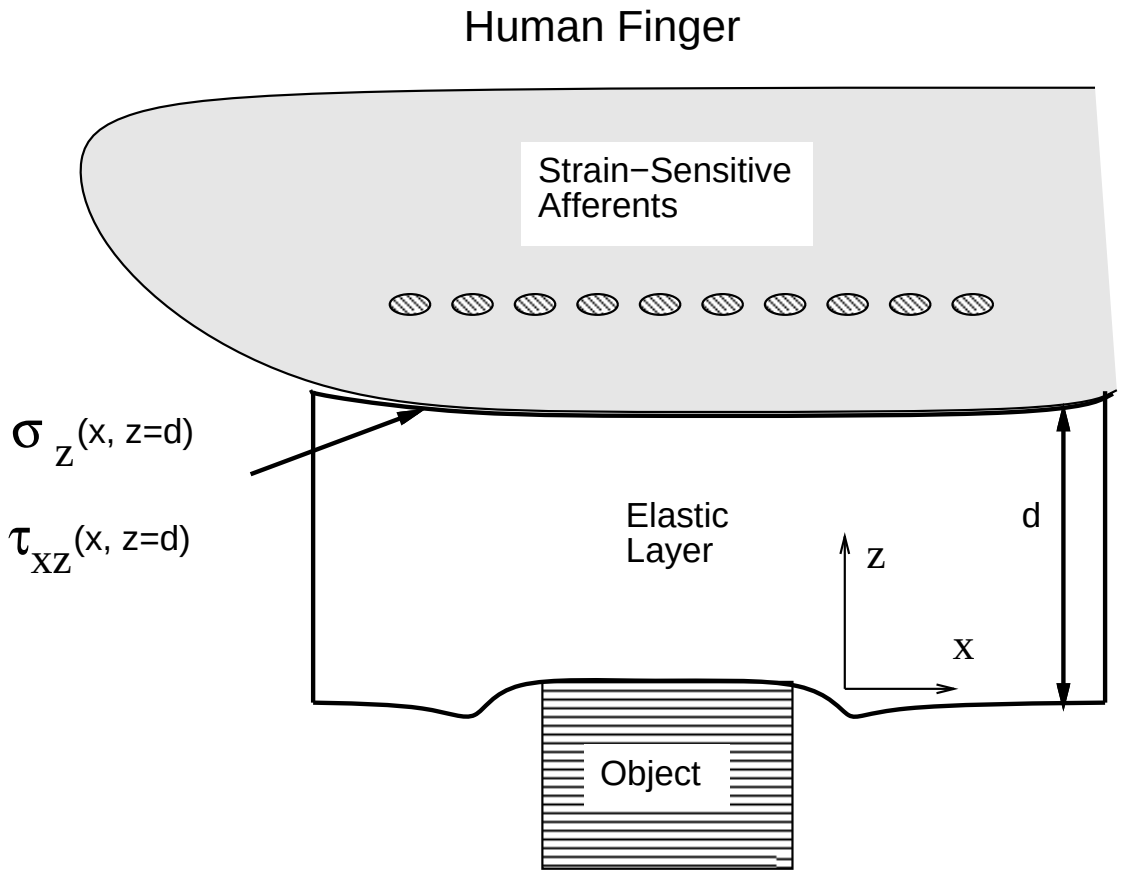

Figure 2.2: Example direct contact with rigid object through elastic layer.

display density, the thinner the glove can be without introducing spatial sampling artifacts.

2.4.1 Stress matching

Consider the real contact of Figure 2.2 replaced with a tactile display such that the normal and shear stresses on the finger $\sigma_z(x, z = d),\ \tau_{xz}(x, z = d)$ are the same to within the noise sensitivity of the finger. Figure 2.4 shows how this could be done.

Ideally, the normal and shear stresses on the boundary $z = \frac{d}{2}$ are continuously sensed and exactly replicated on the elastic layer covering the finger. Since the boundary conditions match at the top of the finger layer and the bottom of the tactile sensor layer, the two layers act as one layer of thickness d. Thus the finger would sense exactly what was sensed in Figure 2.2. Figure 2.3 shows the signal flow for a stress matching teletaction system.

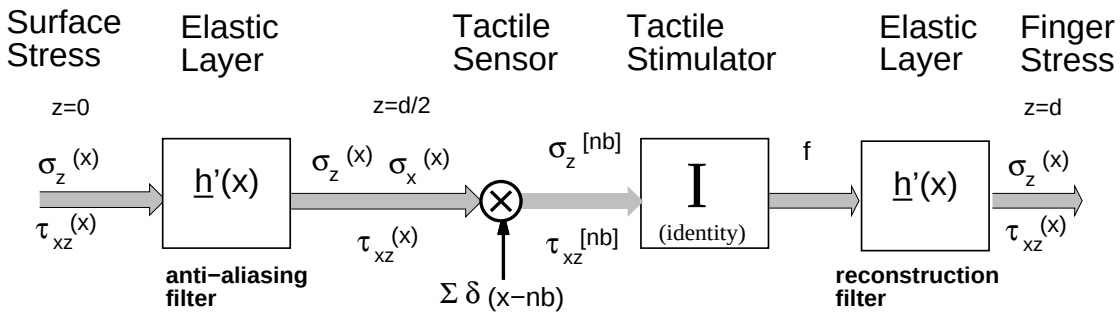

Figure 2.3: Signal flow model for a stress matching tactile sensor and display combination.

In practice, most tactile sensors measure the normal component of the strain (ϵ_z) at depth $\frac{d}{2}$, not both components of stress. An exception is [Domenici, 1992]. Also, the measurements are spatially sampled, not continuous, so information is lost due to aliasing. Further, most current displays apply only normal forces not tangential. The problem is to choose the display element forces, F_{ij}, so that the stress on the human finger is as close as possible to the the real contact stress.

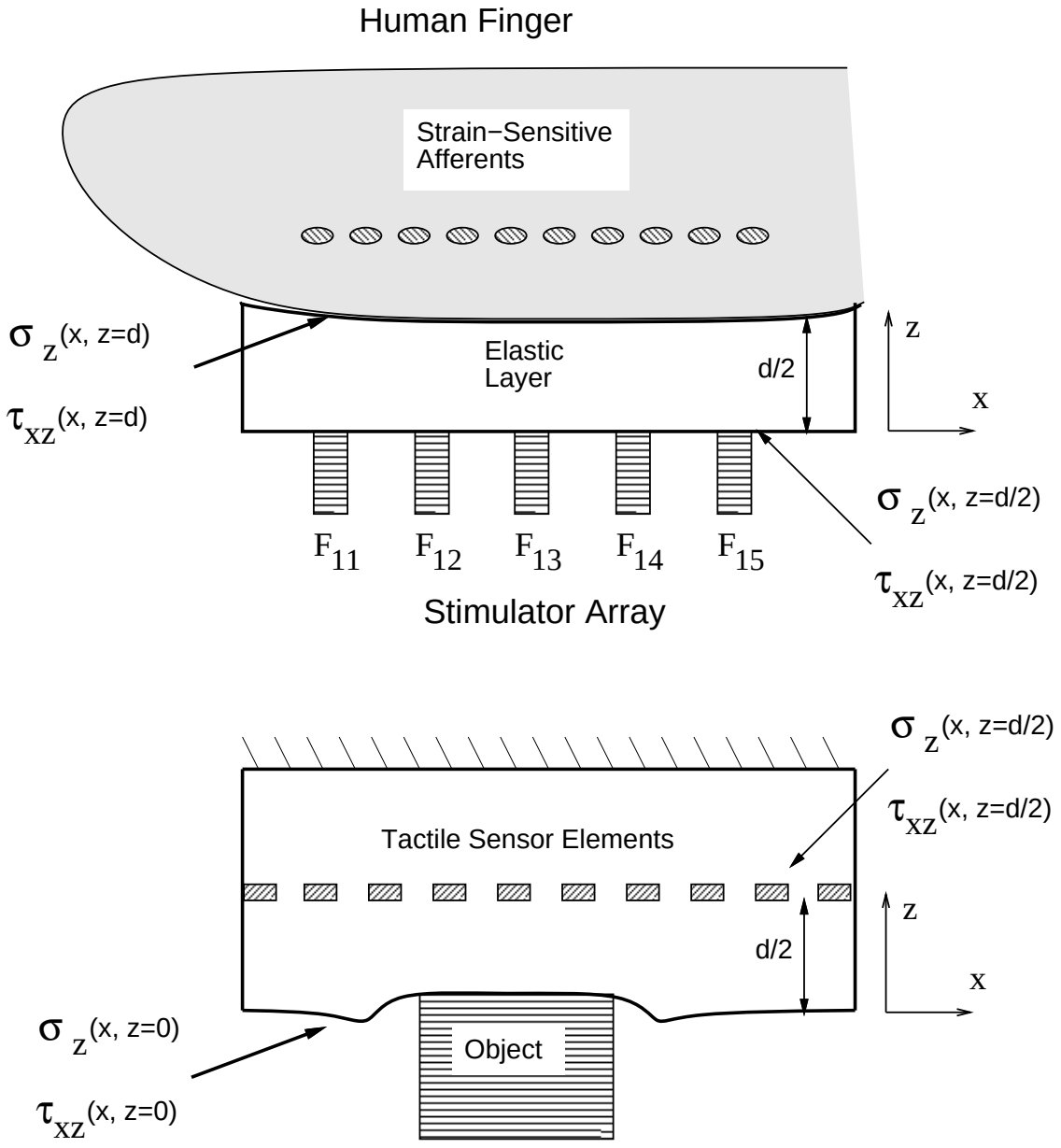

Figure 2.4: Tactile sensor and tactile display principles for stress matching.

2.4.2 Strain matching

Instead of matching surface stresses, we can match strains. This could be an easier problem, as the cutaneous mechanoreceptors may respond best to only one component of strain; i.e. they are scalar rather than tensor sensor elements.

Studies show that individual SA mechanoreceptor's response correlates with maximum compressive strain independent of direction [Phillips, 1981c] or with strain energy density [Srinivasan, 1996]. For this paper, we assume normal strain ϵ_z and frictionless indentation for simplicity. Figure 2.5 shows the signal flow for a strain matching teletaction system. Determination of stresses and strains of a real contact would be complicated without giving more insight to the basic problem.

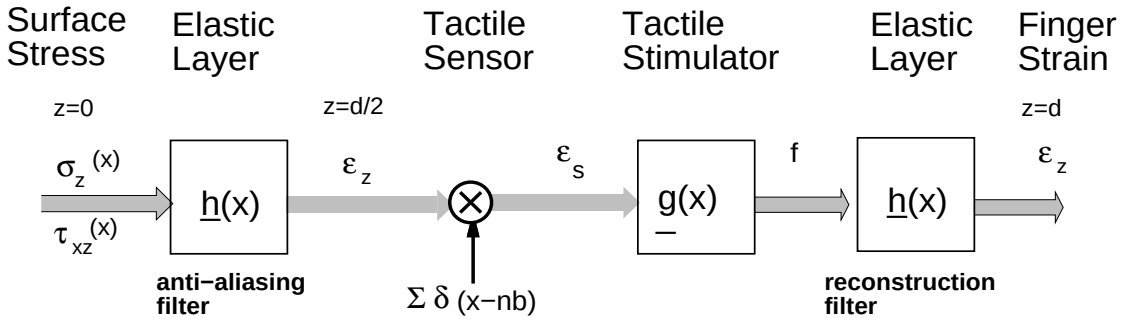

Figure 2.5: Signal flow model for a strain matching tactile sensor and display combination.

Using a linear, space-invariant model for the elastic medium, for surface normal load $p(x)$, the normal strain at depth d is $\epsilon_z(x, z = d) = h_z(x, d) * p(x)$. Discretizing the problem,

$$\epsilon_s = E_s p \tag{2.1}$$

$$\epsilon_f \;=\; E_f S f \tag{2.2}$$

where ϵ_f is the strain in the human finger, ϵ_s is measured strain in the tactile sensor, E_s and E_f are the maps from surface pressure to measured strain in the sensor and finger respectively, p is the pressure on the sensor, f is the discrete set of display points applying normal forces to the finger, and S is a sampling matrix. (The sampling matrix inserts zero force elements to match the size of the map matrix E_f). For the ideal strain matching method, we want $\epsilon_f = \epsilon_s$.

Using a least-squares approach, in principle the optimal force vector can be found from

$$f \;=\; [(E_f S)^T (E_f S)]^{-1} (E_f S)^T \epsilon_s. \tag{2.3}$$

As high sensing density is easier to achieve than high display density, we assume that $\epsilon_s(x)$ can be accurately recovered by interpolation. We note several difficulties with this approach, such as changes in position and temporal scales, hysteresis, non-linearities, and that the human finger likely measures maximum compressive strain, not normal strain. Although low-pass filtering the tactile sensor makes the inverse map poorly conditioned, it also lowers required display spatial resolution. Note that while f may be poorly reconstructed, it will be low-pass filtered by $E_f S$.

Let's consider a numerical example showing strain matching for a rectangular indentor (Fig. 2.6). We assume a display element spacing of 1 mm, sensor depth of 1.5 mm, and rectangular indentor width of 4 mm. (For calculation, pressure and strain are discretized at 0.1 mm spacing). For numerical purposes, Fig. 2.7 shows the

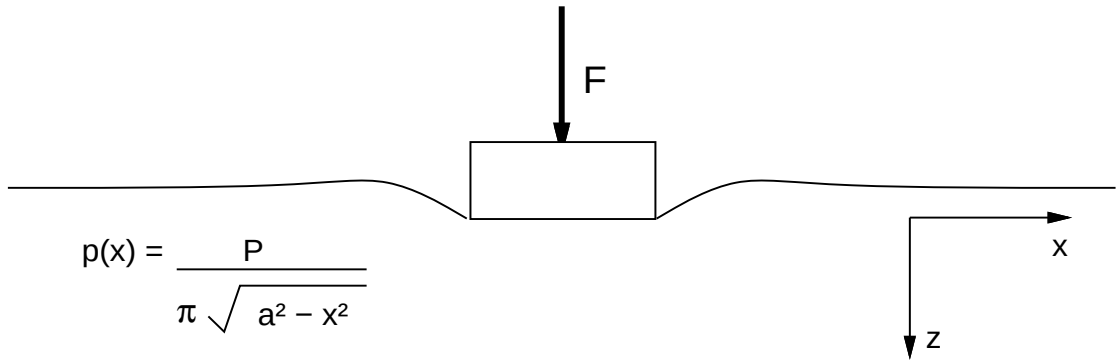

Figure 2.6: Example pressure distribution for rectangular indentor with frictionless indentation.

good matching between normal strain in tactile sensor ϵ_s and the resulting strain in the finger ϵ_f. Note that the display values have not been regularized, hence the noisy appearance. Approaches described in [Nicolson, 1993] or [Ellis, 1992] could regularize the tactor forces and ensure that they are all compressive. The elastic layer between the display pins and finger has in effect regularized the surface stress, and the sensed strain in the finger could be quite similar to the sensed strain in the tactile sensor.

2.4.3 Shape matching

An alternative method for teletaction is to "... reproduce the object's contour so that it contacts the appropriate part of the human hand" [Hagner, 1988]. While the concept seems appealing, it has some limitations. First, as seen in Fig. 2.6, the surface deflection on the tactile sensor is not the same as the object shape – a shape and pressure from strain problem must be solved first to recover object shape and contact extent [Nicolson, 1993]. In fact, a similar poorly conditioned map as in eq. (2.3)

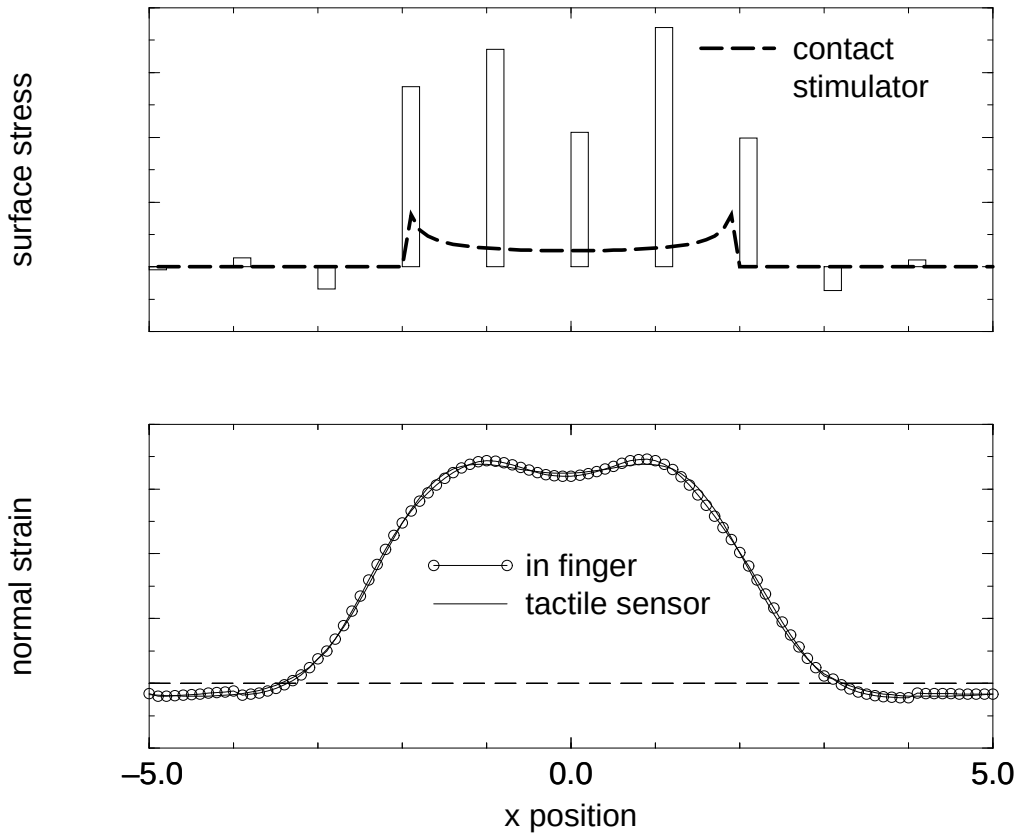

Figure 2.7: Equivalence of sampled surface stress profile and actual surface stress when measured by sub-surface strain sensors such as in the human finger. The top graph compares surface stress on the tactile sensor with the discrete surface stress which would be generated by a tactile display. The bottom graph compares the normal strain component in the tactile sensor and in a user's finger.

would be needed for shape display. The net loading on the finger would need to be controlled to insure that contact areas and stresses were consistent with the tactile sensor. Additionally, the shape display makes it difficult to present shear stresses or tensile forces, which may be possible with the strain matching approach. Finally, it is hard to build a stiff display which feels like a rigid object – the elastic layer is still needed for anti-aliasing.

2.4.4 Aliasing

Aliasing arises in the teletaction system from sampling by the tactile sensor and display. The teletaction system should be designed so that the aliasing energy of the strain signal is undetectable. One way to test whether aliasing is detectable is to consider whether a sampled and low-pass filtered "DC" signal feels like a "DC" signal. We show that a 3:2 thickness ratio of anti-aliasing layer to sensor and display spacing reduces the energy of the sampling effects to undetectable levels [Fearing, 1997].

Chapter 3

Bidigital Teletaction System

The bidigital teletaction system consists of two tactile sensors, two tactile displays, and the communications channel between the devices (Figure 3.1). The stimulus is a phantom corresponding to a blood vessel embedded in tissue. We use capacitive sensor technology for its ease of construction and low cost. Compliant tactile displays with air chambers allow ease of construction, low cost, no pin friction, no extraneous information from air leakage, and response linearity [Moy, 2000].

3.1 Tactile Sensors

Tactile sensors construction is described in Appendix A. Each tactile sensor contains a 4×8 array of capacitive elements [Fearing, 1990] in a cylindrical configuration (Figure 3.2) of which we use the center 4×6 elements. The center-to-center element spacing is 2.7 mm, which translates to an element angle spacing of 12.2 ^{o} on the

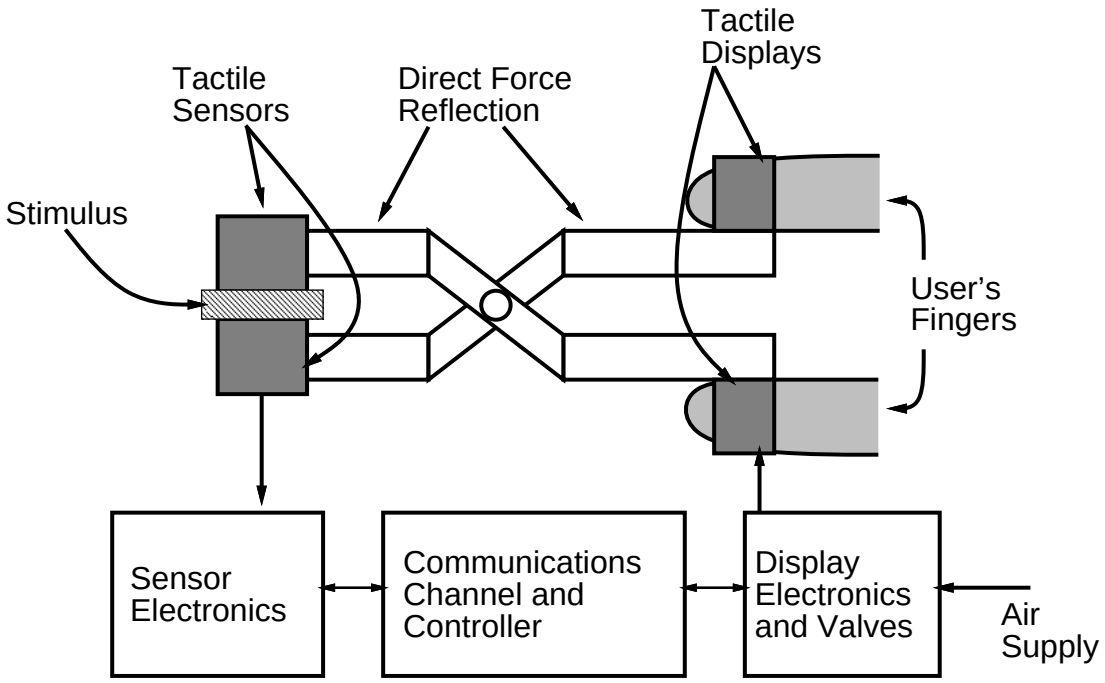

Figure 3.1: Layout of the bidigital teletaction system.

25.4 mm core. Each element is an intersection of two 1.5 mm wide copper strips. Between the copper strips, we use a 1 mm thick dielectric with 0.5 $mm \times 0.5\ mm \times 0.5\ mm$ square bumps at 1 mm spacing. The sensor has a final radius of 16 mm consisting of 12.7 mm core, 0.15 mm sense lines, 1.0 mm dielectric, 0.15 mm drive lines, and a 2.0 mm anti-aliasing layer.

The sensors are calibrated by applying a normal load of 1.10 N along the length of the sensor corresponding to the sense lines (Figure 3.3). We collect and average 100 data points every 0.254 mm and calculate sensor gains (Table 3.1). The tactile sensor system runs at about 100 Hz.

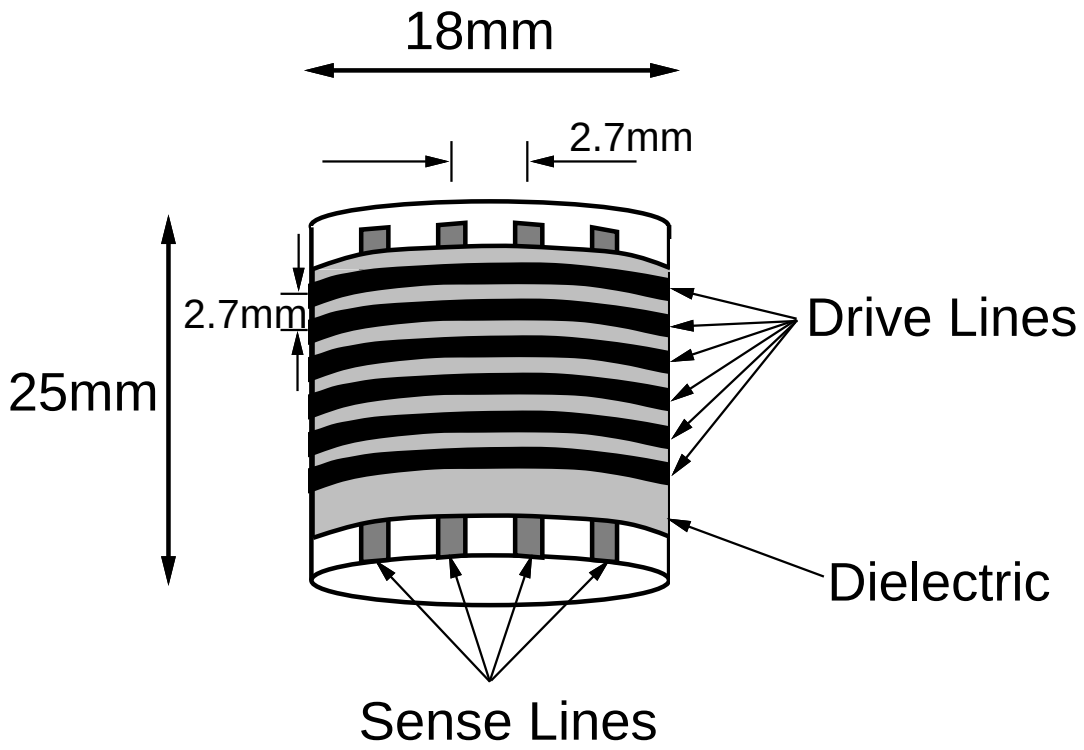

Figure 3.2: The tactile sensor is built on a 25.4 mm core and has an overall diameter of 32 mm. The elements have center-to-center spacing of 2.7 mm and width of 1.5 mm.

Finger 0	Column					
	0	1	2	3	4	5
Row 0	0.474	0.632	0.533	0.395	0.369	0.322
Row 1	0.741	0.786	0.666	0.606	0.608	0.509
Row 2	0.844	0.968	0.994	1.000	0.911	0.820
Row 3	0.548	0.779	0.762	0.778	0.701	0.653

Finger 1	Column					
	0	1	2	3	4	5
Row 4	0.295	0.350	0.344	0.325	0.286	0.295
Row 5	0.591	0.677	0.739	0.717	0.637	0.564
Row 6	0.886	0.903	0.893	0.891	0.869	0.815
Row 7	0.720	0.753	0.755	0.721	0.658	0.571

Table 3.1: Tactile sensor gains.

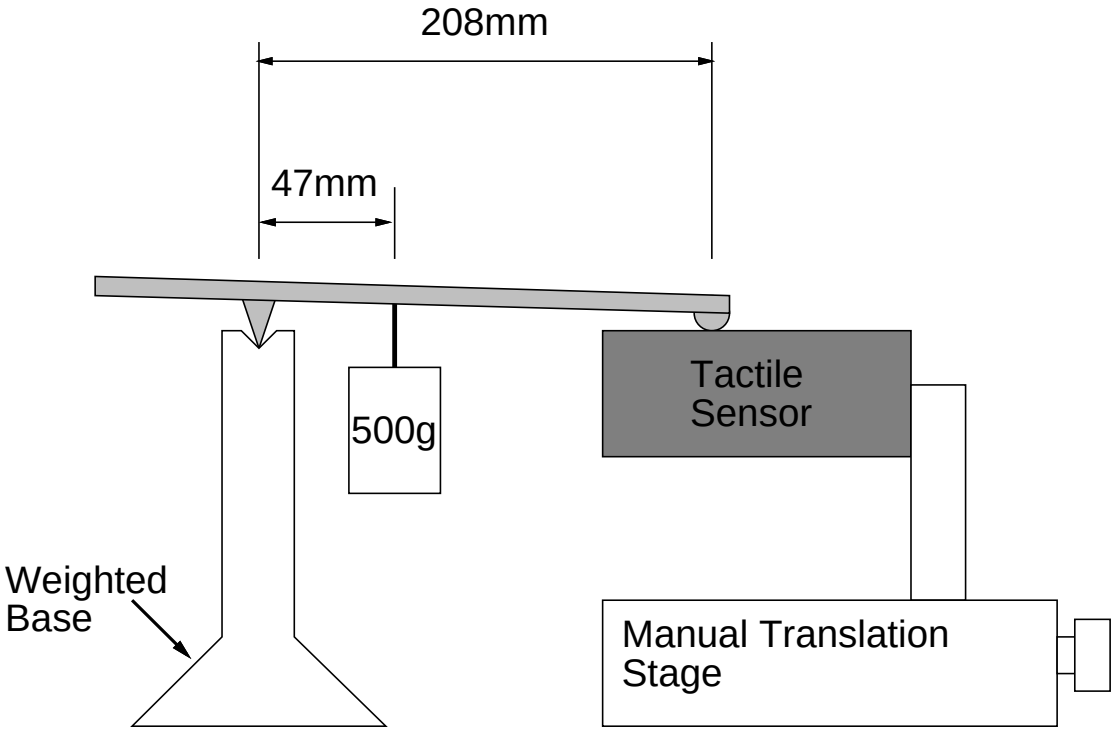

Figure 3.3: Tactile sensor calibration apparatus.

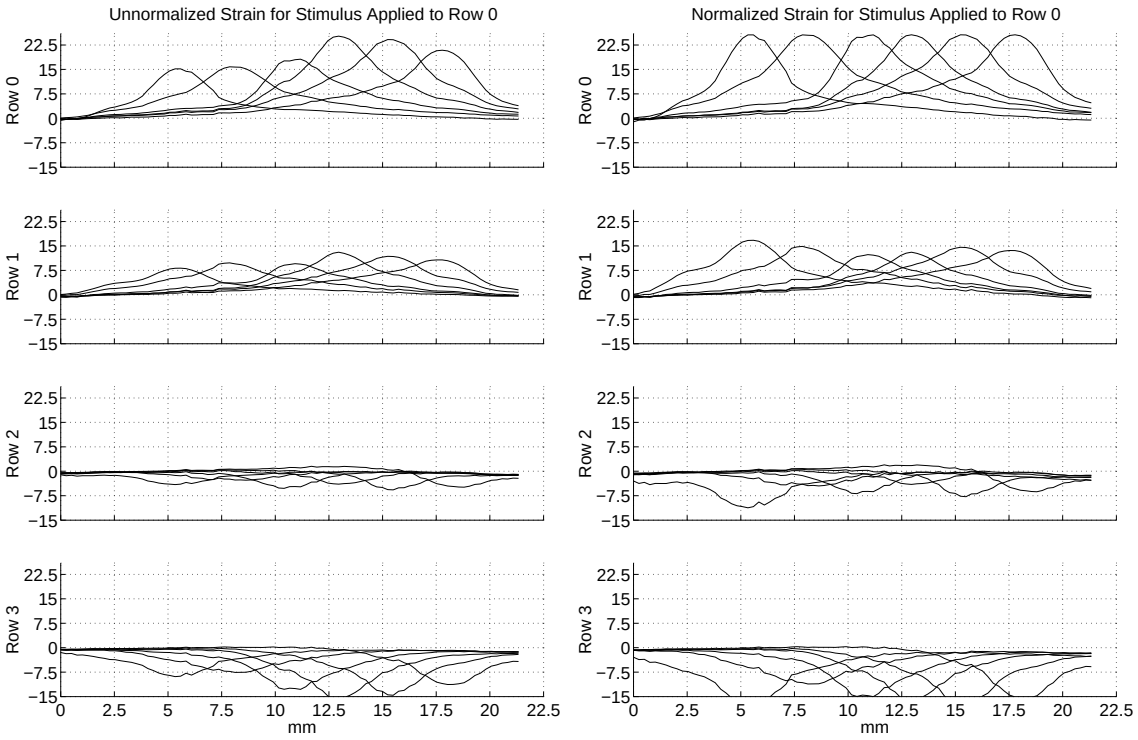

Figure 3.4: Raw and normalized strain for sensor row 0.

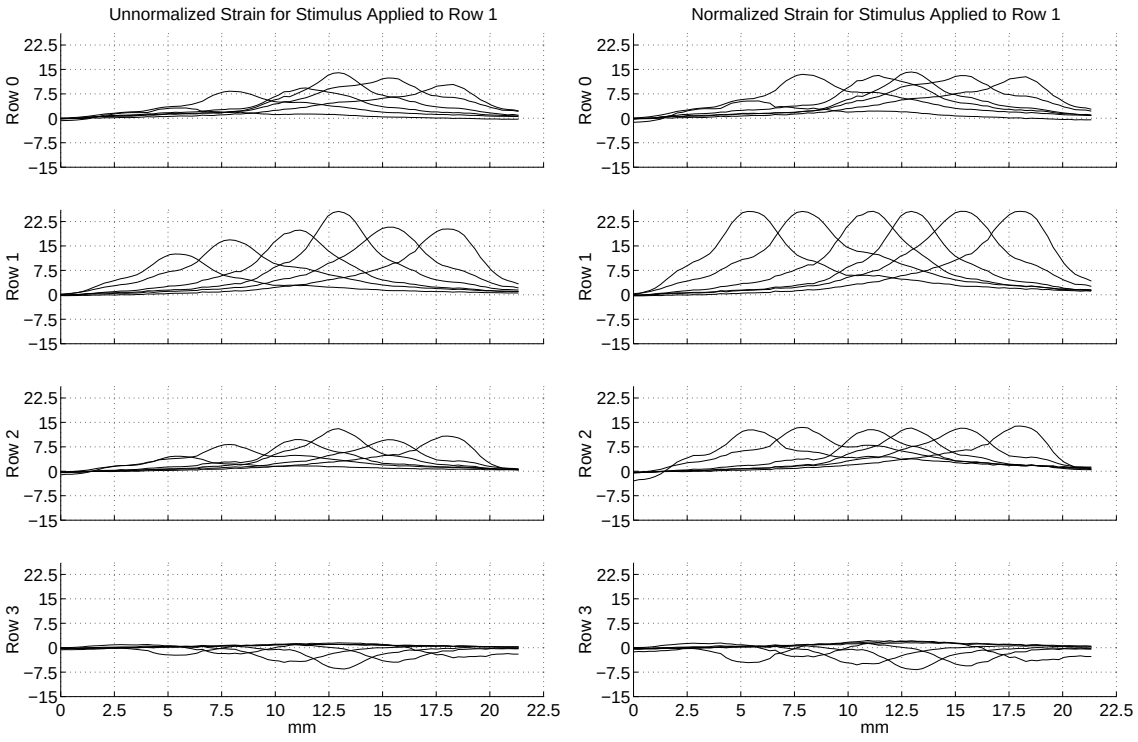

Figure 3.5: Raw and normalized strain for sensor row 1.

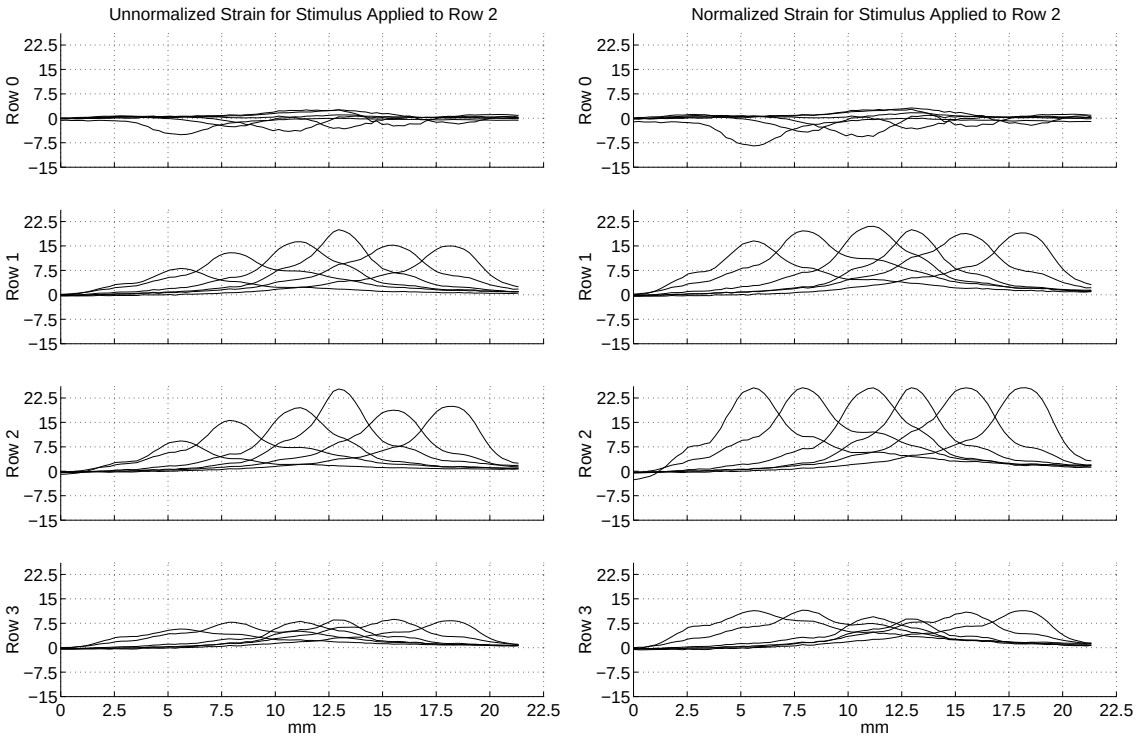

Figure 3.6: Raw and normalized strain for sensor row 2.

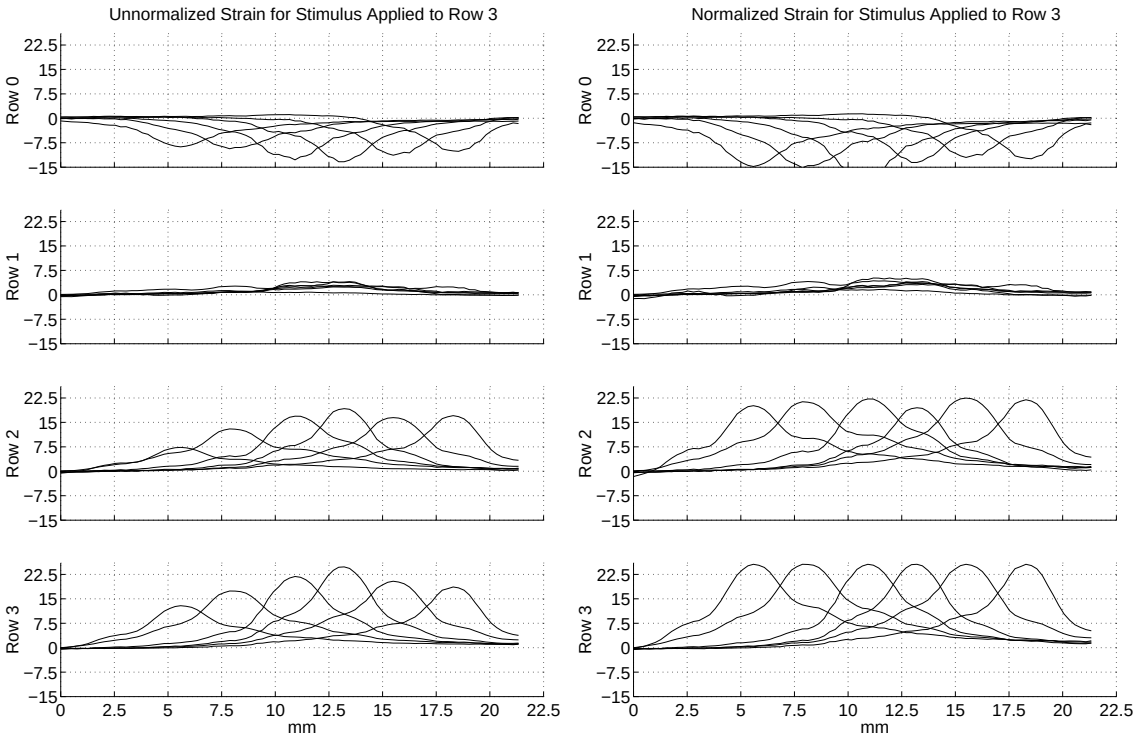

Figure 3.7: Raw and normalized strain for sensor row 3.

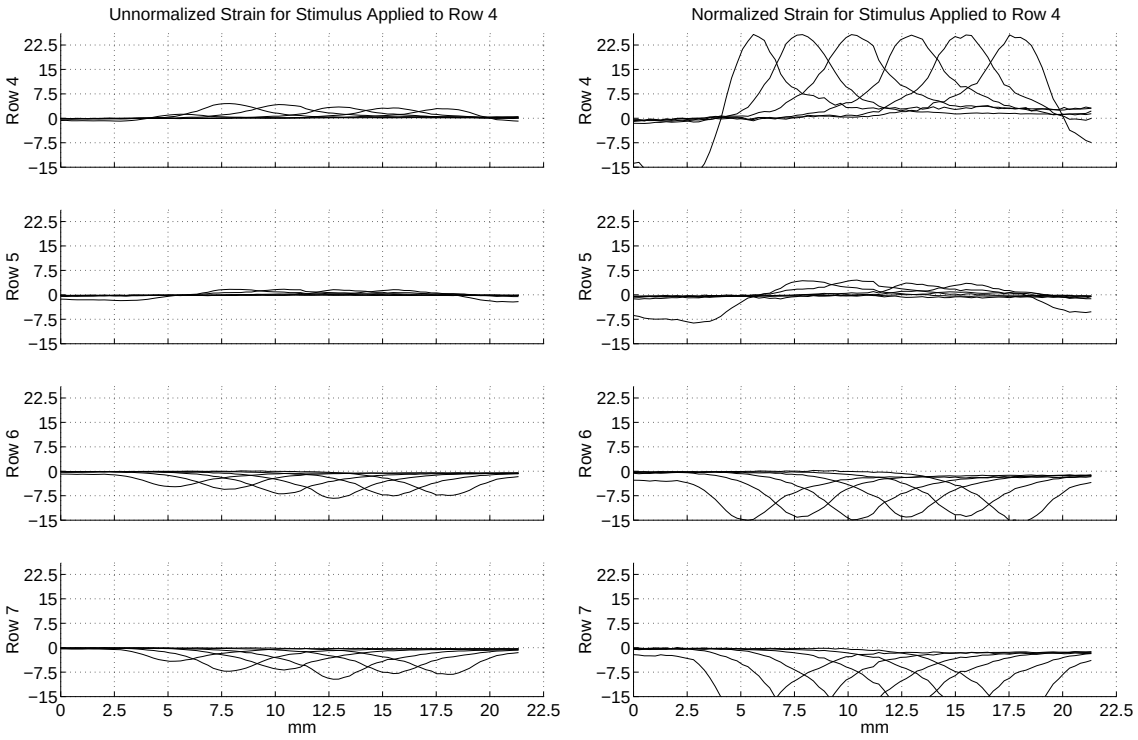

Figure 3.8: Raw and normalized strain for sensor row 4.

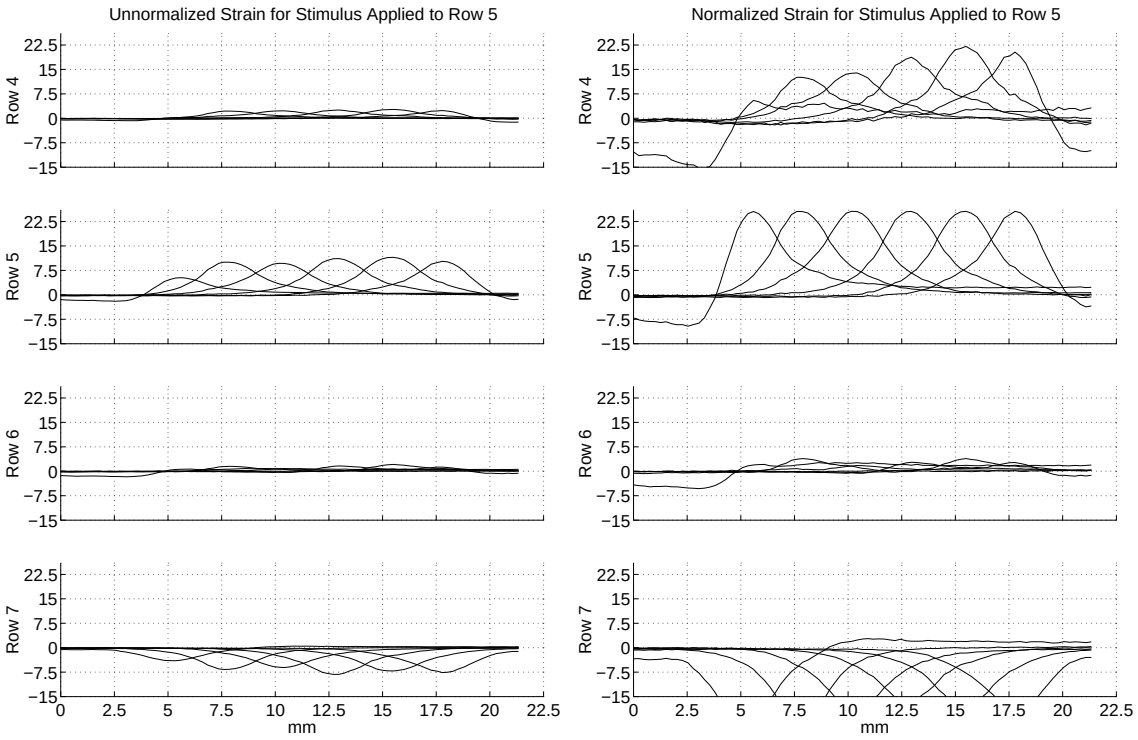

Figure 3.9: Raw and normalized strain for sensor row 5.

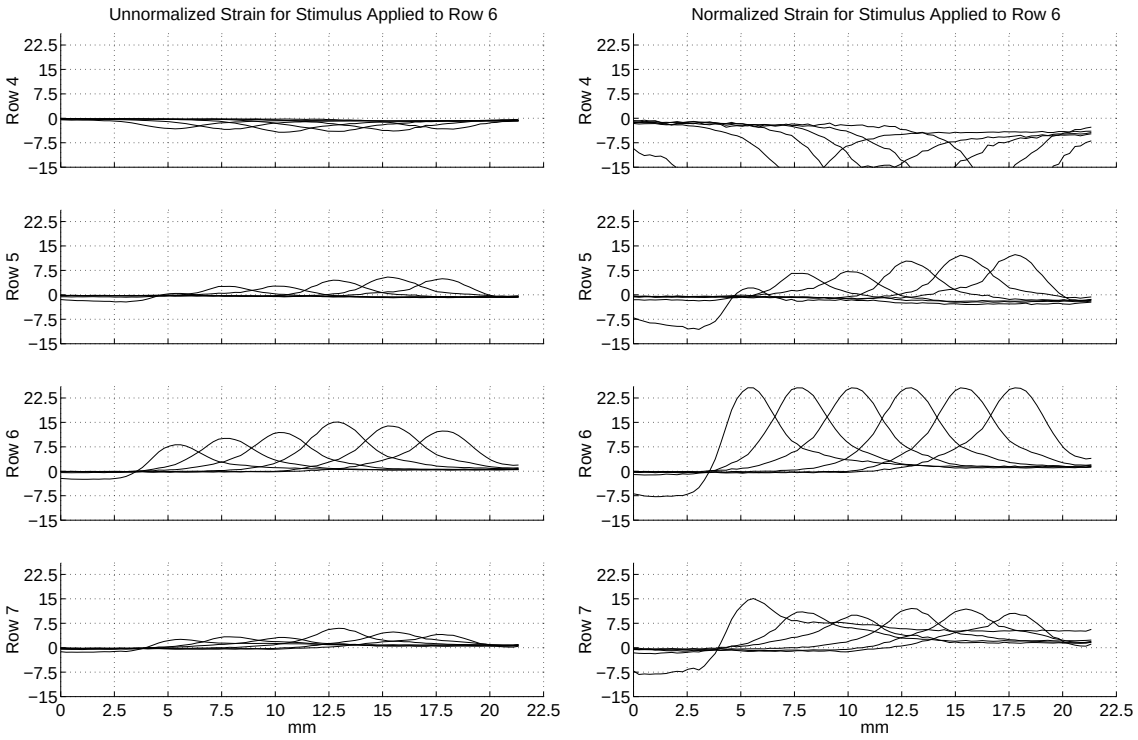

Figure 3.10: Raw and normalized strain for sensor row 6.

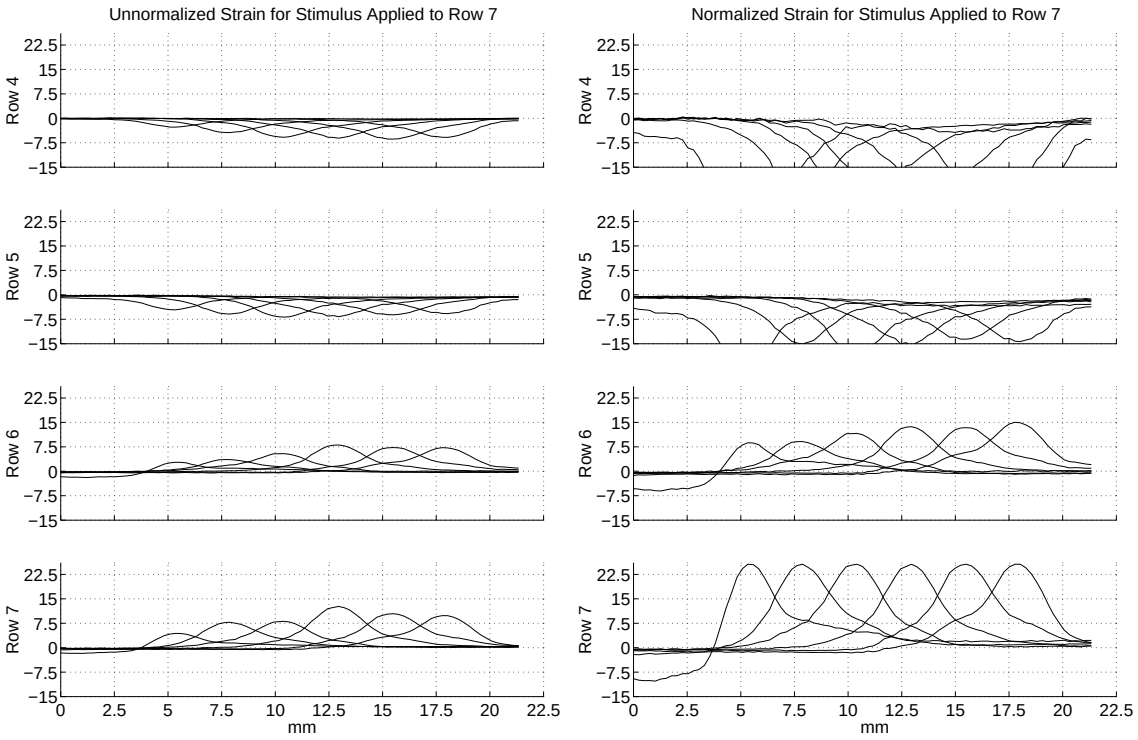

Figure 3.11: Raw and normalized strain for sensor row 7.

3.2 Tactile Display

The tactile display system consists of a Siemens C167CR-LM chip on a Phytec board, 4 power supplies, 32 Matrix valves by Matrix S.p.A., 4 Matrix valve controller boards, 32 orifice/capacitive elements, associated tubing and wires, and 2 display interfaces (Figure 3.12).

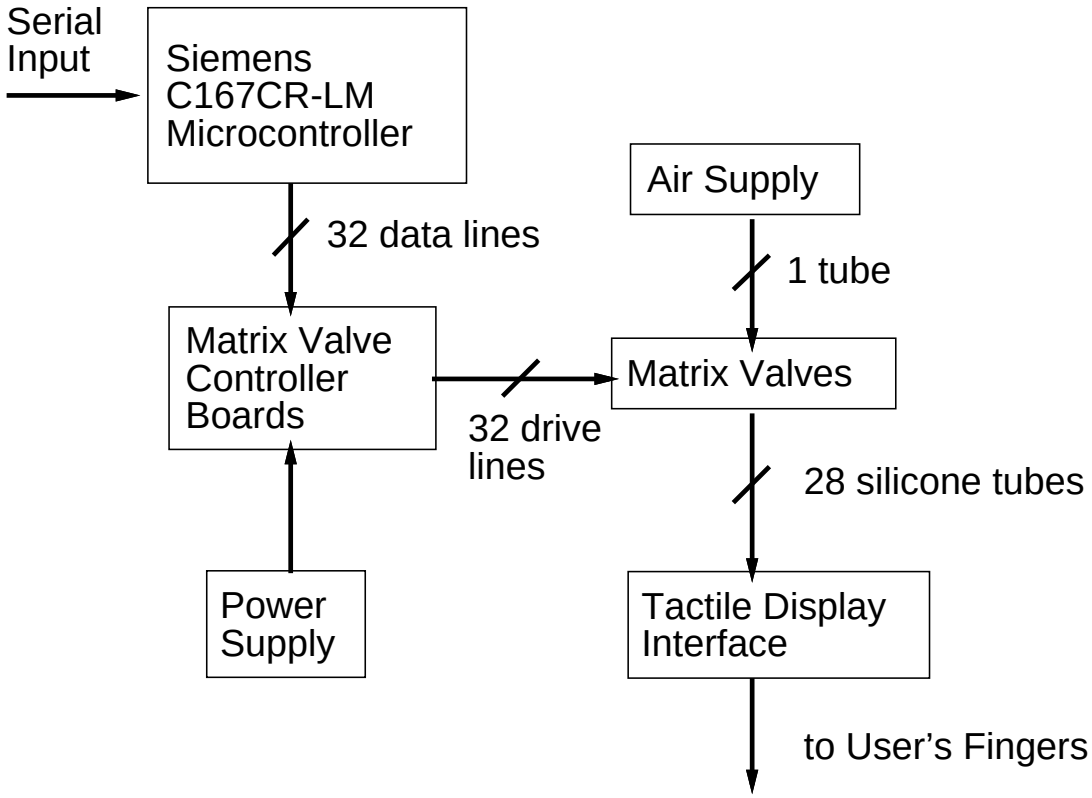

Figure 3.12: Block diagram of tactile display system.

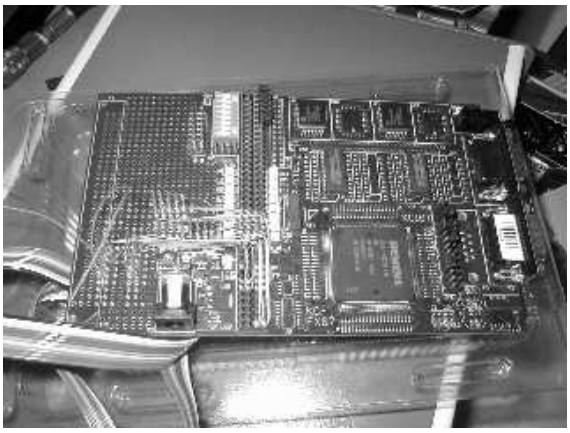

Figure 3.13: The Siemens board wired up.

3.2.1 Siemens C167 board

A Phytec prototype board containing a Siemens C167CR-LM chip connects the PC to the valve controller boards. The Siemens chip runs at 20 MHz and the clock is divided down to 2.5 MHz giving a 400 ns clock period. We run the chip at 2.5 MHz because the Siemens chip uses 16 bit counter registers. If we ran at higher clock speeds, we would need longer registers to obtain the PWM frequency range of 100 Hz to 300 Hz. We tested the valves at PWM frequencies of 300 Hz, 200 Hz, 150 Hz, and 100 Hz, and 150 Hz gave the best tradeoff between pressure range and response time. At 150 Hz, we wait 16667 cycles before resetting the counter register.

On the Siemens chip, we use 28 CAPCOM (CAPture and COMpare) channels as the PWM duty cycle generators. Each channel has a load value and a compare value. The load values for the channels are `0xBEE5`, corresponding to

`65536 (0xFFFF) - 16667 (0x411B) = 48869 (0xBEE5),`

which gives a 150 Hz PWM frequency. The compare values control the PWM duty cycle output of each channel. The counter starts at the load value with a low output. The counter increments each clock cycle and switches to a high output when the counter value is equal to the compare value. The counter is reset to the load value the clock cycle after the counter reaches `0xFFFF`. The input range of `0xBEE5` to `0xFFFF` corresponds linearly to a 100% to 0% duty cycle. We linearly split this range into 128 values to give PWM duty cycle steps of 0.78%. We use the last 7 bits of a serial port input byte as the desired pressure. The 28 CAPCOM channel outputs connect to the Matrix valve driver boards.

We use 1 PWM channel to control the stimulus valve. The PWM channel uses the same idea as the CAPCOM channel but has some options we don't use, such as pulse centering.

On the Siemens board, we also utilize the 4 A/D channels for valve calibration. We control the PWM duty cycles internally to give 0.4% PWM duty cycle steps. We then connect the analog pressure sensors outputs back to the Siemens A/D channels to record the pressure. We calibrate 4 valves at a time. With the calibration curves, we linearize the valves so that the desired pressure from the serial port input byte gives a consistent output across all the valves.

Due to limitations of the Siemens board, we can only run the serial port at 57.6kbps. This baud rate limits the tactile display system to a 100 Hz update rate. Table 3.2 shows the pinout connections for the Phytec board.

Pin #	ID	Description
85	P2.0/CAPCOM0	Valve 0 control
89	P2.1/CAPCOM1	Valve 1 control
86	P2.2/CAPCOM2	Valve 2 control
90	P2.3/CAPCOM3	Valve 3 control
87	P2.4/CAPCOM4	Valve 4 control
91	P2.5/CAPCOM5	Valve 5 control
88	P2.6/CAPCOM6	Valve 6 control
92	P2.7/CAPCOM7	Valve 7 control
93	P2.8/CAPCOM8	Valve 8 control
97	P2.9/CAPCOM9	Valve 9 control
94	P2.10/CAPCOM10	Valve 10 control
98	P2.11/CAPCOM11	Valve 11 control
95	P2.12/CAPCOM12	Valve 12 control
99	P2.13/CAPCOM13	Valve 13 control
96	P2.14/CAPCOM14	Valve 14 control
100	P2.15/CAPCOM15	Valve 15 control
125	P8.0/CAPCOM16	Valve 16 control
129	P8.1/CAPCOM17	Valve 17 control
126	P8.2/CAPCOM18	Valve 18 control
130	P8.3/CAPCOM19	Valve 19 control
127	P8.4/CAPCOM20	Valve 20 control
131	P8.5/CAPCOM21	Valve 21 control
128	P8.6/CAPCOM22	Valve 22 control
132	P8.7/CAPCOM23	Valve 23 control
119	P7.4/CAPCOM28	Valve 24 control
123	P7.5/CAPCOM29	Valve 25 control
120	P7.6/CAPCOM30	Valve 26 control
124	P7.7/CAPCOM31	Valve 27 control
117	P7.0/PWM0	Valve 28 control (stimulus)
121	P7.1/PWM1	Valve 29 control (extra)
118	P7.2/PWM2	Valve 30 control (extra)
122	P7.3/PWM3	Valve 31 control (extra)
69	P5.0/ADC0	A/D Channel 0
73	P5.1/ADC1	A/D Channel 1
70	P5.2/ADC2	A/D Channel 2
74	P5.3/ADC3	A/D Channel 3
151	Ground	
152	Ground	

Table 3.2: Pinout of Phytec board, associated Siemens ID, and output connection.

3.2.2 Valve controller boards

The Matrix valve controller boards take 8 TTL inputs, +24V, ground, and outputs drive signals to the Matrix valves. There is a DB-25 connecting the board to the inputs and a DB-15 connecting the board to the valves. Pinouts are shown in Figure 3.14. Each board controls 1 Matrix valve array. Figures 3.15-3.16 show the input/output characteristics.

3.2.3 Power supply

A PowerOne 3.6A 24V linear power supply (Digikey part number 179-2054-ND) drives each of the valve controller boards. A separate quad output PowerOne switching supply (Digikey part number 179-2019-ND) drives for the tactile sensors and Siemens board. The tactile sensors use the +5, +12V, -12V, and ground line. The Siemens board uses the +5V and ground line.

3.2.4 Matrix valves

Matrix 2-way solenoid valves increase the pressure in each tactile display element. Instead of using another 2-way valve for deflation, an orifice allows deflation of the display elements when the valve is off. Capacitive chambers act as a low pass filter to reduce PWM buzz. The buzz is caused by the rapid switching on and off of the valve. The Matrix valves come packaged with one input and 8 outputs, as shown in Figure 3.17.

15 Pin D-Sub Connector

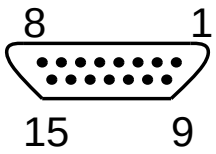

1 Valve 1 Output Control (Brown)
2 Valve 2 Output Control (Red)
3 Valve 3 Output Control (Orange)
4 Valve 4 Output Control (Yellow)
5 Valve 5 Output Control (Green)
6 Valve 6 Output Control (Blue)
7 Valve 7 Output Control (Violet)
8 Valve 8 Output Control Greyn)
9 Valve Common (Black)
10 Valve Common (Black)
11 Valve Common (Black)
12 Valve Common (Black)
13 Unconnected
14 Unconnected
15 Unconnected

25 Pin D-Sub Connector

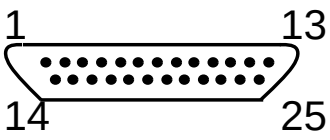

1 + Supply
2 + Supply
3 - Supply
4 - Supply
5 + Channel 1 Input
6 + Channel 2 Input
7 + Channel 3 Input
8 + Channel 4 Input
9 + Channel 5 Input
10 + Channel 6 Input
11 + Channel 7 Input
12 + Channel 8 Input
13 Unconnected
14 + Supply
15 + Supply
16 - Supply
17 - Supply
18 - Channel 1 Input
19 - Channel 2 Input
20 - Channel 3 Input
21 - Channel 4 Input
22 - Channel 5 Input
23 - Channel 6 Input
24 - Channel 7 Input
25 - Channel 8 Input

Figure 3.14: Valve controller board pinouts.

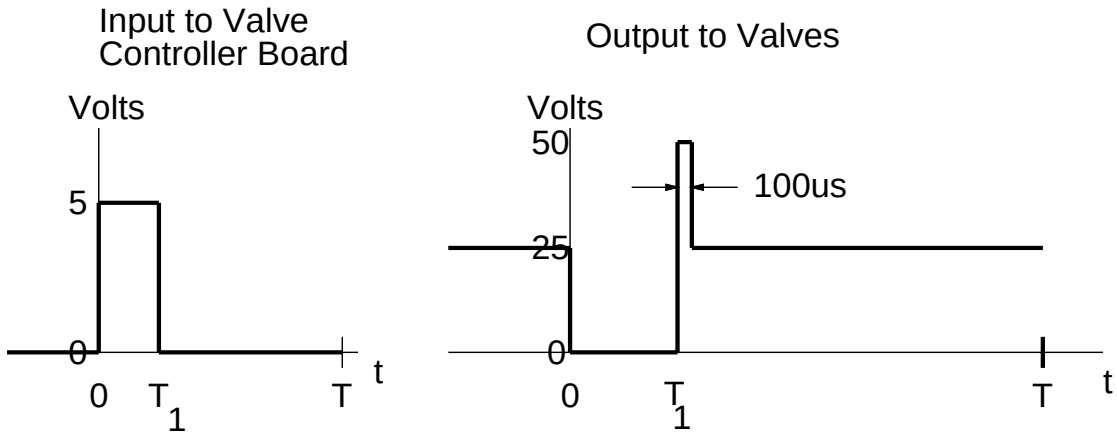

Figure 3.15: Valve controller output for a high input signal of $T_1 \leq 2\ ms$. $T = 6.67\ ms$ for a 150 Hz PWM frequency.

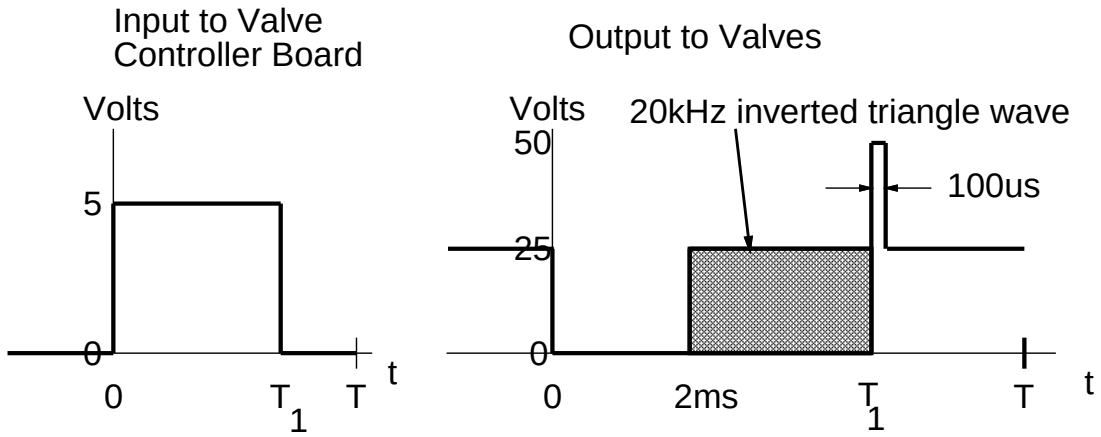

Figure 3.16: Valve controller output for a high input signal of $T_1 \geq 2\ ms$. $T = 6.67\ ms$ for a 150 Hz PWM frequency.

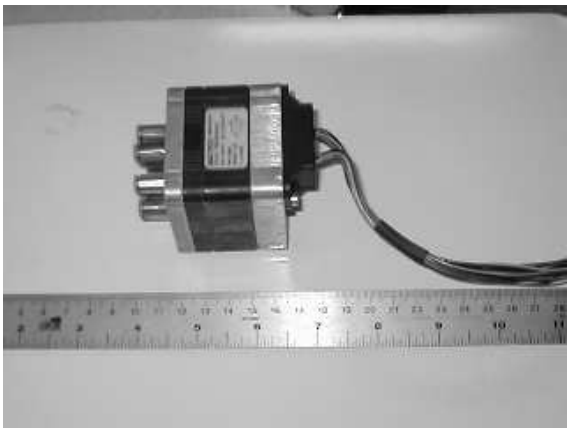

Figure 3.17: A Matrix valve array with one input and 8 outputs.

We run the valves at a PWM frequency of 150 Hz. The valve output pressures are controlled by a PWM input. We calibrate and linearize the valves to 128 PWM levels as discussed in the section above and Appendix D. The PWM buzz is less than 10% peak-to-peak for duty cycles greater than 20%. Across all valves and PWM duty cycles, the average PWM buzz is 5.55 PSI peak-to-peak and the standard deviation is 1.30 PSI.

We look at the response times to step inputs corresponding to a 0 to 10 PSI jump, a 10 to 50 PSI jump, a 50 to 10 PSI jump, and a 10 to 0 PSI jump. The output pressure is shown in Figure 3.18 and agrees with the 2 ms transition time claimed by Matrix.

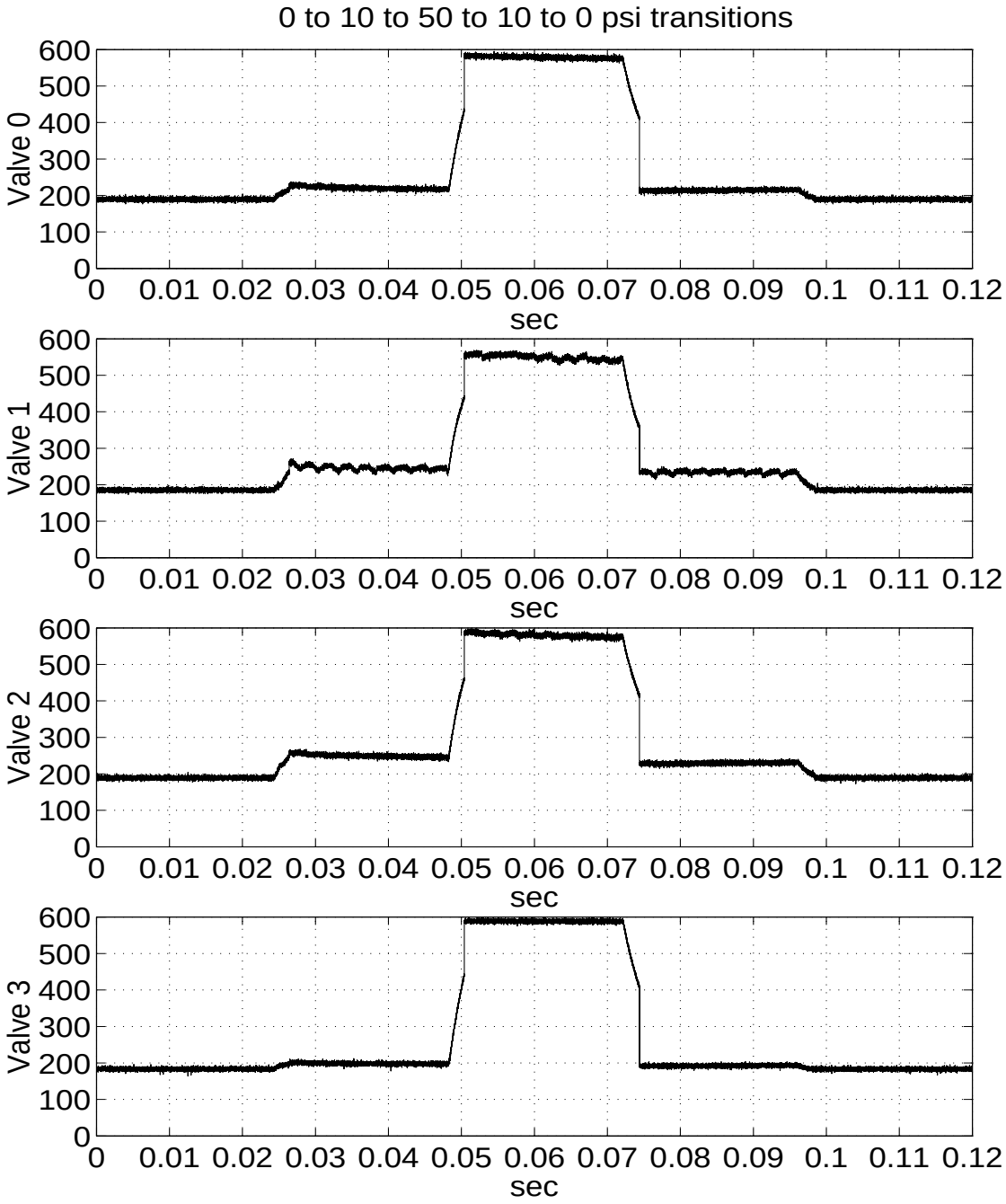

Figure 3.18: Output pressures while changing from 0 (0% PWM) to 10 (20% PWM) to 50 (100% PWM) to 10 to 0 PSI with unlinearized valves.

3.2.5 Display interface

Each tactile display interface contains 14 display elements in a hexagonally packed 5-4-5 configuration (Figure 3.19) with 2 mm spacing between elements and rows. Construction of the tactile display interface is described in Appendix B.

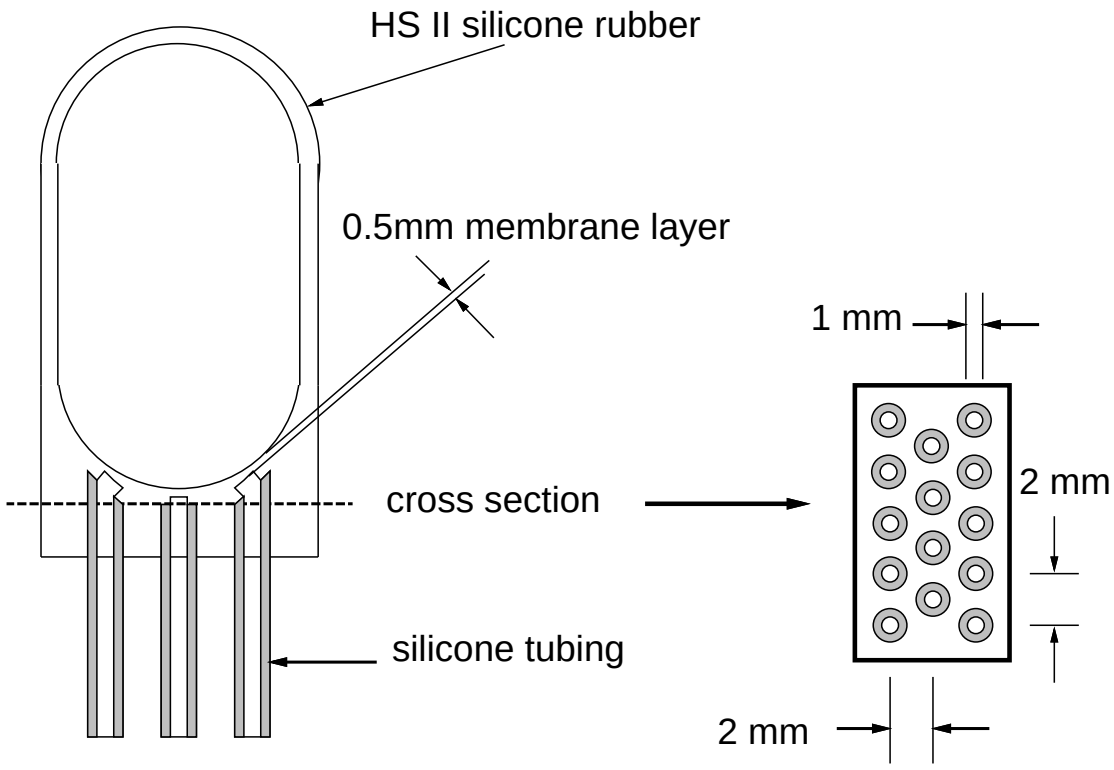

Figure 3.19: The tactile display with 14 elements and a center-to-center spacing of 2 mm.

3.3 Control Program and Communication Channels

The program `tactile.exe` controls all communication between the tactile sensor and tactile display. We modified the code to convert tactile sensor data to tactile display data and transmit the tactile display data to the Siemens board over the serial port. The Siemens board receives the header byte then an `unsigned char` from 128 to 255 which corresponds to a duty cycle between 0% and 100% in 1.28% increments.

The control program runs at 35-50 Hz, depending on the interpolation algorithm we use and whether we query for a keyboard input. A linear interpolation algorithm takes 2 ms while a sum of sinc functions takes 4 ms. The keyboard query for the experiment adds another 4 ms. It takes about 10 ms to read the sensors and another 10 ms to transmit tactile display data over the serial port. All programs run on a Pentium based PC running Windows 95.

3.3.1 Strain matching

The tactile sensors collect normal strain data from the contact. Since there was a resolution difference between the tactile sensor and display spacing and element configuration, we applied an interpolation algorithm. The tactile display was a 5-4-5 hexagonal pattern with 2 mm between elements. The tactile sensor was a 4×6

rectangular pattern with 2.7 mm between elements. We used a sum of sinc functions to interpolate intermediate points as follows:

$$\epsilon_d(i) = \sum_{j=0}^{n_s} \epsilon_s(j) sinc(\frac{x_i - x_j}{2.7}) sinc(\frac{y_i - y_j}{2.7})$$

where $\epsilon_d(i)$ is the strain to present in display element i, where $\epsilon_s(j)$ is the strain recorded in sensor element j, and x_i, x_j, y_i, y_j are the x and y locations of the sensor and display elements. Using MATLAB simulations of the linear elastic model [Fearing, 1997], we find that applying the 0.5 mm reconstruction filter on the tactile display would change a neighboring element by less than 2%. We decided that the extra time needed for the matrix multiplication was not worth the extra accuracy.

3.3.2 Contrast

We added a contrast factor so that we used a wide range of valve PWM duty cycles. The tactile sensors ranged from 0% strain for no contact to 40% strain for really strong contact. We used a 2.5 multiplicative contrast factor to use 0% to 100/128 = 78% PWM duty cycles on the valves. This contrast factor was chosen to make sure a 35 PSI peak pressure stimulus waveform was easily detected.

3.4 Direct force feedback

Through the design of our teletaction system (Figure 3.1), we have direct force feedback. The grasping force applied to the displays is proportional to the grasping

force applied by the sensors to the environment. By eliminating a complex force reflection system and associated time delay, we can focus on the teletaction system.

3.5 Stimulus

Our stimulus is a mock blood vessel embedded in tissue. The stimulus is made from silicone tubing, GE 6166 silicone gel, and plastic wrap. Stimulus construction is detailed in Appendix C. One of the Matrix valves (#28) controls the pressure in the embedded silicone tubing. We present an aortic pressure curve at approximately 1 Hz [PWV Medical, 1999]. We use 8 peak pressure levels of 0, 5, 10, 15, 20, 25, 30, and 35 PSI. (Figure 3.20). We use such high pressures after pilot tests show that 35 PSI is easily felt through both direct touch and the teletaction system. For comparison, the peak pressure in the aorta is approximately 2.7 PSI ($140mm$Hg) [PWV Medical, 1999].

3.6 Complete system

The complete system of tactile sensors, tactile displays, associated electronics, and electrical and pneumatic connections are shown in Figure 3.21. A picture of the sensors squeezing the mock blood vessel is shown in Figure 3.22. The system is packaged such that the controller PC only needs a parallel port connection to read the sensors and a serial port connection to control the display. The tactile sensors have

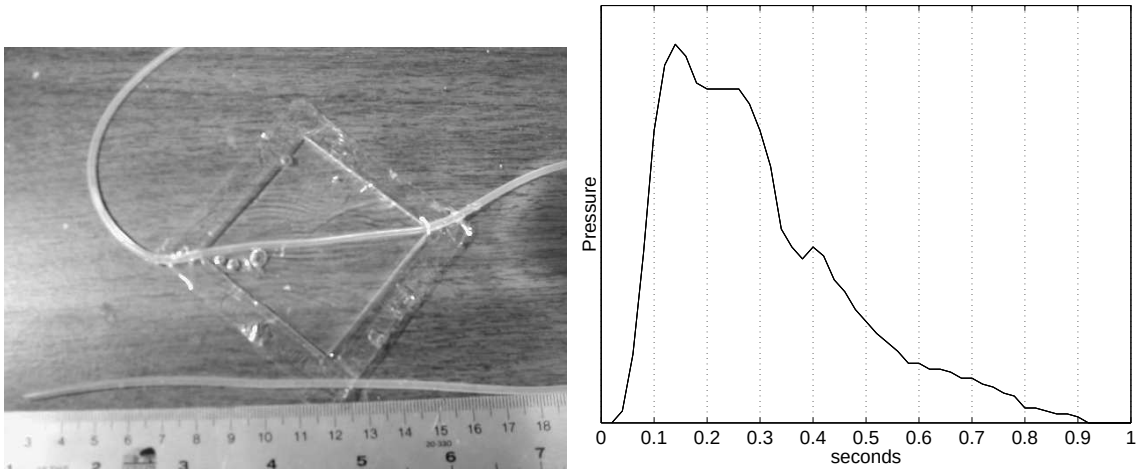

Figure 3.20: Stimulus and stimulus pressure waveform.

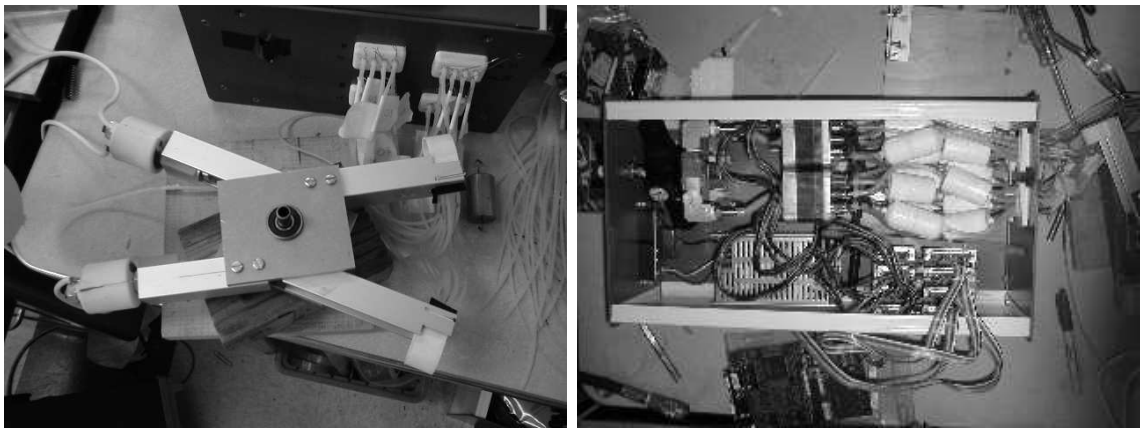

Figure 3.21: Pictures of the bidigital teletaction system along with the tactile display valves, low pass filters, and electronics.

Figure 3.22: Picture of the sensors squeezing the stimulus.

2 small boxes of electronics and the tactile displays have one large box of electronics and pneumatics and an array of 4 power supplies.

Chapter 4

Grating Detection

Using an early version of the tactile display, we tested the human performance in grating detection. We also verified the uniformity and linearity of the molded display process. We use a simulated 5 mm grating to determine the necessary amplitude resolution to detect grating orientation.

We tested the molded tactile display technology for its physical properties as well as the ability to transmit tactile information. We discuss the display construction, uniformity and linearity testing, and human psychophysics testing of grating detection.

4.1 Tactile display construction

The tactile display consists of a 5x5 array of tactor elements (Figure 4.1 and 4.2). The elements are spaced 2.5 mm apart and are 1 mm in diameter, as seen in the

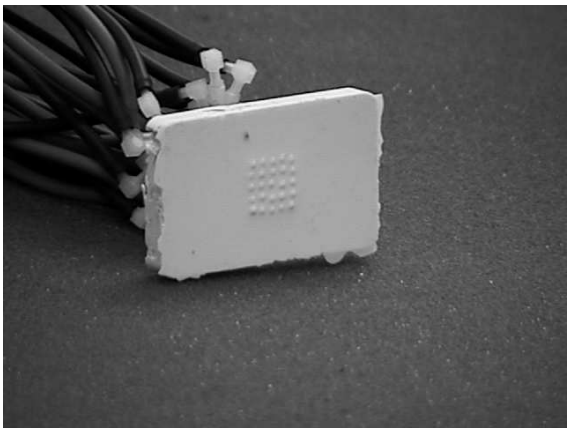

Figure 4.1: A 5 × 5 chamber array with all chambers inflated.

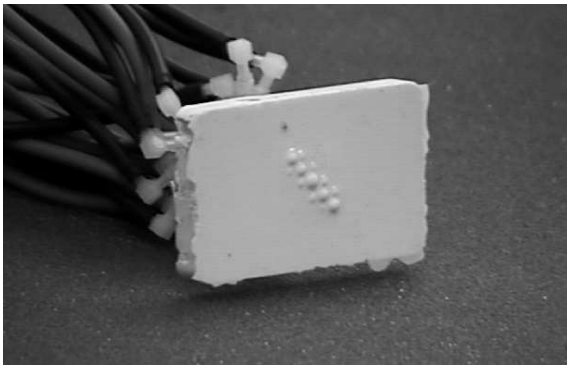

Figure 4.2: A 5 × 5 chamber array with a diagonal pattern inflated.

cross section (Figure 4.3). The effective contact area is 25 mm^2 in a 12 mm × 12 mm area. Instead of an array of actuated pins, we use an array of pressurized chambers as the stimuli. The enclosed pressurized chamber design ensures no extraneous stimuli from air leakage. We used 25 Clippard solenoid 3-way valves [Cohn, 1992] with pulse width modulated (PWM) square waves to control the pressure in each chamber.

The tactile display was molded from silicone rubber (HS II by Dow Corning) in

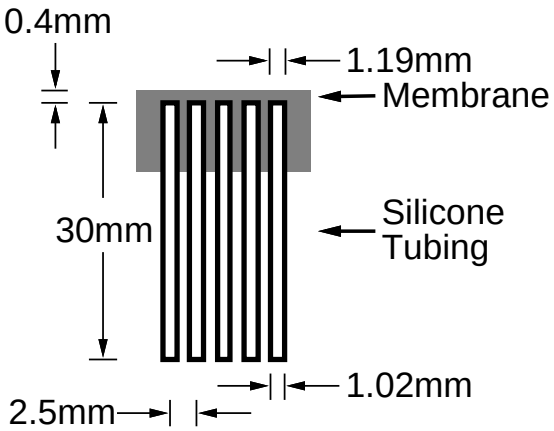

Figure 4.3: Cross section of the contact interface.

a one-step process. The mold is shown in Figure 4.4. Twenty-five stainless steel pins (diameter 1.19 mm) extend 30 mm from the baseplate of the mold and were soldered to the back of the baseplate. The pins were planarized with the contact interface mold by a milling machine.

Silicone tubing (inner/outer diameter = 1.02/2.16 mm) was placed around each of the pins. The tubing does not extend to the end of the pins. The chamber size was determined by the diameter of the pin. The membrane thickness of the chambers was precisely controlled by spacers between the baseplate structure and contact interface mold. We used 0.4 mm of brass shim which leads to a membrane thickness of 0.4 mm. The spacing between elements was kept uniform by the contact interface mold.

The silicone rubber was poured into the mold and the mold was pressed against a flat surface. It took 24 hours for the silicone rubber to cure. The silicone rubber bonds with the silicone tubing to form an airtight chamber. The flexibility of the

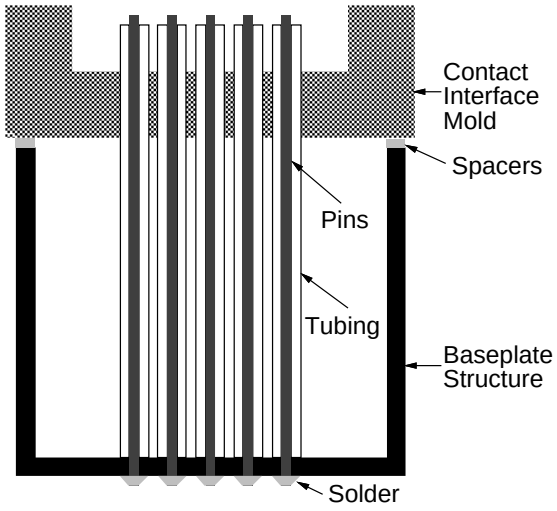

Figure 4.4: The contact interface mold used in fabrication.

contact interface provides constant contact between all the tactors and the finger (Figure 4.5). Since the tactile display was always in contact with the finger, we do not worry about a dead zone before the elements made contact. Attachment force of the contact interface to the finger can be controlled. The contact interface was connected to the pneumatic valve array by hoses and barbed connectors.

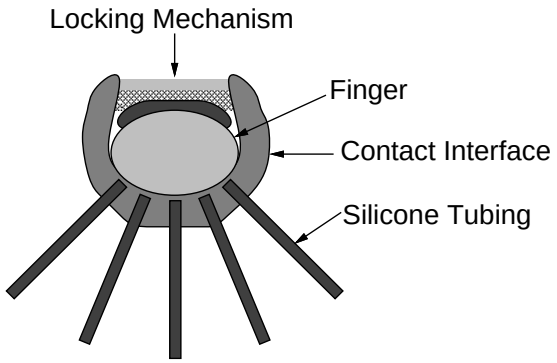

Figure 4.5: The contact interface wrapped around the finger with a locking mechanism above the fingernail.

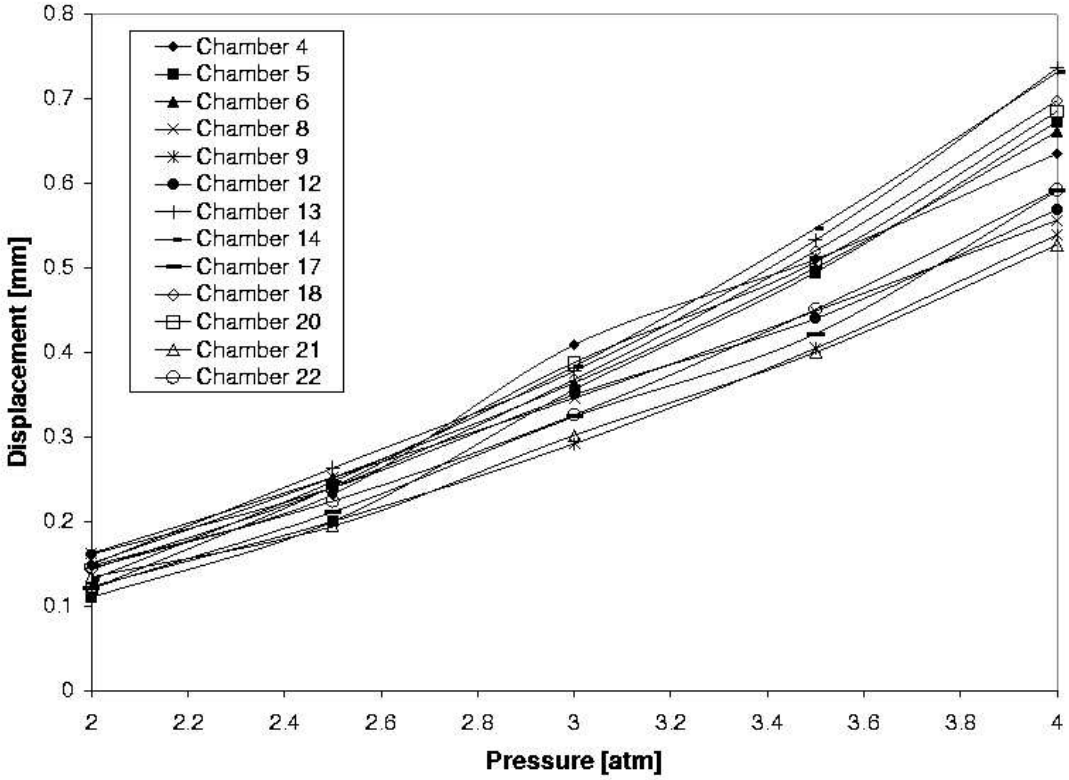

Figure 4.6: Uniformity test results.

4.2 Static performance

To measure the uniformity of the display and the quality of the manufacturing process, we applied pressures of 29.4 to 58.8 PSI (2 to 4 atm) to the chambers. We measured the corresponding display displacement for each pressure and chamber. The displacement was determined using a mounted micrometer, adjusted to the point of contact with the display. The results are shown in Figure 4.6. At each pressure, the variation between chambers was about 15% from the average value.

Because the thickness of the membrane is the main variable between chambers, the uniform displacement distribution also demonstrates the regularity of the manufacturing process. The process is thus shown to provide a uniform membrane thickness over every chamber. We are assuming that the material itself is uniform, as any inconsistencies in the rubber are minor compared to slight imperfections in the mold and molding process. If the spread of 15% is too high and the manufacturing process cannot easily be refined, the fidelity can be improved in software by a calibration matrix.

We measured the force vs. displacement curves for 7.3 to 53.8 PSI (0.5 to 4 atm) of pressure in 7.3 PSI (0.5 atm) steps to determine a complete mapping of supply pressure, force, and displacement. One representative chamber was used for the characterization because of the high similarity between chambers. The force at various displacements was measured by mounting a force/torque sensor on a micrometer driven stage, which has an accuracy of 0.001 mm along the axis of expansion of the display. The stage was set to a given displacement and a static supply pressure is applied to the chamber. The force was read from the force/torque sensor. This procedure was repeated for the range of displacements and pressures. The results are shown in Figure 4.7.

For each static supply pressure, the force vs. displacement curve is linear. This conclusion is the most important consideration, because the tactile display cannot be fixed at a certain force or displacement across all users due to the differences in

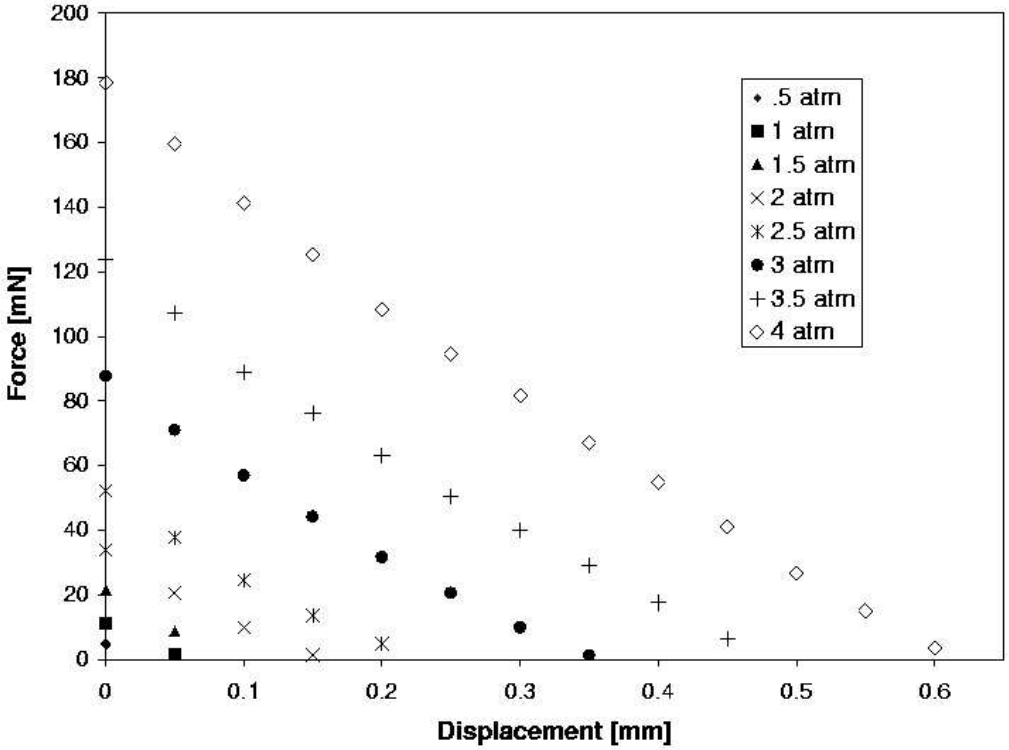

Figure 4.7: Force vs. displacement at various pressures.

stiffness of the finger pad. Due to the linearity of the individual curves, the same information can be transmitted regardless of the indentation and placement of the individual finger.

4.3 Tactile display and human performance

To test the performance of the tactile display, we conducted a psychophysics experiment using simulated gratings, with a 5 mm period. We compared the results

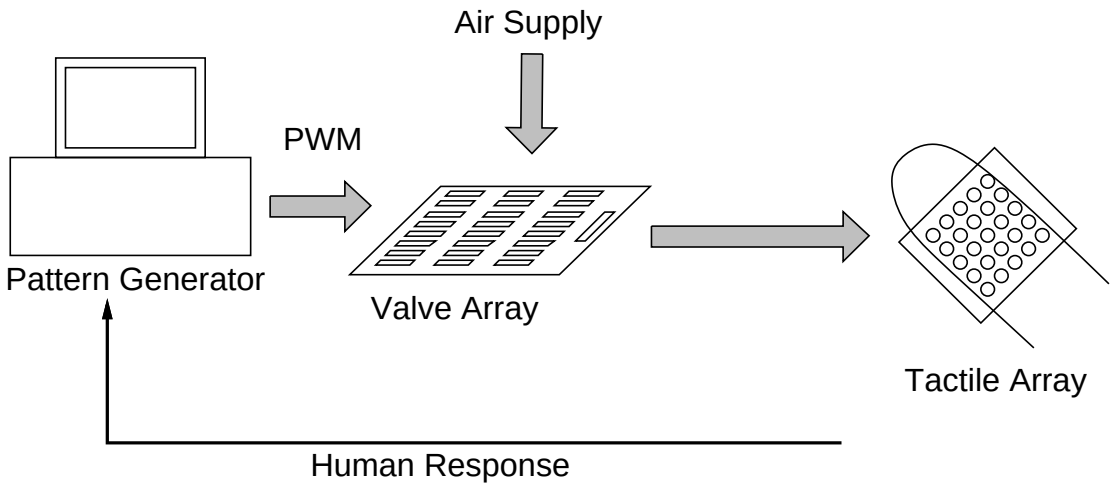

Figure 4.8: Test apparatus.

with contacts with real gratings. In the experiment, subjects were asked to determine the direction of a grating pattern presented to them on the tactile display. The apparatus is shown in Figure 4.8.

We generated simulated square gratings with 5 mm period in horizontal and vertical orientations as shown in Figure 4.9. The grating troughs were at 20%, 34%, 50%, 69% or 90% of the grating peak pressure of 44 PSI (3 atm). The experiment consisted of presenting 300 patterns to each subject. The 300 patterns consisted of 30 grating patterns in each orientation at five different trough pressure levels. The experiment was broken down into 6 sessions of 50 trials each.

The tactile display was secured to the subject's finger with two wires wrapped around the display and finger (Figure 4.10). The grating pattern was presented for 3 seconds and the subject is given an additional 3 seconds to respond. One second of

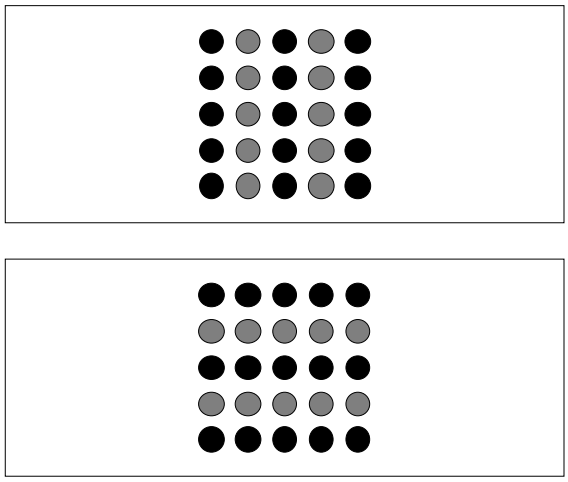

Figure 4.9: The vertical and horizontal grating patterns used as stimuli. Black dots indicate full pressure. Grey dots indicate 20%, 34%, 50%, 69% or 90% of full pressure.

Subject	90%	69%	50%	34%	20%
1	15	32	47	49	56
2	26	41	48	47	46
3	24	34	45	44	52
4	29	30	47	47	50
5	36	31	41	42	43
6	25	42	47	49	51

Table 4.1: Raw data for grating detection experiments. The numbers represent the number of correct orientation detections out of 60 trials at each trough pressure.

rest was given after the response is recorded. The subject was instructed to respond whether the grating was "across" or "along" the finger. The experiment used a forced choice method. Subjects listened to white noise through headphones to remove audio cues from the valve array.

The experiment was conducted on 6 volunteer subjects with no known impairments in tactile sensory functions. The raw data is shown in Table 4.1. The average results are shown in Figure 4.11. We compare these results with previous results

Figure 4.10: The tactile display attached to the finger.

shown in Figure 4.12 [Moy, 2000]. We convert the results to use the modulation index, defined as:

$$\sigma_z(x) \sim \alpha_\sigma(1 + \mu_\sigma \cos(\omega x))$$

where $\sigma_z(x)$ is the applied normal stress profile, α is the scaling factor, μ_σ is the modulation index, and ω is the frequency of the grating. The converted results are shown in Figure 4.13. Our results correlate well with previous data. The just noticeable difference point is approximately 0.1 modulation index units (a 10% amplitude variation). As the modulation index gets higher (trough pressures get lower), the perception of grating orientation also gets higher. We thus conclude that our tactile display has sufficient amplitude resolution to match human perceptual limits.

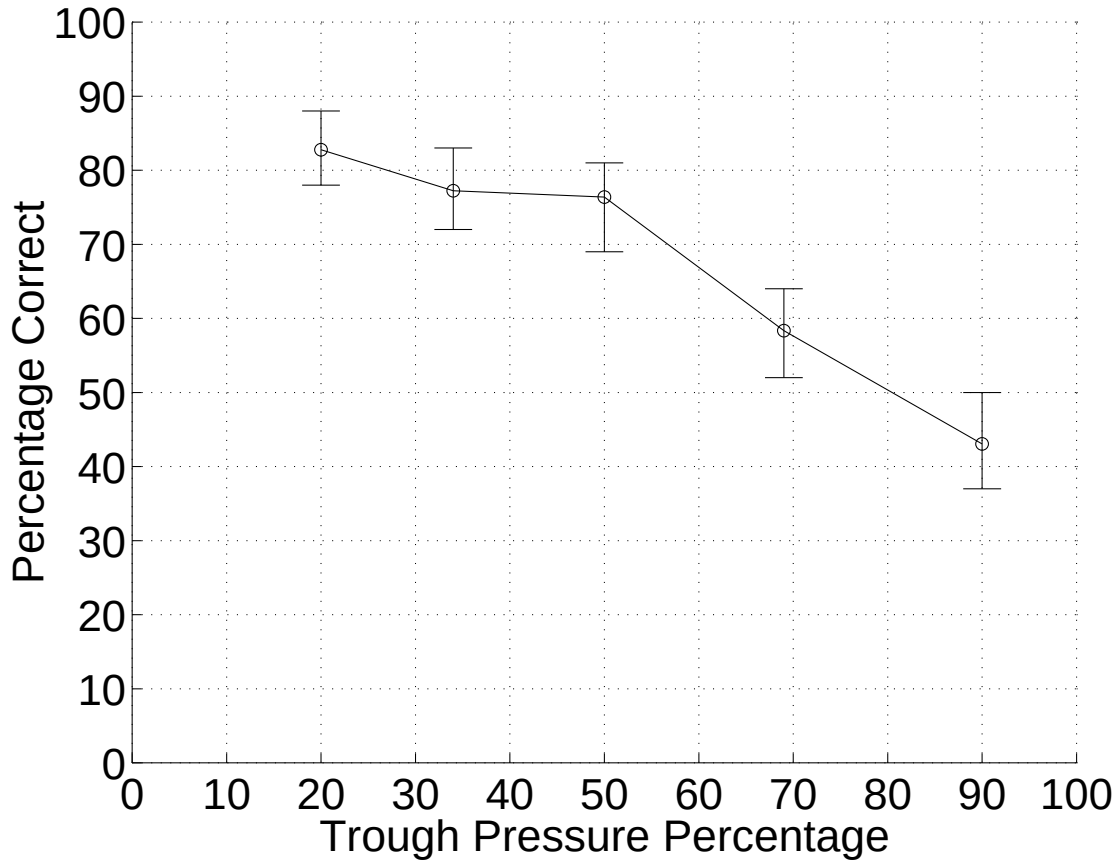

Figure 4.11: Results of the psychophysics experiment with 95% confidence intervals [Natrella, 1963].

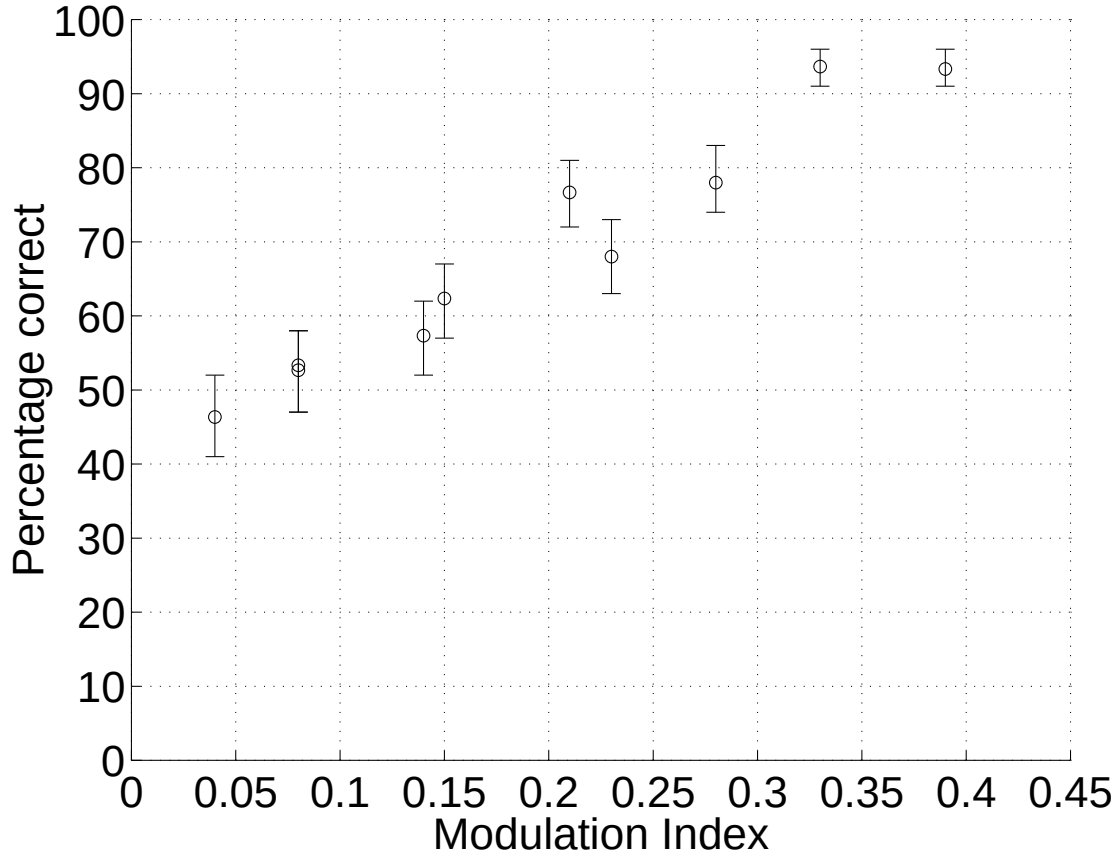

Figure 4.12: Results from previous psychophysics experiments relating grating orientation perception and modulation index for contacts with machined wax blocks [Moy, 2000]. Error bars represent 95% confidence intervals for n=300.

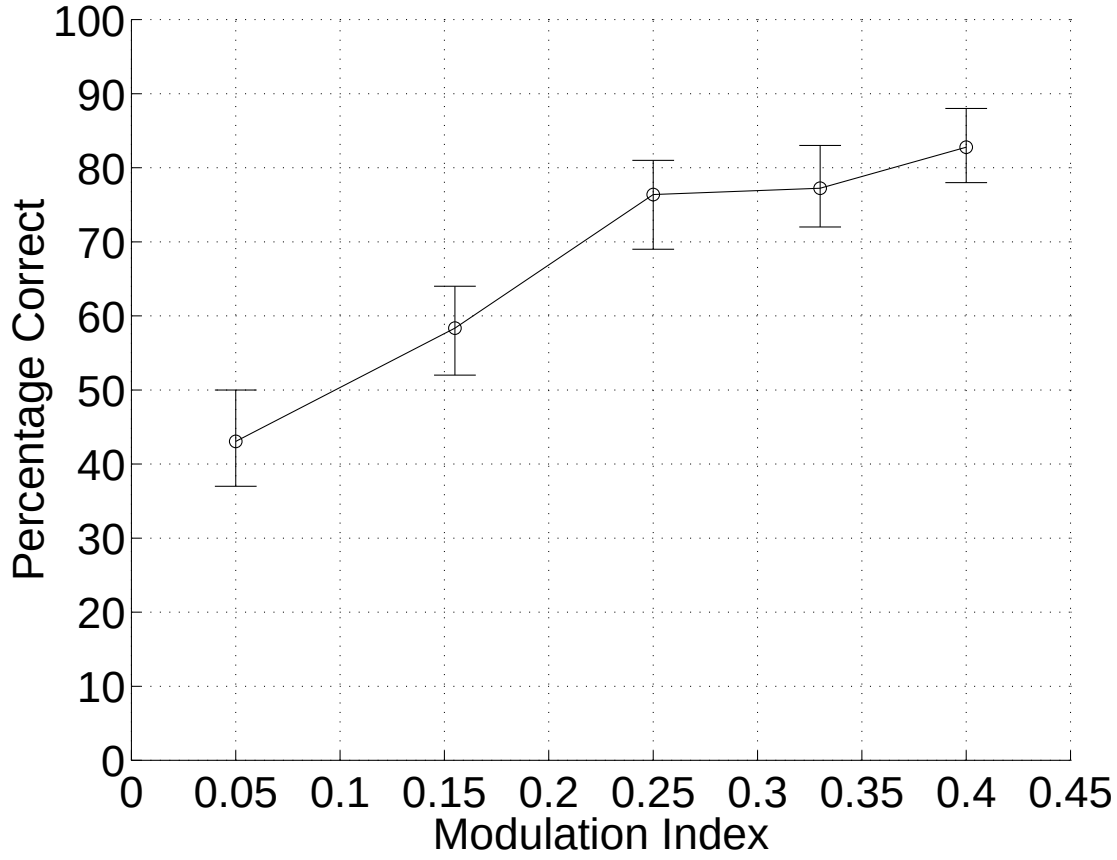

Figure 4.13: Results from the psychophysics experiment relating grating orientation perception and modulation index for the compliant tactile display. Error bars represent 95% confidence intervals for n=360.

Chapter 5

Pulsing Blood Vessel Detection

With the bidigital teletaction system described in Chapter 3, we tested the teletaction system and human performance in detecting a pulsing blood vessel. We also compared the effect of having tactile feedback in one finger and both fingers, similar to the experiment comparing monocular or stereo visual feedback through an endoscope [Tendick, 1993]. A final experiment compared direct touch to bidigital teletaction in the pulse detection task.

Previous experiments included artery tracking [Beasley, 2002] and single finger artery localization [Howe, 1995]. Our experiments tested the limits of the bidigital teletaction system for pulsing blood vessel detection. We compared having tactile feedback in both fingers versus having tactile feedback in only one finger.

5.1 Methods

In laparoscopic surgery, the surgeon's loss of tactile feedback makes it difficult to identify blood vessels if they are visually occluded. In order for the surgeon to fully identify a blood vessel, they must first detect it, then localize its position. We designed experiments to see how well our teletaction system can transmit tactile information about a pulsing blood vessel. We used multielement sensors and displays since this system can be extended to test localization, but we leave that for future experiments. We also tested whether having tactile information in both the thumb and finger can better detect pulsing blood vessels versus having tactile information only on the finger. The basic experiment of blood vessel detection with monodigital and bidigital tactile feedback will help determine future generations of the teletaction system.

5.2 Procedure

Our goal was to test if the bidigital teletaction system transmits enough tactile information to detect a pulsing blood vessel and if there was a statistically significant difference in having one or two active fingers in the bidigital teletaction system. When running the experiment with only one active finger, one sensor and display supply feedback to the subject while the unused display supplies a DC response to the other finger. The information received by the subject can be represented as:

$$Data_{2fingers} = Noise(p_1(t)) + Info(p_1(t)) + Noise(p_2(t)) + Info(p_2(t))$$

$$Data_{1finger} = Noise(p_1(t)) + Info(p_1(t)) + Noise(DC\ level)$$

where $p_1(t)$ and $p_2(t)$ are the sensed pressure profiles, $Noise(\cdot)$ is the noise produced by the teletaction system, and $Info(\cdot)$ is the pulse information.

We designed an experiment that measures the threshold of pulse detection using a dual staircase method to find the 71% response stimulus level. The experiment consists of 64 trials. Each trial consisted of one or two test cases depending on the test subjects response. Since we are looking for the 71% detection level, the trial follows the state diagram in Figure 5.1 [Levitt, 1970].

In order to decrease the stimulus pressure, the subject had to respond with two consecutive 'positive detect' answers on the same staircase. In each test case the subject squeezed the stimulus with the tactile sensors and responded whether they felt a pulse or not on the tactile displays. The pulse has 8 levels of peak pressure from 0 PSI to 35 PSI in 5 PSI steps. Each experiment was repeated for the case of having both sensors and displays active and for the case of having only one sensor and one display active.

The dual staircase method randomly interleaves two staircases. One staircase starts at maximum pressure. The second staircase starts at minimum pressure. We

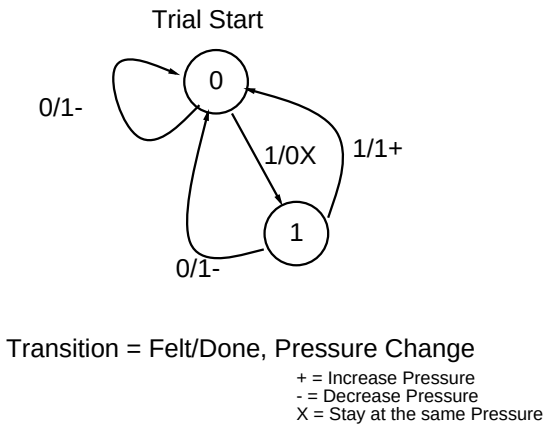

Figure 5.1: Mealy machine state diagram for a 71% detection trial.

randomly selected the starting staircase. Depending on the subject's response, we determined the next stimulus pressure for that staircase. If the subject felt the pulse, we decreased the pressure. If the subject did not feel the pulse, we increased the pressure. The experiment continued by randomly selecting the staircase for the next test case. Since there were two staircases, the subject did not know which staircase they were being tested on. The control program kept track of the current state of the trial so that trials can be interleaved, if the random number generator so chose. Once a staircase completed its 32 trials, the other staircase finished the rest of its 32 trials in sequence [Cornsweet, 1962, Levitt, 1970].

The whole experiment took approximately 30 minutes. Subjects wore noise canceling headphones to remove audio cues from the valves. The apparatus was covered by cloth to remove visual cues of the pulsing tube.

5.3 Results

The experiment was conducted on 10 volunteer subjects with no known impairments in tactile sensory functions. The raw data and separated staircases from the experiments are shown in Figures 5.2–5.11.

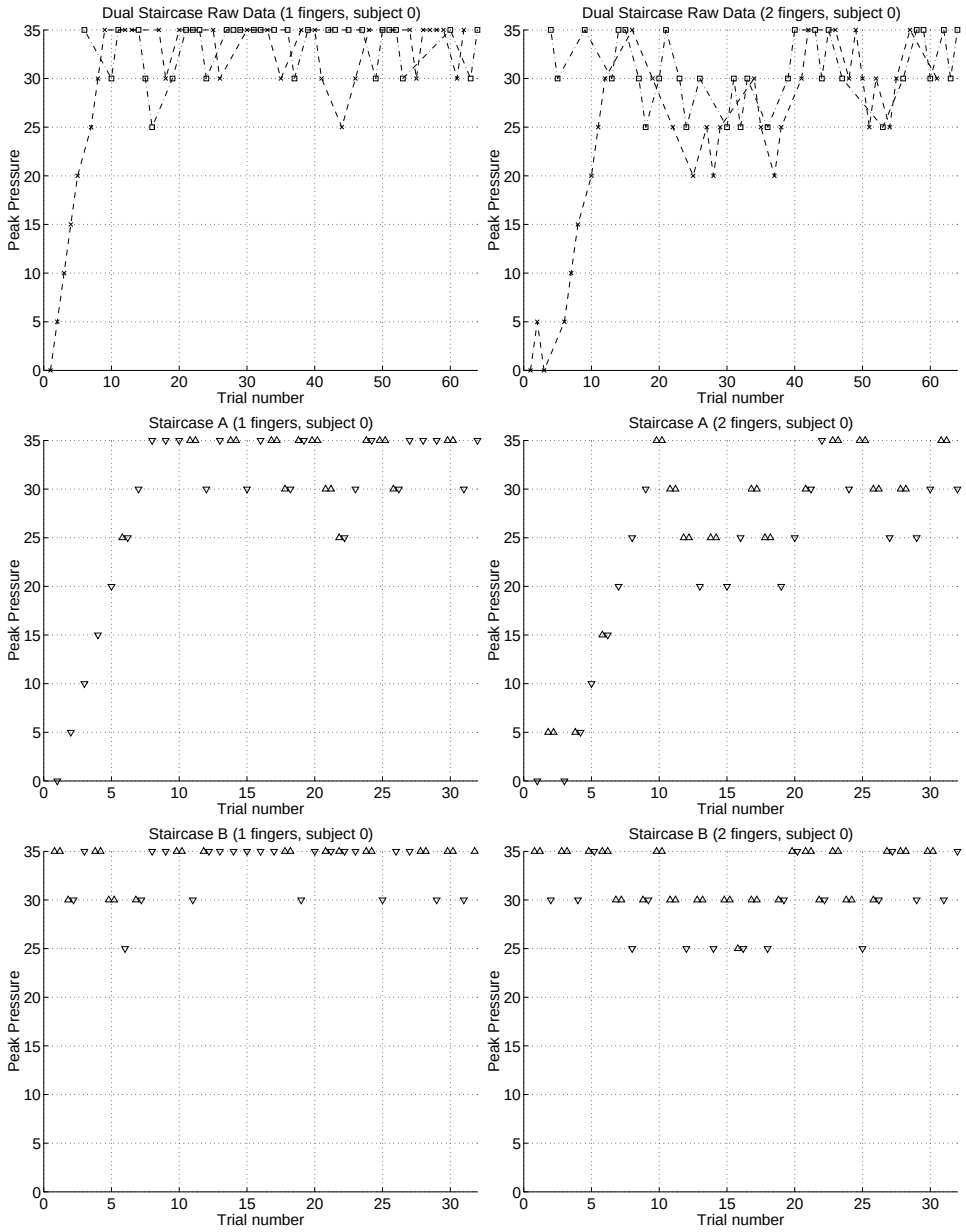

Figure 5.2: Raw data and separated staircases for subject 0.

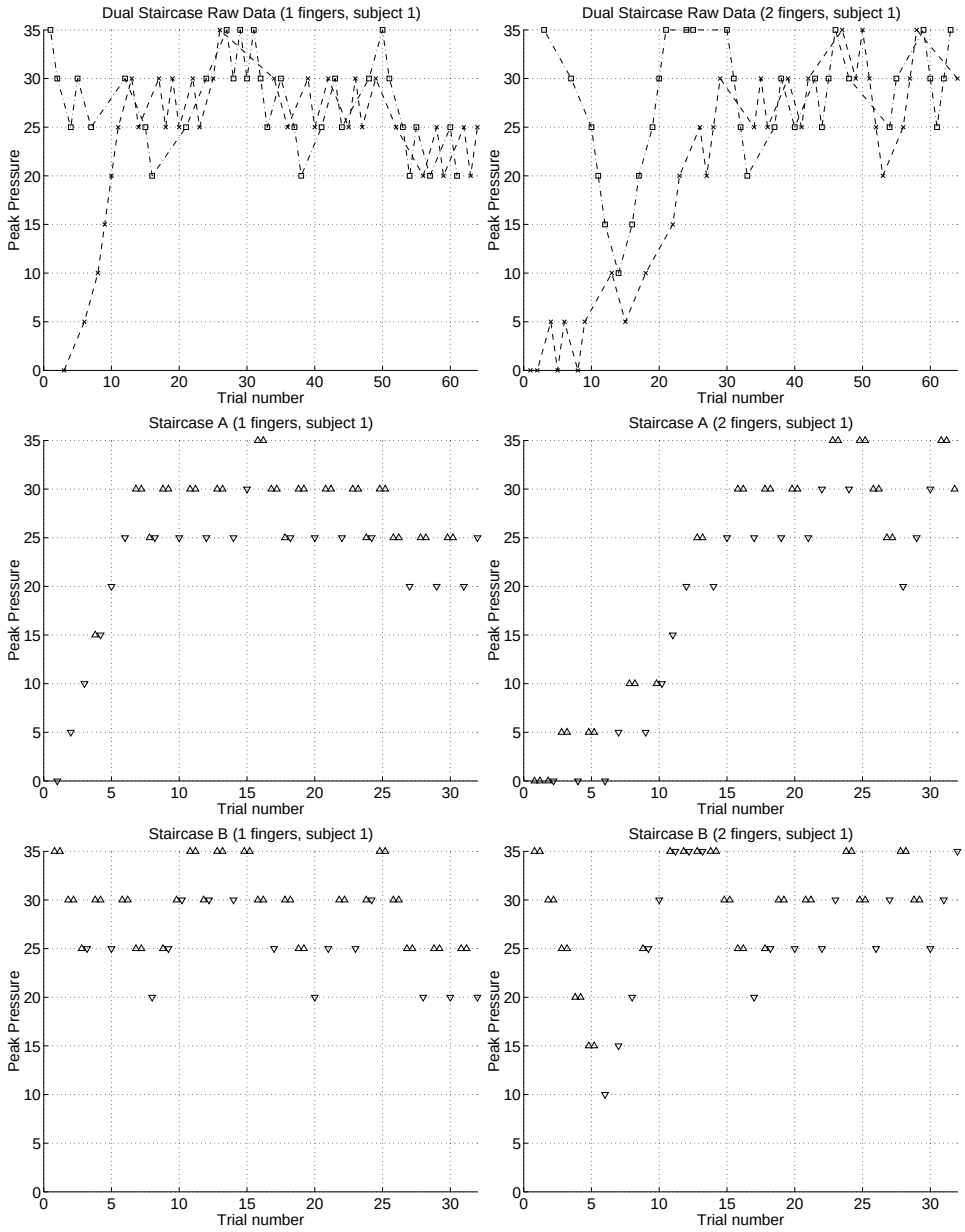

Figure 5.3: Raw data and separated staircases for subject 1.

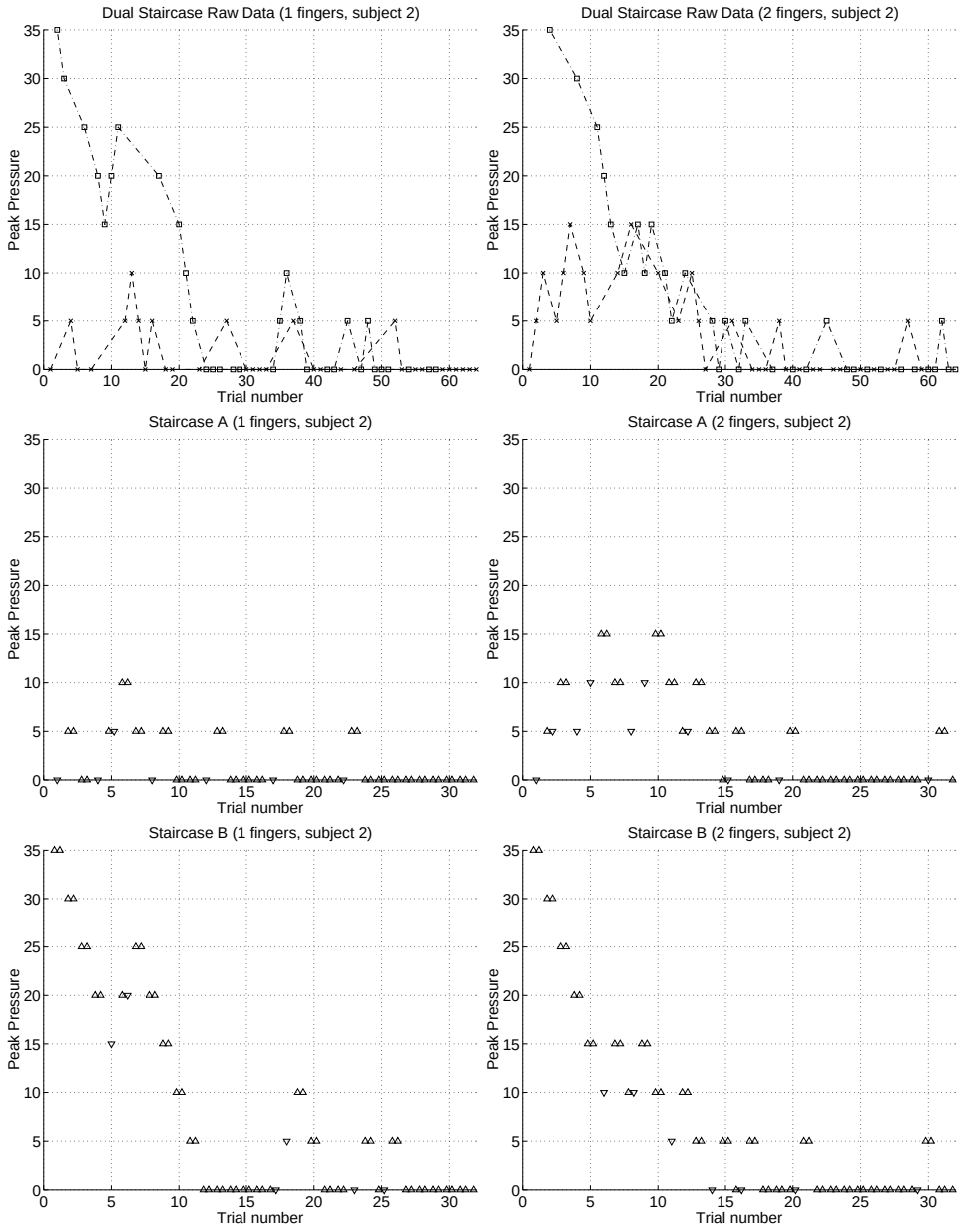

Figure 5.4: Raw data and separated staircases for subject 2.

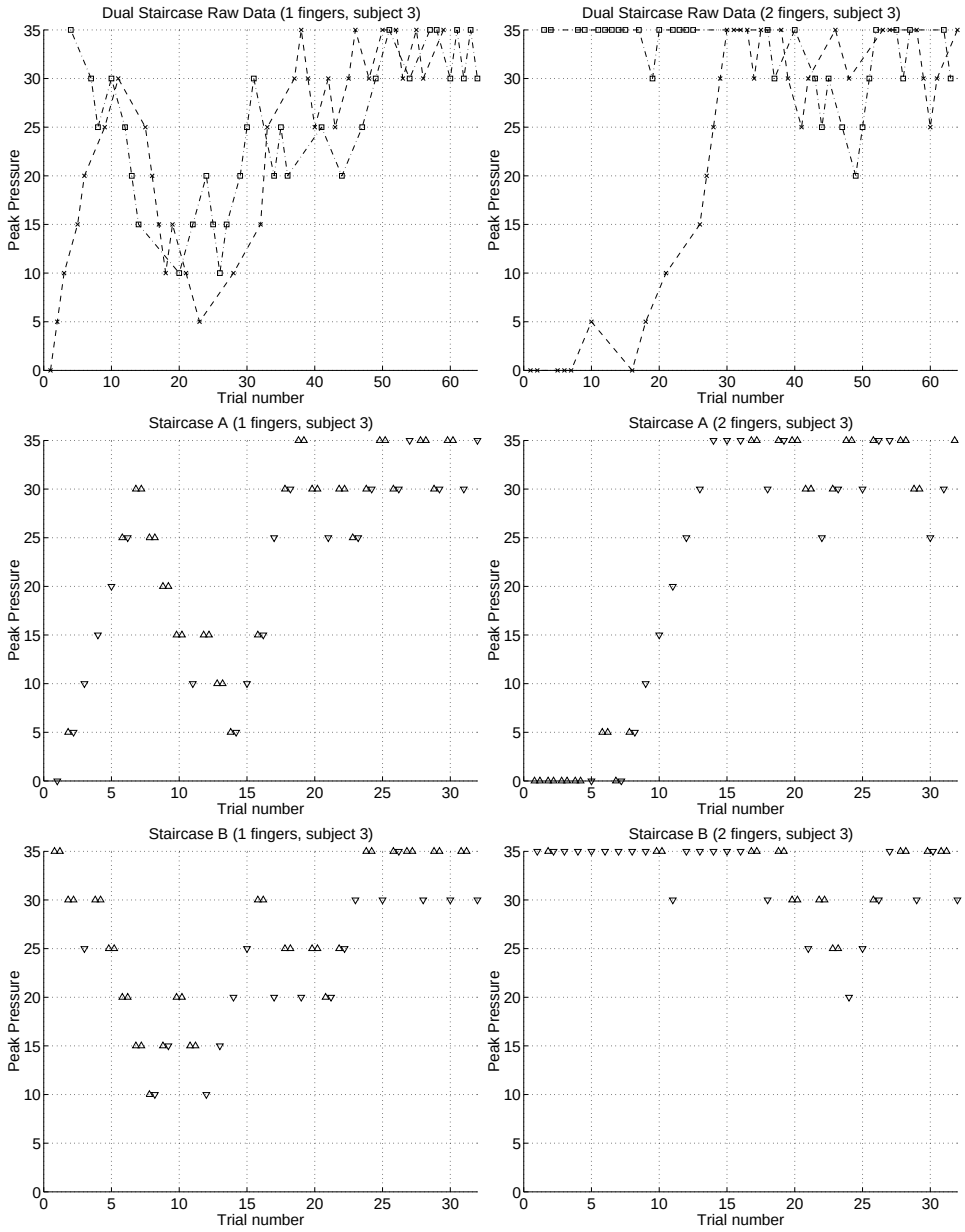

Figure 5.5: Raw data and separated staircases for subject 3.

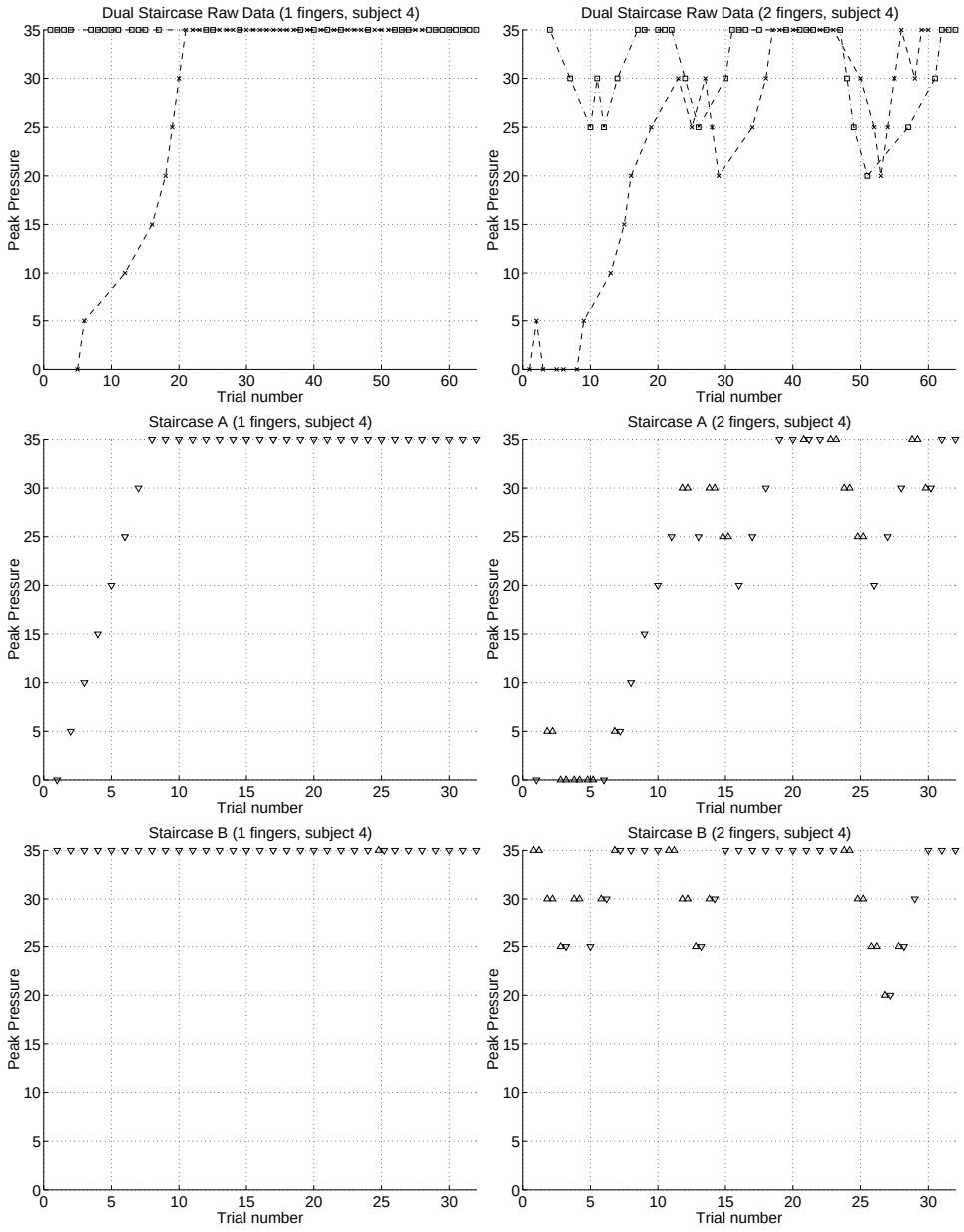

Figure 5.6: Raw data and separated staircases for subject 4.

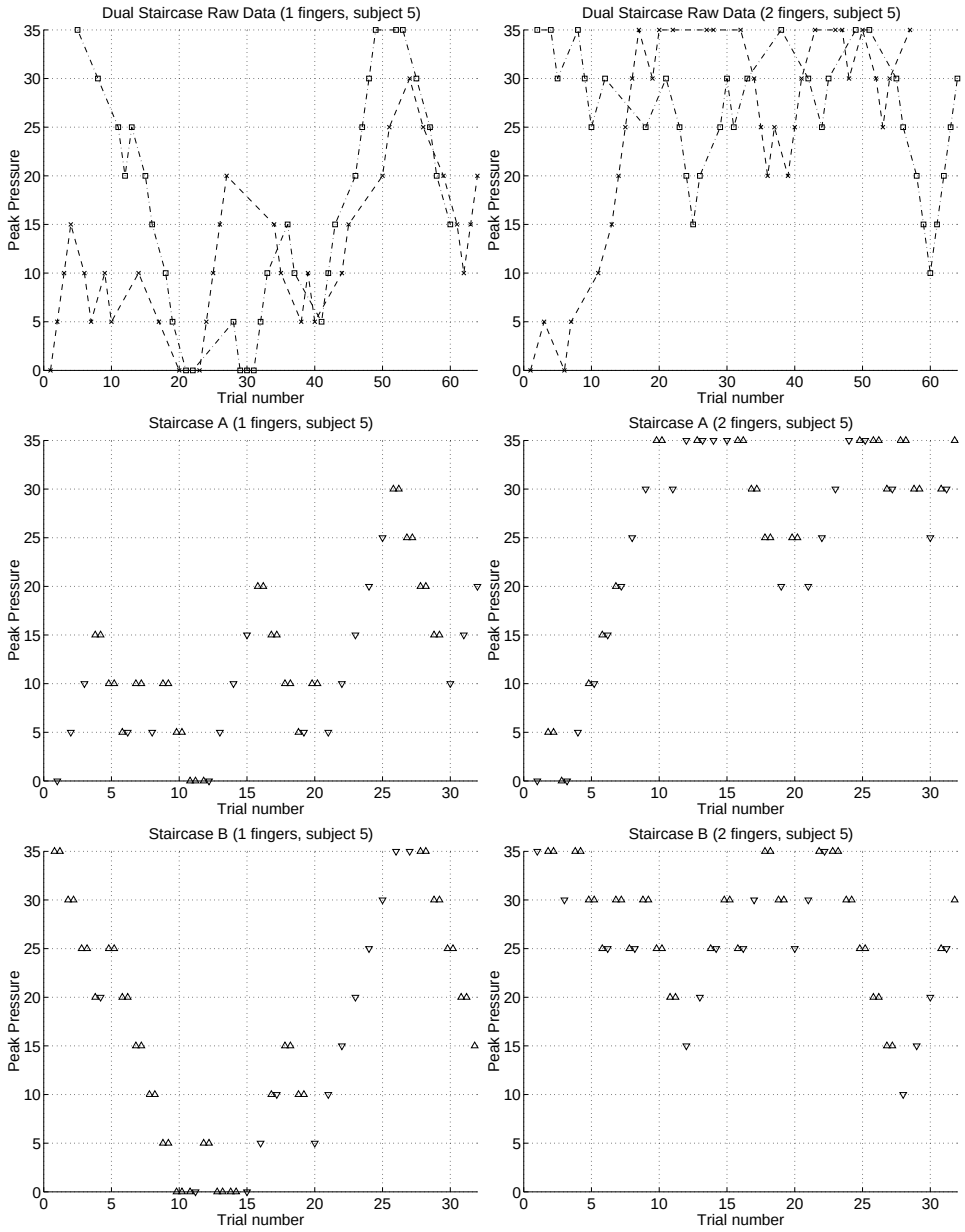

Figure 5.7: Raw data and separated staircases for subject 5.

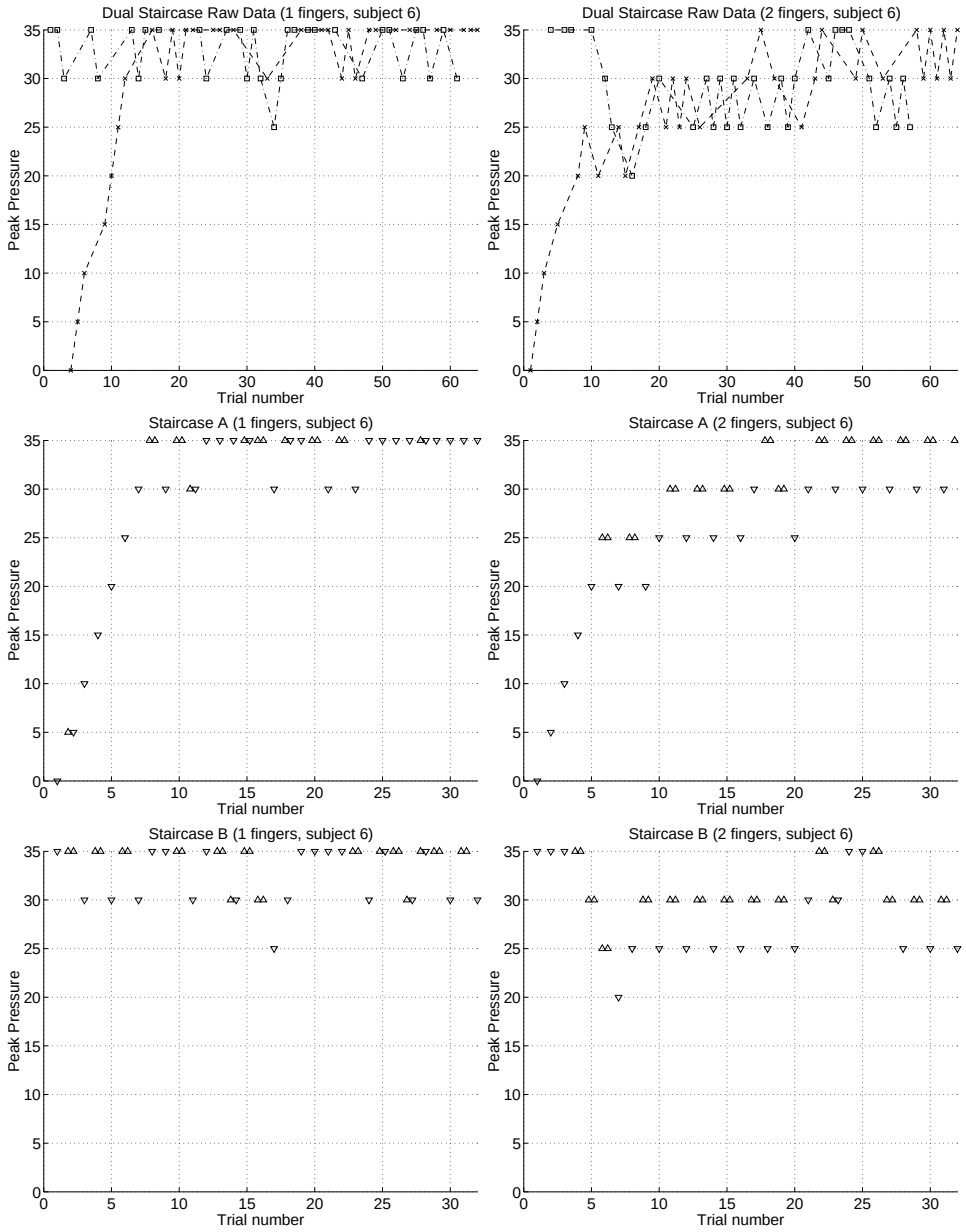

Figure 5.8: Raw data and separated staircases for subject 6.

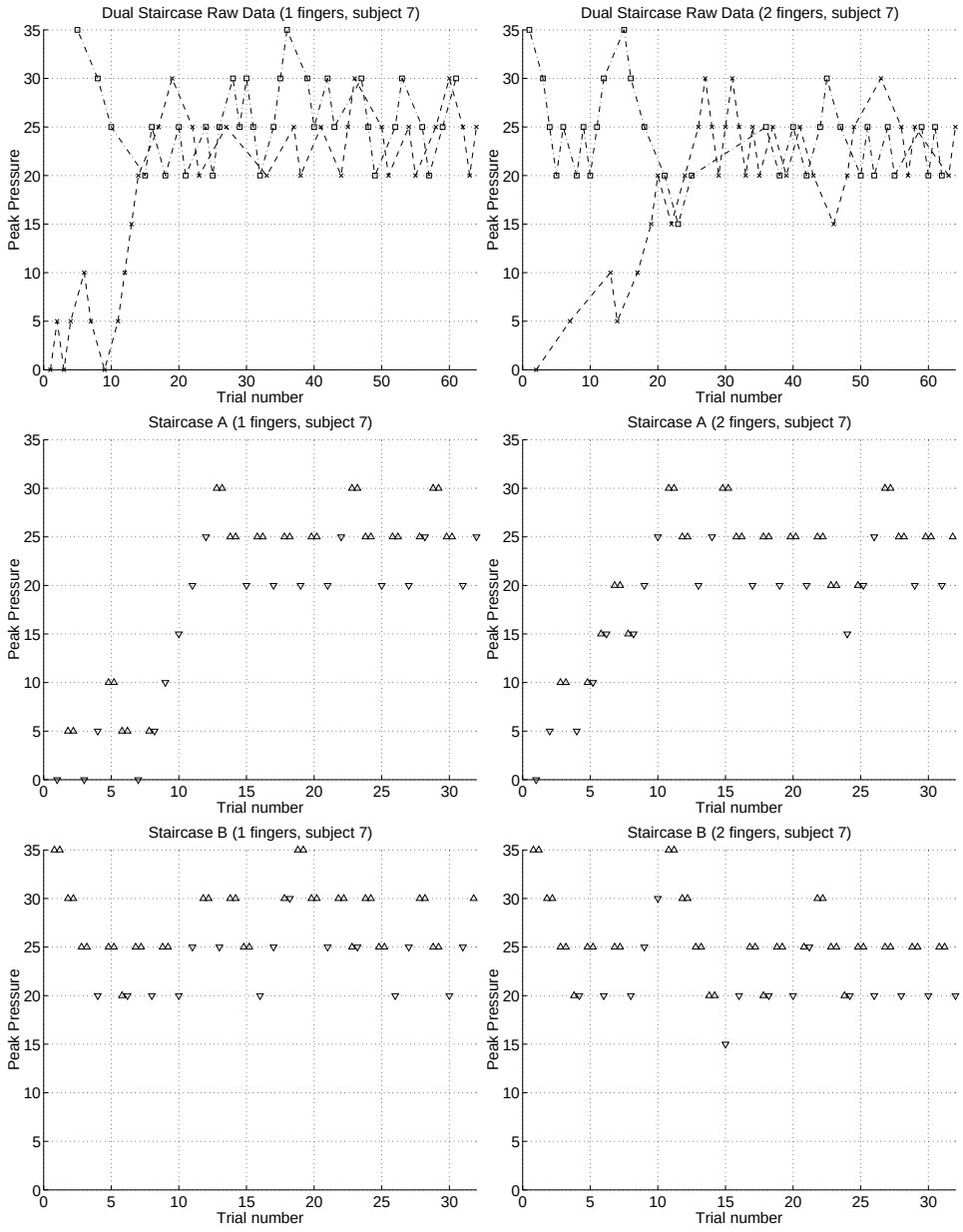

Figure 5.9: Raw data and separated staircases for subject 7.

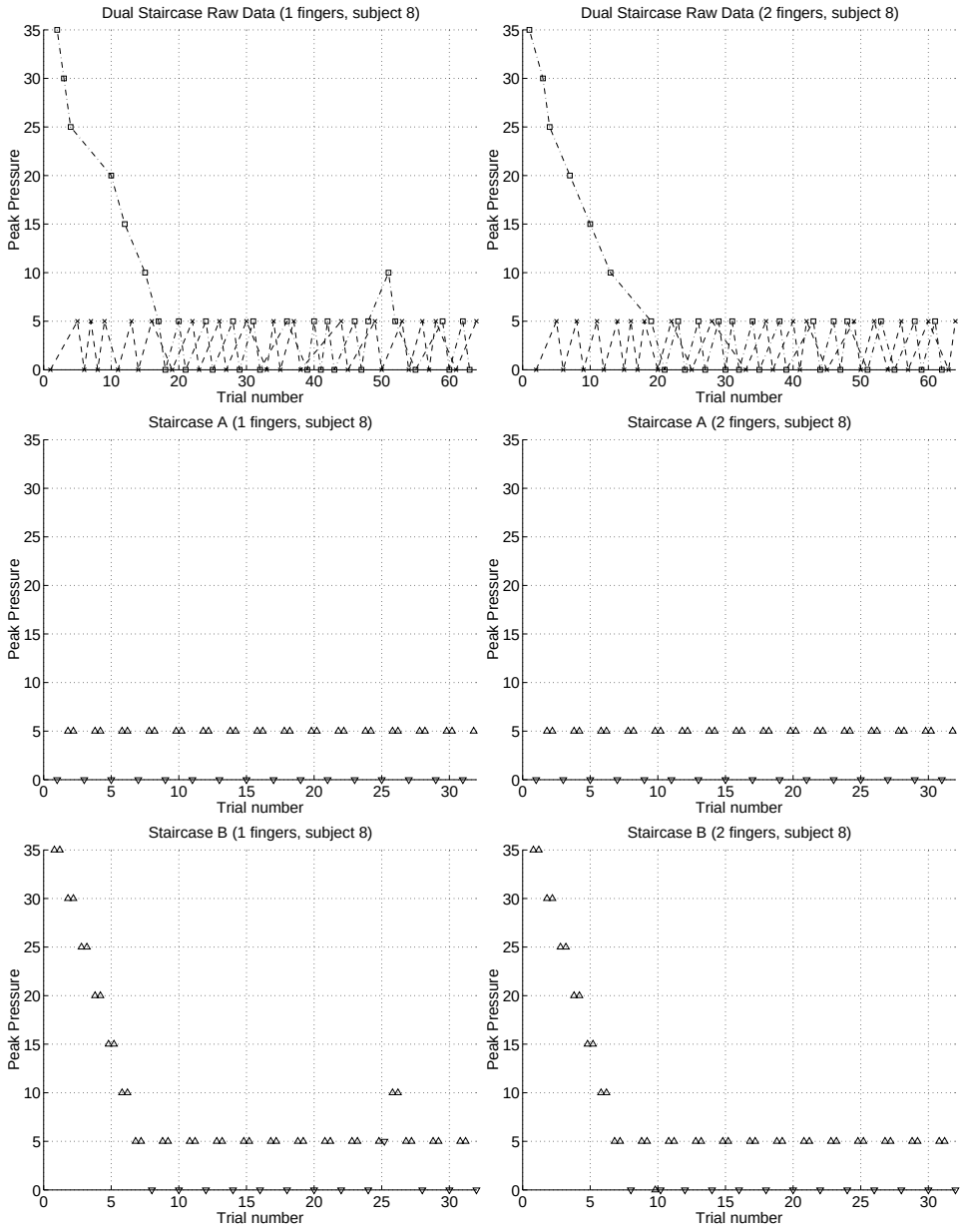

Figure 5.10: Raw data and separated staircases for subject 8.

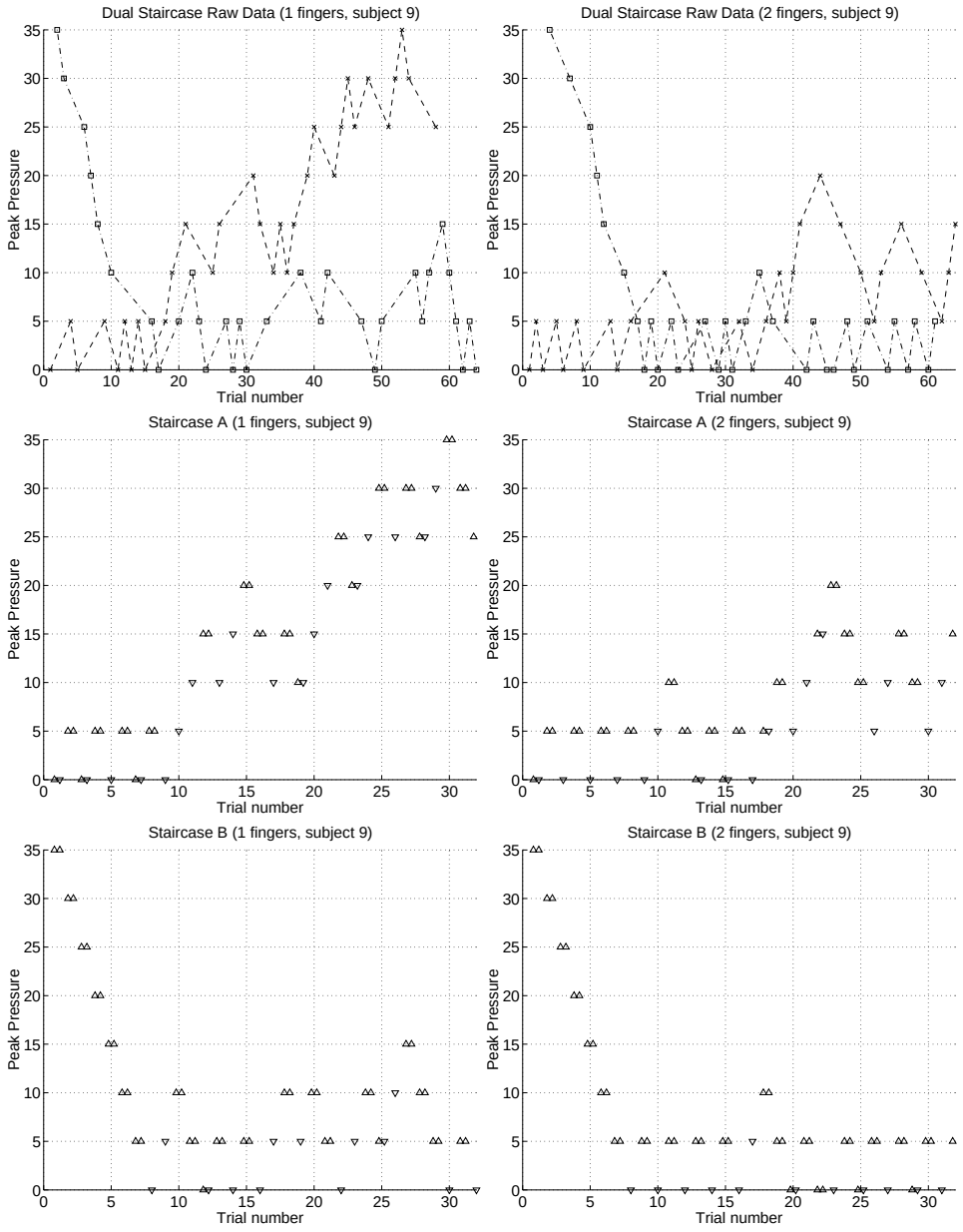

Figure 5.11: Raw data and separated staircases for subject 9.

Table 5.1 shows the raw data tabulated into the number of times each peak pressure received a "felt" or "not felt" response along with the means and standard deviations. The means and standard deviations were estimated following the procedure in [Dixon, 1948] and [Natrella, 1963]. The bold faced lines show which data is actually used for further analysis. We then calculate confidence intervals for each subject and across all subjects.

The mean and standard deviation calculation algorithm is as follows:

1. Count the number of total responses (R) and total non-responses (N-R), where N is the total number of trials. Use the set of data corresponding to the smaller of R and N-R.

2. Let $n_0, n_1, ..., n_k$ denote the frequency at each level where n_0 corresponds to the lowest level and n_k the highest level on which the event occurs.

3. Let $A = \sum i f_i$ and $B = \sum i^2 f_i$.

4. If $R < N - R$, then we count the responses and obtain estimated mean and standard deviation by:

$$m = y_0 + d(\frac{A}{R} - 0.5)$$
$$s = 1.62d\{\frac{RB - A^2}{R^2} + 0.029\}$$

5. If $N - R < R$, then we count the non-responses and obtain estimated mean and

Subject	Trial Type	Peak Pressure 0	5	10	15	20	25	30	35	# of trials	Mean m	Std. Dev. s
0	1 felt	0	0	0	0	0	0	2	13	**15**	**31.83**	**1.17**
	1 not felt	1	1	1	1	1	3	14	27	49	32.91	20.02
	2 felt	0	1	0	0	0	3	10	12	**26**	**28.27**	**12.50**
	2 not felt	2	1	1	1	4	11	13	5	38	27.50	24.96
1	1 felt	0	0	0	0	0	8	16	6	**30**	**27.17**	**3.98**
	1 not felt	1	1	1	1	9	16	5	0	34	24.85	14.16
	2 felt	1	2	1	1	1	4	11	7	**28**	**23.57**	**31.68**
	2 not felt	3	2	2	2	5	11	7	4	36	24.31	33.15
2	1 felt	31	10	3	1	2	2	1	1	51	2.40	23.90
	1 not felt	9	2	0	1	1	0	0	0	**13**	**5.96**	**13.18**
	2 felt	22	9	6	5	1	1	1	1	46	3.80	23.28
	2 not felt	9	5	4	0	0	0	0	0	**18**	**6.11**	**5.46**
3	1 felt	0	0	1	4	3	4	6	9	**27**	**24.35**	**20.12**
	1 not felt	1	2	5	4	5	7	10	3	37	24.12	28.28
	2 felt	4	1	0	0	0	1	4	10	**20**	**22.50**	**65.03**
	2 not felt	2	1	1	1	2	5	10	22	44	31.25	28.63
4	1 felt	0	0	0	0	0	0	0	0	**0**	**35.00**	**0.00**
	1 not felt	1	1	1	1	1	1	1	57	64	35.31	16.40
	2 felt	3	1	0	0	0	3	7	5	**19**	**21.97**	**50.45**
	2 not felt	2	1	1	1	4	8	6	22	45	30.50	29.18
5	1 felt	4	3	7	5	4	4	3	2	32	13.12	34.03
	1 not felt	4	8	6	5	4	2	1	2	32	15.16	30.60
	2 felt	0	1	0	1	2	4	9	9	**26**	**26.15**	**16.78**
	2 not felt	2	1	2	3	5	9	8	8	38	26.58	30.02
6	1 felt	0	0	0	0	0	0	1	15	**16**	**32.19**	**0.71**
	1 not felt	1	1	1	1	1	2	16	25	48	32.81	19.95
	2 felt	0	0	0	0	0	3	14	9	**26**	**28.65**	**3.54**
	2 not felt	1	1	1	1	4	15	9	6	38	27.89	19.58
7	1 felt	0	2	1	0	0	14	11	2	**30**	**23.17**	**16.29**
	1 not felt	3	2	1	1	15	11	1	0	34	21.32	20.27
	2 felt	0	0	1	0	3	19	6	2	**31**	**23.15**	**6.89**
	2 not felt	1	2	1	4	19	5	1	0	33	21.14	12.15
8	1 felt	0	28	2	1	1	1	1	1	35	5.64	18.33
	1 not felt	28	1	0	0	0	0	0	0	**29**	**2.67**	**0.50**
	2 felt	0	29	1	1	1	1	1	1	35	5.50	18.38
	2 not felt	29	0	0	0	0	0	0	0	**29**	**2.50**	**0.23**
9	1 felt	0	11	6	5	2	3	4	2	33	12.50	32.63
	1 not felt	12	6	5	2	2	3	1	0	**31**	**10.73**	**27.17**
	2 felt	1	18	6	4	2	1	1	1	34	7.50	20.25
	2 not felt	19	7	3	1	0	0	0	0	**30**	**5.17**	**5.49**

Table 5.1: Tabulated pulse detection data with mean and standard deviation.

standard deviation by:

$$m = y_0 + d(\frac{A}{(N-R)} + 0.5)$$
$$s = 1.62d\{\frac{(N-R)B - A^2}{(N-R)^2} + 0.029\}$$

We then continue by calculating confidence intervals for the data. Since we used a staircase method, the standard error of the mean is

$$\sigma_m = G\sigma/\sqrt{N}$$

where G is a factor between 0.9 and 1.25 dependent on the ratio d/σ. We read G off a figure in [Dixon, 1948]. Table 5.2 shows s_m the estimated standard deviations of the mean calculated from G, s, and N, the number of points in the small data set. The confidence interval for mean, m, is estimated by $m \pm ks_m$. For a 90% confidence interval, $k = 1.64$. Confidence intervals for each subject using monodigital and bidigital feedback are shown in Table 5.3.

We plot the results comparing 1 and 2 finger feedback with a 90% confidence intervals in Figure 5.12. For all subjects except subject 6, there is no statistically significant difference in having feedback with one or both fingers at the 90% confidence levels. Looking at the raw data, we see that subject 2 had lots of false positives and subject 4 missed a lot easily detectable stimuli. Subject 8 was exceptionally good and distinguished between the smallest peak pressure pulse and no pulse. We conclude that eight out of 10 subjects were able to detect the pulse at a 71% correctness level. The detectable peak pressure range across all subjects except subject 2 and 4

Subject	# of fingers	d/s	G	s	N	$Gs/\sqrt{N}$
0	1	4.27	1.25	1.17	15	0.38
	2	0.40	0.92	12.50	26	2.26
1	1	1.26	1.04	3.98	30	0.76
	2	0.16	0.90	31.68	28	5.39
2	1	0.38	0.91	13.18	13	3.33
	2	0.92	0.99	5.46	18	1.27
3	1	0.25	0.91	20.12	27	3.52
	2	0.08	0.90	65.03	20	13.09
4	1	Inf	1.25	0.00	0	0.00
	2	0.10	0.90	50.45	19	10.42
5	1	0.16	0.90	30.60	32	4.87
	2	0.30	0.91	16.78	26	3.00
6	1	7.05	1.25	0.71	16	0.22
	2	1.41	1.05	3.54	26	0.73
7	1	0.31	0.91	16.29	30	2.71
	2	0.73	0.96	6.89	31	1.19
8	1	9.91	1.25	0.50	29	0.12
	2	21.29	1.25	0.23	29	0.05
9	1	0.18	0.90	27.17	31	4.39
	2	0.91	0.99	5.49	30	0.99

Table 5.2: Adjusted standard deviations.

Subject	# of fingers	Mean m	Std. Dev. s_m	Confidence Interval 90% (k=1.64)
0	1	31.83	0.38	31.21 - 32.45
	2	28.27	2.26	24.57 - 31.97
1	1	27.17	0.76	25.93 - 28.41
	2	23.57	5.39	14.73 - 32.41
2	1	5.96	3.33	0.51 - 11.42
	2	6.11	1.27	4.02 - 8.20
3	1	24.35	3.52	18.57 - 30.13
	2	22.50	13.09	1.04 - 43.96
4	1	35.00	0.00	35.00 - 35.00
	2	21.97	10.42	4.89 - 39.06
5	1	15.16	4.87	7.17 - 23.14
	2	26.15	3.00	21.24 - 31.07
6	1	32.19	0.22	31.82 - 32.55
	2	28.65	0.73	27.46 - 29.85
7	1	23.17	2.71	18.73 - 27.61
	2	23.15	1.19	21.20 - 25.09
8	1	2.67	0.12	2.48 - 2.86
	2	2.50	0.05	2.41 - 2.59
9	1	10.73	4.39	3.52 - 17.93
	2	5.17	0.99	3.54 - 6.79

Table 5.3: 90% Confidence intervals for each subject.

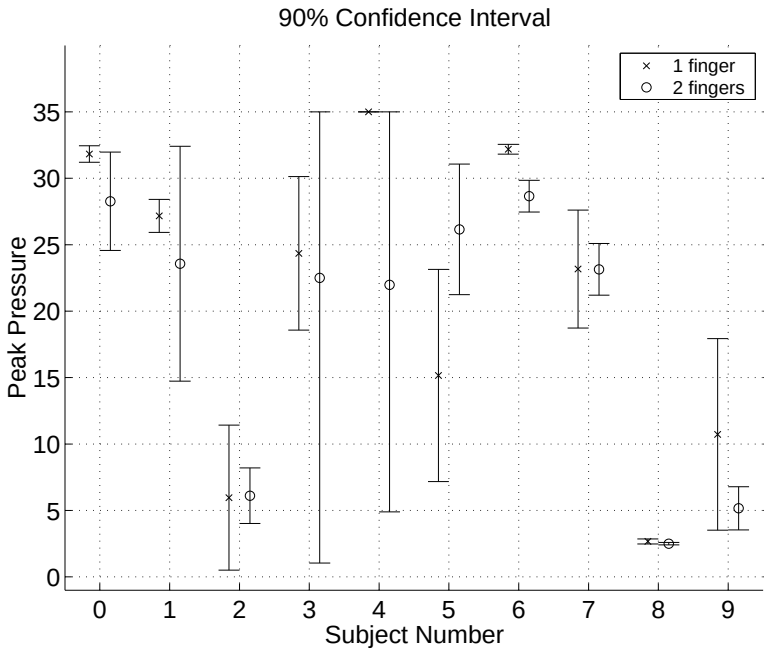

Figure 5.12: Comparing 1 and 2 finger results at a 90% confidence interval.

is 2.5 PSI to 32.2 PSI. With such a wide range of threshold pressures, it would be invalid to average the data across all subjects. Instead, we compare the difference in means across all subjects according to the following t-test algorithm [Natrella, 1963]:

Subject	$m_{1finger}$	$m_{2fingers}$	$m_d = m_{1finger} - m_{2fingers}$
0	31.83	28.27	3.56
1	27.17	23.57	3.60
2	5.96	6.11	-0.15
3	24.35	22.50	1.85
4	35.00	21.97	13.03
5	15.16	26.15	-10.99
6	32.19	28.65	3.54
7	23.17	23.15	0.02
8	2.67	2.50	0.17
9	10.73	5.17	5.56

1. Choose α to calculate the $100(1-\alpha)\%$ confidence interval. For a 90% confidence interval, $\alpha = 0.1$.

2. Calculate the mean, $\overline{m_d}$, and standard deviation, s_d, for the n differences, m_d. $\overline{m_d} = 2.02$ and $s_d = 5.98$.

3. Look up $t_{1-\alpha/2}$ for $n-1$ degrees of freedom in a t-distribution table. For 9 degrees of freedom, $t_{0.95} = 1.833$.

4. Compute $\mu = t_{1-\alpha/2}\frac{s_d}{\sqrt{n}} = 3.66$.

5. If $\|\overline{m_d}\| < \mu$, decide that the averages do not differ. In our case, $2.02 < 3.66$, so we conclude that there is no difference in detection pressure threshold between monodigital and bidigital feedback. The range $\overline{m_d} \pm \mu = -1.64$ to 5.68 is the

90% confidence interval estimate of the average difference in detection pressure thresholds.

Some subjects had very consistent results while other subjects had a very wide range of detection thresholds. Some subjects had a very low mean detection pressure threshold while other subjects had a medium to high mean detection pressure threshold. The large subject variation could be caused by differences in applied grasping force, valve PWM buzz artifact perception, and lack of training. Future experiments can include software to record and provide visual feedback about the grasping force to achieve less grasping force variation between subjects. Better valves will reduce PWM buzz artifacts which might be giving additional information that some subjects use as a detection criteria. Additional training with the apparatus will give subjects a better understanding of the stimulus they are trying to detect.

5.4 Direct touch comparison

In order to determine the bidigital teletaction system performance, we conducted direct touch experiments. Instead of using the bidigital teletaction system to grasp the stimulus, subjects grasped the stimulus with their thumb and middle finger while wearing a 2 mm thick HS II glove over each digit. The 2 mm glove corresponds to the combination of the tactile sensors' anti-aliasing layer and the tactile displays' reconstruction layer [Fearing, 1997].

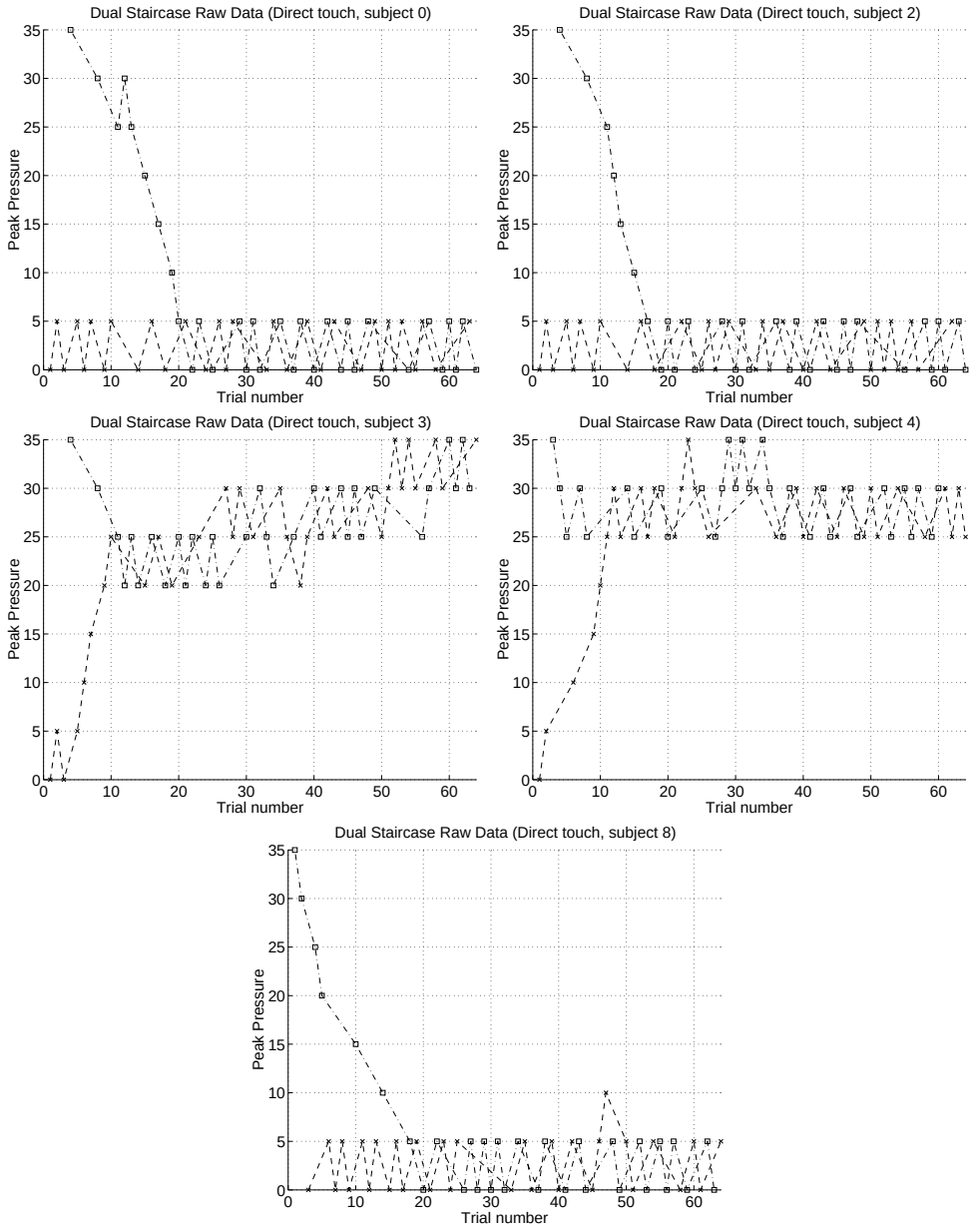

Figure 5.13: Raw data for direct touch experiments.

The experiment was conducted on 5 volunteer subjects who also participated in the bidigital teletaction experiments above. The raw data are shown in Figures 5.13.

Following the same procedure for data analysis, we obtained the means, standard deviations, and 90% confidence intervals for the 5 subjects. Results are shown in Tables 5.4, 5.5, and 5.6, and Figure 5.14. Taking each subject individually, with 90% confidence, subjects 0 and 2 did significantly better with direct touch while subjects 3, 4, and 8 did not do significantly better. Direct touch and bidigital teletaction are compared in Figure 5.15.

Subject	Trial Type	Peak Pressure								# of trials	Mean m	Std. Dev. s
		0	5	10	15	20	25	30	35			
0	felt	0	28	1	1	1	1	2	1	35	6.21	22.61
	not felt	28	0	0	0	0	1	0	0	**29**	**3.36**	**6.98**
2	felt	0	29	1	1	1	1	1	1	35	5.50	18.38
	not felt	29	0	0	0	0	0	0	0	**29**	**2.50**	**0.23**
3	felt	0	1	0	0	0	10	11	7	**29**	**26.12**	**11.35**
	not felt	2	1	1	1	11	12	7	0	35	24.21	19.19
4	felt	0	0	0	0	0	0	25	5	**30**	**28.33**	**1.36**
	not felt	1	1	1	1	1	25	4	0	34	25.88	13.44
8	felt	0	28	2	1	1	1	1	1	35	5.64	18.33
	not felt	28	1	0	0	0	0	0	0	**29**	**2.67**	**0.50**

Table 5.4: Tabulated direct touch pulse detection data with mean and standard deviation.

Subject	d/s	G	s	N	$Gs/\sqrt{N}$
0	0.72	0.95	6.98	29	1.23
2	21.29	1.25	0.23	29	0.05
3	0.44	0.92	11.35	29	1.94
4	3.68	1.20	1.36	30	0.30
8	9.91	1.25	0.50	29	0.12

Table 5.5: Adjusted standard deviations for direct touch pulse detection data.

Although two subjects showed significant improvement, one subject stayed at a

Subject	Mean m	Std. Dev. s_m	Confidence Interval 90% (k=1.64)
0	3.36	1.23	1.34 - 5.38
2	2.50	0.05	2.41 - 2.59
3	26.12	1.94	22.94 - 29.30
4	28.33	0.30	27.84 - 28.82
8	2.67	0.12	2.48 - 2.86

Table 5.6: 90% Confidence intervals for each subject's direct touch pulse detection data.

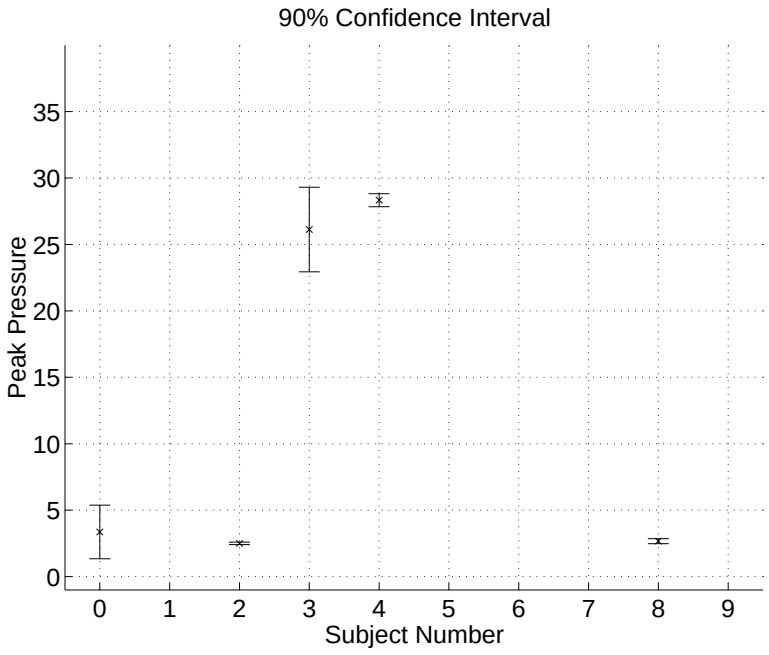

Figure 5.14: 90% confidence interval for direct touch.

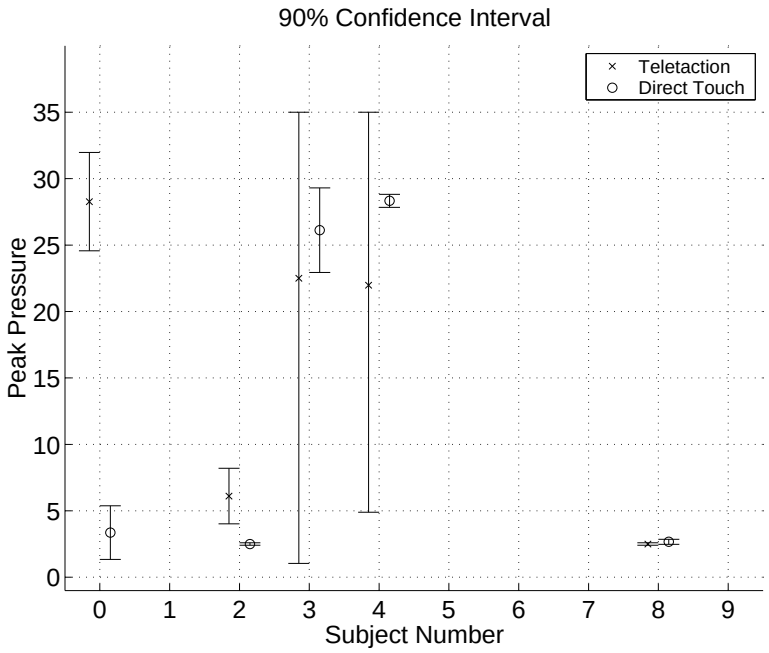

Figure 5.15: A 90% confidence interval comparison between direct touch and bidigital teletaction.

low detection pressure threshold, and two subjects showed no significant improvement, we can not say whether direct touch or the bidigital feedback would have lower pulse detection pressure thresholds. We conclude that the bidigital teletaction system is not quite as good as direct touch in pulsing blood vessel detection. This result is not surprising as the teletaction system does not have a spatial or temporal resolution as good as the mechanoreceptors.

5.5 Discussion

In this section, we discuss our hypotheses and the possible reasons for unexpected results. We expected that bidigital teletaction performance would be significantly better than monodigital performance. Results from this experiment show that there was not a significant difference between bidigital and monodigital teletaction (Figure 5.12). We expected that pulse pressure detection thresholds for bidigital teletaction and direct touch would be similar. With 90% confidence, the results show that there is no difference in pulse pressure detection thresholds between direct touch and bidigital teletaction in a majority of the subjects (Figure 5.15).

We now look into more detail about the possible reasons that bidigital teletaction performance was not significantly better than monodigital performance. We expected that bidigital teletaction would give better performance, by having a lower pulse detection threshold, for the following fundamental reason:

- There were twice the number of elements giving $\sqrt{2}$ more information.

The possible reasons that there was no significant difference are as follows:

1. There could have been spatial misalignments. A spatial misalignment occurs when the pulse grasped directly between the sensors is displayed onto the fingers as being offset from each other. The pulse could be misaligned on the axial and/or radial direction.

2. The extra information provided by the second finger was not enough to overcome

a 5 PSI difference between peak pressure steps.

3. There was a significant difference between thumb and middle finger sensitivity.

We now discuss each of the reasons:

1. The similarity of detectable pressure thresholds in direct touch and bidigital teletaction shows that possible spatial misalignment did not effect peak pressure thresholds.

2. With twice as many elements, we would expect some improvement. We believe that the noise in the valves overwhelms any advantage the extra information provides. The valves have a maximum of 10% PWM buzz with an average of 5.55 PSI peak-to-peak (or ±2.78 PSI) buzz and standard deviation of 1.30 PSI. To analyze the noise, we look at the SNR ratio of the tactile display using the maximum of 10% PWM buzz criteria. For a 20% PWM duty cycle, the output is an 7±0.7 PSI pressure. The SNR for the display is as follows:

$$SNR = 10log_{10}(\frac{7^2}{0.5 * 0.7^2}) = 23.0dB$$

For a 20 PSI peak pressure, we assume a 10% PWM buzz of ±2 PSI for an SNR of 23.0dB. Using an ideal case of having the same ±2 PSI of noise for a 25 PSI peak pressure, the SNR is 24.9dB. We use the assumption that the noise is the same because it falls into the average and standard deviation of the PWM buzz (Figure D.30) across all valves and PWM duty cycles, and we are comparing PWM duty cycles that are relatively close.

Having twice the data would provide a SNR of 24.5dB, which is slightly less than the SNR of a 5 PSI increase in peak pressure with the same amount of noise. So in theory, the additional information from the second finger is not enough to overcome a 5 PSI peak pressure difference. Additional experiments with more intermediate pressures and more subjects will give us a stronger statistical analysis to determine if bidigital teletaction is any better than monodigital teletaction.

3. We assumed, possibly incorrectly, that the thumb and middle finger have relatively similar sensitivities to pressure profiles. We have not found any reason to believe that the thumb's sensitivity would overwhelm any more information the middle finger provides. The fingers are probably more sensitive than the thumb since we instinctively feel textures with the fingers and not the thumb. Further experiments giving only feedback to the middle finger would determine if there is any sensitivity difference for this task. We do not believe that the sensitivity difference, if it exists, would be able to explain the lack of detection pressure threshold difference in pulse detection with monodigital and bidigital teletaction.

The conditions of our experiment are as follows:

1. Capacitive sensors collecting normal strain data in a 4×6 configuration with 2.7 mm interelement spacing with less than 0.5% noise, giving 7-8 bits of infor-

mation

2. Strain matching between tactile sensors and tactile displays, quantizing to 128 levels, giving a maximum of 7 bits of information

3. A maximum of 10% PWM buzz on the valves driving the tactile displays, giving a maximum of 3.3 bits of information

4. Pneumatically actuated compliant tactile displays with 14 elements in a 5-4-5 configuration and 2 *mm* interelement spacing

5. A mock blood vessel made of silicone tubing and silicone gel

6. Peak pressure waveforms in 5 PSI steps

7. Opposing sensors in a 1 degree of freedom grasping configuration

8. Uncontrolled and direct force feedback

In the calibration and design of the system, we find that the tactile sensors with 0.5% strain noise give 7-8 bits, the strain matching algorithm and quantization to 128 levels give a maximum of 7 bits, and the valve PWM buzz of 10% give a maximum of 3.3 bits. The teletaction system is most limited by the PWM buzz from the valves. Using less noisy valves would improve the system more than using better tactile sensors, strain matching algorithms, or tactile displays.

The addition of a second finger did not significantly improve detection pressure thresholds. The noise introduced by the PWM buzz overwhelmed any information

advantage the second finger added. The peak pressure steps of 5 PSI were too large to show any advantage the second finger added. With a smaller interval between steps, the SNR of the bidigital teletaction system at pressure level N would have been greater than the monodigitial teletaction system at pressure level $N + 1$.

The 5 PSI step size between peak pressures was chosen such that the dual staircase method would reach a threshold point in a reasonable number of trials. We see that the 5 PSI difference is more than the 90% confidence interval in 10 of the 20 teletaction cases (Figure 5.12), so for half the cases, a difference of 5 PSI in the stimulus was statistically significant. With more trials and smaller step sizes, the 90% confidence interval would get smaller and we would have a more accurate interval for the detectable peak pressure threshold. The lack of a statistically significant difference in the majority of the bidigital teletaction system and direct touch results verified that the correct contrast ratio was used. A 5 PSI difference in direct touch felt like a 5 PSI difference through the bidigital teletaction system.

Overall, the past two chapters show that a basic tactile display and teletaction system provides enough feedback to determine grating orientation and detect pulsing blood vessels, respectively. We show that the limiting factor of the system is the PWM buzz from the valves. Two ways to get around the PWM buzz is to sacrifice response time and use larger low pass filters (air chambers) or to use precise, accurate, and compact 2-way or 3-way valves. Unfortunately, these valves do not currently exist. While the tactile sensors and displays were sufficient for these experiments,

there is room for improvement. Tactile sensor element density and uniformity can be improved by more advanced construction techniques such as etching. Improvements to tactile display element density down to the sampling limit of twice the SA I density of $70/cm^2$ will provide more realistic tactile information. As predicted, the 2 mm spacing between tactile display elements was able to present tactile information of a grating with a 5 mm period. Even though the stimulus was only 2 mm wide, the anti-aliasing layer on the tactile sensor was thick enough so that the teletaction system was able to detect and transmit the tactile information.

Chapter 6

Conclusions

In this chapter, we discuss what we have accomplished, the limitations of our bidigital teletaction system, what improvements we want to pursue, and direct applications of our system.

6.1 Discussion

In this thesis, we designed and tested a molded tactile display and a bidigital teletaction system. One of the goals driving the design of the teletaction system was its portability. We would like to be able to move all the hardware around, plug it into any Windows based machine, and install the control software for demonstrations. We started the design process by considering all relevant sensing and actuation technologies. We chose capacitive sensing for its ease of construction, low cost, and scalability. We chose pneumatic actuation of closed chambers for its small actuator

size, no leakage or pin binding, ease of molding the tactile display, and low cost.

We started with a flat conformable display and moved on to a curved display when we obtained a 3D Systems ThermalJet wax printer. Using CAD software, Solidworks, and the ThermalJet, we designed and fabricated the necessary pieces for a sacrificial mold that was cheap and precise. The membrane thickness and display curvature was controlled precisely by the Solidworks model.

For the pneumatic actuators, we started with 3-way Clippard valves driven by a Xilinx board running at a PWM frequency of 81 Hz. We moved to 2-way Matrix valves driven by a Siemens board running at a PWM frequency of 150 Hz. The Matrix valves are smaller, quieter, and faster. We implemented a passive leak in the valve/display loop to compensate for using a 2-way valve. We tested the Matrix valves at 100 Hz, 200 Hz, and 300 Hz and determined that 150 Hz was a good tradeoff between response time, PWM buzz, and usable pressure range.

The human psychophysics experiments showed the basic fundamental parameters of spatial, amplitude, and temporal resolution for recording and displaying tactile feedback. Through grating detection tests, we showed that a 10% amplitude resolution difference was sufficient to present a simulated 5 mm period grating. The pulse detection experiment verifies that the sensor and display combination was capable of presenting time and amplitude varying signals. Tactile information was transmitted in both the one finger and two finger case. Neither case was shown to be statistically significantly better for this simple pulse detection task.

While we have used the basic test patterns of a grating and pulse, we need to test more practical applications such as scanning, orientation determination, and localization. For future experiments, the tactile sensors and displays of our bidigital teletaction system can be mounted on a force reflecting master-slave robot. The sensors and displays were designed to have low mass and low cost.

6.2 Future developments

The bidigital teletaction system we built was adequate for the simple experiments we ran. In the future, we would like to have 28 elements on each display. To do this, we will need to run two Siemens boards in parallel or find another microprocessor with more output pins as well as have another set of Matrix valves and associated electronics and pneumatics. With more elements, we will be able to run localization and orientation determination experiments. Further tactile display development should include increasing spatial resolution to 1 element/mm^2, adding feedback to ensure correct pressures in the chambers, and ease of connection the display to the valve array.

We ran the teletaction control software on a Pentium Pro 166 machine running Windows 95 via a DOS window. Software and hardware upgrades include moving from serial and parallel ports to USB ports for faster communication, and moving to a native Windows based control program. Software enhancements include contrast control, brightness control, feature extraction, and resolution magnification.

The ultimate goal is to integrate the bidigital teletaction onto a telesurgical robot and run tactile and force feedback experiments.

6.3 Applications

In this section, we discuss two applications which are directly applicable to the current bidigital teletaction system.

6.3.1 Minimally invasive surgery

By using a smaller tactile sensor and having the surgeon wear the tactile displays, we can add tactile feedback to minimally invasive procedures. One of the major deficiencies in minimally invasive surgery is the lack of tactile feedback. The addition of tactile feedback to an endoscope, a catheter, or a laparoscopic instrument will provide surgeons with more information about the surrounding tissue.

6.3.2 Functional MRI tests

Another application of the tactile display is in functional MRI tests. In these tests, MRI data are collected while a touch stimulus is applied somewhere to the subject. Since the stimulus needs to be uniform across all subjects, we need an automated and repeatable process. A key limitation of the stimulus generator is that it have no metallic pieces, as the strong magnetic fields generated by the MRI machine would

attract any metallic piece. Our tactile display design separates the actuators and contact interface by a series of silicone tubes. With sufficient length of tubing, the valve array can be located in another room.

Bibliography

[Asamura, 2001] N. Asamura, T. Shinohara, Y. Tojo, N. Koshida, and H. Shinoda, "Necessary spatial resolution for realistic tactile feeling display," *Proceedings of IEEE International Conference on Robotics and Automation*, vol. 2, Seoul, South Korea, 21-26 May 2001, pp. 1851-1856.

[Bach-y-Rita, 1998] P. Bach-y-Rita, K. A. Kaczmarek, M. E. Tyler and M. Garcia-Lara, "Form perception with a 49-point electrotactile stimulus array on the tongue: A technical note", *Journal of Rehabilitation Research and Development*, vol. 35, 1998, pp. 427-430.

[Beasley, 2002] R.A. Beasley and R.D. Howe, "Tactile tracking of arteries in robotics surgery," *Proceedings of IEEE International Conference on Robotics and Automation*, vol. 4, Washington, DC, 11-15 May 2002, pp. 3801-3806.

[Beebe, 1995] D.J. Beebe, C.M. Hymel, K.A. Kaczmarek, and M.E. Tyler, "A polyimide-on-silicon electrostatic fingertip tactile display," *1995 IEEE Engineer-*

ing in Medicine and Biology, vol.2, Montreal, Que., Canada, 20-23 September 1995, pp. 1545-1546.

[Biagiotti, 2002] L. Biagotti, M. Gavesi, C. Melchiorri, and B. Riccò, "A new stress sensor for force/torque measurements," *Proceedings of IEEE International Conference on Robotics and Automation*, vol. 2, Washington, DC, 11-15 May 2002, pp. 1655-1660.

[Bliss, 1969] J.C. Bliss, "A Relatively High-Resolution Reading Aid for the Blind", *IEEE Trans. on Man-Machine Sys.*, vol. 10, pp. 1-9, 1969.

[Caldwell, 1999] D.G. Caldwell, N. Tsagarakis, and C. Giesler, "An integrated tactile/shear feedback array for stimulation of finger mechanoreceptor," *Proceedings IEEE International Conference on Robotics and Automation*, vol. 1, Detroit, MI, 10-15 May 1999, pp. 287-292.

[Chiang, 2000] K.H. Chiang, "Limits on Microvalve Design", *UC Berkeley Doctoral Dissertation*, 2000.

[Cohn, 1992] M.B. Cohn, M. Lam, and R.S. Fearing, "Tactile feedback for teleoperation," *Proceedings of the SPIE - The International Society for Optical Engineering*, vol. 1833, Boston, MA, 15-16 November 1992, pp. 240-254.

[Cornsweet, 1962] T.N. Cornsweet, "The staircase method in psychophysics", *American Journal of Psychology*, vol. 75, 1962, pp. 485-491.

[Dargahi, 1999] J. Dargahi, S. Payandeh, and M. Parameswaran, "A micromachined piezoelectric teeth-like laparoscopic tactile sensor: theory, fabrication and experiments," *Proceedings of IEEE International Conference on Robotics and Automation*, vol. 1, Detroit, MI, 10-15 May 1999, pp. 299-304.

[Debus, 2002] T. Debus, T. Jang, P. Dupont, and R.D. Howe, "Multi-channel vibrotactile display for teleoperated assembly," *Proceedings of IEEE International Conference on Robotics and Automation*, vol. 1, Washington, DC, 11-15 May 2002, pp. 592-597.

[Dellon, 1995] E.S. Dellon, K. Keller, V. Moratz, and A.L. Dellon, "The relationships between skin hardness, pressure perception and two-point discrimination in the fingertip," *The Journal of Hand Surgery*, vol. 20B, no. 1, February 1995, pp. 44-48.

[Dixon, 1948] W.J. Dixon and A.M. Mood, "A Method for Obtaining and Analyzing Sensitivity Data", *Journal of American Statistical Association*, vol. 43, no. 241, March 1948, pp. 109-126.

[Domenici, 1992] C. Domenici and D. DeRossi, "A Stress-component-selective tactile sensor array", *Sensors and Actuators A*, vol. 13, pp. 97-100, 1992.

[Ellis, 1992] R.E. Ellis and M. Qin, "Singular Value and Finite-Element Analysis of Tactile Shape Recognition", *IEEE Int. Conf. on Robotics and Automation*, vol. 3, pp. 2529-2535, San Diego, CA, May 8-13, 1994.

[Fearing, 1985] R.S. Fearing and J.M. Hollerbach, "Basic solid mechanics for tactile sensing," *International Journal of Robotics Research*, Fall 1985, vol.4, no. 3, pp. 40-54.

[Fearing, 1990] R.S. Fearing, "Tactile sensing mechanisms," *International Journal of Robotics Research*, June 1990, vol.9, no. 3, pp. 3-23.

[Fearing, 1997] R.S. Fearing, G. Moy, and E. Tan, "Some basic issues in teletaction," *Proceedings of IEEE International Conference on Robotics and Automation*, vol. 4, Albuquerque, NM, 20-25 April 1997, pp. 3093-3099.

[Fischer, 1995] H. Fischer, B. Neisius, and R. Trapp, "Tactile Feedback for Endoscopic Surgery" in *Interactive Technology and New Paradigm for Healthcare*, edited by K. Morgan, R. M. Satava, H. B. Sieburg, R. Mattheus, J. P. Christensen, pp. 114-117, IOS Press 1995.

[Frisken-Gibson, 1987] S.F. Frisken-Gibson, P. Bach-y-Rita, W.J. Tompkins, and J.G. Webster, "A 64-solenoid, four-level fingertip search display for the blind," *IEEE Transactions on Biomedical Engineering*, vol. BME-34, no. 12, December 1987, pp. 963-965.

[Gemperle, 2001] F. Gemperle, N. Ota, and D. Siewiorek, "Design of a wearable tactile display," *Proceedings Fifth International Symposium on Wearable Computers*, Zurich, Switzerland, 8-9 October 2001, pp. 5-12.

[Gray, 1996] B.L. Gray and R.S. Fearing, "A surface-micromachined microtactile sensor array," *Proceedings of IEEE International Conference on Robotics and Automation*, vol. 1, Minneapolis, MN, 22-28 April 1996, pp. 1-6.

[Hagner, 1988] D.G. Hagner and J.G. Webster, "Telepresence for Touch and Proprioception in Teleoperator Systems", *IEEE Trans. on Systems, Man, and Cybernetics*, vol. 18, no. 6, pp. 1020-1023, November/December 1988.

[Hakozaki, 2002] M. Hakozaki and H. Shinoda, "Digital tactile sensing elements communicating through conductive skin layers," *Proceedings of IEEE International Conference on Robotics and Automation*, vol. 4, Washington, DC, 11-15 May 2002, pp. 3813-3817.

[Hardwick, 1998] A. Hardwick, S. Furner, and J. Rush, "Tactile display of virtual reality from the World Wide Web-a potential access method for blind people," *Displays*, vol. 18, no. 3, 15 May 1998, pp. 153-161.

[Hasser, 1996] C. J. Hasser and M. W. Daniels, "Tactile Feedback with Adaptive Controller for a Force-Reflecting Haptic Display", *15th Southern Biomedical Engineering Conf.*, pp. 526-533, Dayton, OH, March 29-31, 1996.

[Howe, 1994] R.D. Howe, "Tactile Sensing and control of robotic manipulation", Advanced Robotics, vol. 8, no. 3, 1994, pp. 245-261.

[Howe, 1995] R.D. Howe, W.J. Peine, D.A. Kantarinis, and J.S. Son, "Remote pal-

pation technology," IEEE Engineering in Medicine and Biology Magazine, vol. 14, no. 3, May-June 1995, pp. 318-323.

[Johansson, 1982a] Johansson, R. S., Landström, U., and Lundström, R., "Responses of Mechanoreceptive Afferent Units in the Glabrous Skin of the Human Hand to Sinusoidal Displacements", *Brain Research*, vol. 244, 1982, pp. 17-25.

[Johansson, 1982b] Johansson, R. S., Landström, U., and Lundström, R., "Sensitivity to edges of mechanoreceptive afferent units innervating the glabrous skin of the human hand," *Brain Research*, vol. 244, 1982, pp. 27-32.

[Johansson, 1983] R.S. Johansson and R.H. Lamotte, "Tactile Detection thresholds for a single asperity on an otherwise smooth surface", *Somatosensory Research*, vol. 1, no 1, 1983, pp. 21-31.

[Johnson, 1981a] K.O. Johnson and J.R. Phillips, "Tactile spatial resolution I. Two point discrimination, gap detection, grating resolution, and letter recognition", *J. Neurophysiology*, vol. 46, no. 6, 1981, pp. 1177-1191.

[Kaczmarek, 1991] K.A. Kaczmarek, J.G. Webster, P. Bach-y-Rita, and W.J. Tompkins, "Electrotactile and vibrotactile displays for sensory substitution systems," *IEEE Transactions on Biomedical Engineering*, vol. 38, no. 1, January 1991, pp. 1-16.

[Kajimoto, 2001] H. Kajimoto, N. Kawakami, T. Maeda, and S. Tachi, "Electrocu-

taneous display as an interface to a virtual tactile world," *Proceedings IEEE Virtual Reality 2001*, Yokohama, Japan, 13-17 March 2001, pp. 289-290.

[Kontarinis, 1995] D.A. Kontarinis, J.S. Son, W. Peine, and R.D. Howe, "A tactile shape sensing and display system for teleoperated manipulation," *Proceedings of IEEE International Conference on Robotics and Automation*, vol. 1, Nagoya, Japan, 21-27 May 1995, pp. 641-646.

[Konyo, 2000] M. Konyo, S. Tadokoro, and T. Takamori, "Artificial tactile feel display using soft gel actuators," *Proceedings of IEEE International Conference on Robotics and Automation*, vol. 4, San Francisco, CA, 24-28 April 2000, pp. 3416-3421.

[Kowalik, 1994] R. Kowalik and I. Postawka, "The concept of a full screen tactile display (FSTD) driven by electrochemical reactions," *Proceedings of 4th International Conference, Computers for Handicapped Persons*, Vienna, Austria, 14-16 September 1994, pp. 455-460.

[Lederman, 1978] S.J. Lederman, "Heightening tactile impressions of surface texture," *Active Touch*, ed. G. Gordon. Oxford: Pergamon Press, 1978, pp. 205-214.

[Lederman, 1999] S.J. Lederman and R.L. Klatzky, "Sensing and displaying spatially distributed fingertip forces in haptic interfaces for teleoperator and virtual environment systems," *Presence: Teleoperators and Virtual Environments*, vol. 8, no. 1, February 1999, pp. 86-103.

[Lee, 2000] M. Lee, "Tactile Sensing: New Directions, New Challenges," *The International Journal of Robotics Research*, vol. 19, no. 7, July 2000, pp. 636-643.

[Levitt, 1970] H. Levitt, "Transformed up-down methods in psychoacoustics", *Journal of the Acoustical Society of America*, vol. 49, no. 2, 1970, pp. 467-477.

[Loomis, 1986] J.M. Loomis and S.J. Lederman, "Tactual Perception", in *Handbook of Perception and Human Performance*, edited by K.R. Boff, L. Kaufman and J.P. Thomas, pp. 31-1:31-41, John Wiley and Sons: New York, 1986.

[Maeno, 1998a] T. Maeno, T. Kawai, and K. Kobayashi, "Analysis and design of a tactile sensor detecting strain distribution inside an elastic finger," *Proceedings of IEEE/RSJ International Conference on Intelligent Robots and Systems*, vol. 3, Victoria, BC, Canada, 13-17 October 1998, pp. 1658-63.

[Maeno, 1998b] T. Maeno and K. Kobayashi, "FE Analysis of the Dynamic Characteristics of the Human Finger Pad in Contact with Objects with/without Surface Roughness," *Proceedings of the ASME Dynamic Systems and Control Division*, Anaheim, CA, 15-20 November 1998, pp. 279-286.

[Maeno, 1998c] T. Maeno, K. Kobayashi, and N. Yamazaki, "Relationship between the structure of human finger tissue and the location of tactile receptors," *JSME International Journal, Series C*, vol. 41, no. 1, March 1998, pp. 94-100.

[Moy, 2000] G. Moy, C. Wagner, and R.S. Fearing, "A compliant tactile display for

teletaction," *Proceedings of IEEE International Conference on Robotics and Automation*, vol. 4, San Francisco, CA, 24-28 April 2000, pp. 3409-3415.

[Murray, 1998] A.M. Murray, R.L. Klatzky, and P.K. Khosla, "Enhancing subjective sensitivity to vibrotactile stimuli," *Proceedings of the ASME Dynamic Systems and Control Division*, Anaheim, CA, 15-20 November 1998, pp. 157-162.

[Natrella, 1963] M.G. Natrella, *Experimental Statistics*, Department of Commerce, National Bureau of Standards, 1963.

[Nicolson, 1993] E.J. Nicolson and R.S. Fearing, "Sensing Capabilities of Linear Elastic Cylindrical Fingers", *IEEE/RSJ Int. Conf. on Intelligent Robots and Systems*, vol. 1, pp. 178-85, Yokohama, Japan, July 1993.

[Ostrom, 1999] N.P. Ostrom, K.A. Kaczmarek, and D.J. Beebe, "A microfabricated electrocutaneous tactile display," *Proceedings of the First Joint BMES/EMBS Conference*, vol. 2, Atlanta, GA, 13-16 October 1999, p. 838.

[Pawluk, 1998] D.T.V. Pawluk, C.P. van Buskirk, J.H. Killebrew, S.S. Hsiao, and K.O. Johnson, "Control and pattern specification for a high density tactile array," *Proceedings of the ASME Dynamic Systems and Control Division*, Anaheim, CA, 15-20 November 1998, pp. 97-102.

[Phillips, 1981b] J.R. Phillips and K.O. Johnson, "Tactile spatial resolution II. Neural

representation of bars, edges, and gratings in monkey primary affarents," *J. Neurophysiology*, vol. 46, no. 6, 1981, pp. 1192-1203.

[Phillips, 1981c] J.R. Phillips and K.O. Johnson, "Tactile spatial resolution III. A continuum mechanics model of skin predicting mechanoreceptor reponses to bars, edges, and gratings," *J. Neurophysiology*, vol. 46, no. 6, 1981, pp. 1204-1225.

[PWV Medical, 1999] "Sphygmocor: Non-invasive aortic blood pressure pulse wave analysis," Retrieved from http://www.pwvmedical.com/pdf/pr-004-1099.pdf

[Serina, 1997] E.R. Serina, C.D. Mote Jr., and D. Rempel, "Force response of the fingertip pulp to repeated compression-effects of loading rate, loading angle and anthropometry", *J. Biomechanics*, vol.30, (no.10), pp. 1035-40, Oct. 1997.

[Shimoga, 1992] K.B. Shimoga, "Finger Force and Touch Feedback Issues in Dextrous Telemanipulation", *NASA-CIRSSE Int. Conf. on Intelligent Robotic Systems for Space Exploration*, Troy, NY, September 30 - October 1, 1992.

[Shimojo, 1999] M. Shimojo, M. Shinohara, and Y. Fukui, "Human Shape Recognition Performance for 3D Tactile Display," *IEEE Transactions on Systems, Man & Cybernetics, Part A (Systems & Humans)*, vol. 29, no. 6, Nov. 1999, pp. 637-644.

[Srinivasan, 1987] M.A. Srinivasan and R.H. Lamotte, "Tactile discrimination of

shape: responses of slowly and rapidly adapting mechanoreceptive aferents to a step indented into the monkey finger pad", *The Jnl. of Neuroscience*, vol. 7, no. 6, June 1987, pp. 1682-1697.

[Srinivasan, 1996] M.A. Srinivasan and K. Dandekar, " An investigation of the mechanics of tactile sense using two-dimensional models of the primate fingertip," *Transactions of the ASME. Journal of Biomechanical Engineering*, vol. 118, no. 1, February 1996, pp. 48-55.

[Taylor, 1998a] P.M. Taylor, D.M. Pollet, A. Hosseini-Sianaki, and C.J. Varley, "Advances in an electrorheological fluid based tactile array," *Displays*, vol. 18, no. 3, 15 May 1998, pp. 135-141.

[Taylor, 1998b] P.M. Taylor, A. Moser, and A. Creed, "A sixty-four element tactile display using shape memory alloy wires," *Displays*, vol. 18, no. 3, 15 May 1998, pp. 163-168.

[Tendick, 1993] "Sensing and Manipulation Problems in Endoscopic Surgery: Experiment, Analysis, and Observation", *Presence*, vol. 2, no. 1, Winter 1993, pp. 66-81.

[Valbo, 1979] A.B. Valbo and R.S. Johansson, "Detection of Tactile Stimuli. Thresholds of Afferent Units related to psychophysical thresholds in the human hand", *J. Physiology*, vol. 297, pp. 405-422, 1979.

[VanBoven, 1994] R.B. VanBoven and K.O. Johnson, "The limit of tactile spatial resolution in humans: Grating orientation discrimination at the lip, tongue, and finger," *Neurology*, vol. 44, December 1994, pp. 2361-2366.

[VanDoren, 1987] C.L. VanDoren, D.G. Pelli, R.T. Verrillo "A device for measureing tactile spatiotemporal sensitivity," *Journal of the Acoustical Society of America*, vol. 81, no. 6, June 1987, pp. 1906-1916.

[Wagner, 2002] C.R. Wagner, S.J. Lederman, and R.D. Howe, "A tactile shape display using RC servomotors," *Proceedings 10th Symposium on Haptic Interfaces for Virtual Environment and Teleoperator Systems. HAPTICS 2002*, Orlando, FL, USA, 24-25 March 2002, pp. 354-355.

[Way, 1997a] T.P. Way and K.E. Barner, "Automatic visual to tactile translation - Part I: Human factors, access methods, and image manipulation," *IEEE Transactions on Rehabilitation Engineering*, vol. 5, no. 1 March 1997, pp. 81-94.

[Way, 1997b] T.P. Way and K.E. Barner, "Automatic visual to tactile translation - Part II: Evaluation of the TACTile image creation system," *IEEE Transactions on Rehabilitation Engineering*, vol. 5, no. 1 March 1997, pp. 95-105.

[Weisenberger, 1998] J.M. Weisenberger, M.J. Krier, and M.A. Rinker, "Resolution of Virtual Grating Orientation with 2-DOF and 3-DOF Force Feedback Systems", *IMECE Proc. of the ASME Dyn. Sys. and Control Div.*, vol. 64, pp. 295-301, Anaheim, CA, November 1998.

[Wellman, 1997] P.S. Wellman, W.J. Peine, G. Favalora, and R.D. Howe, "Mechanical design and control of a high-bandwidth shape memory alloy tactile display," *Experimental Robotics V. The Fifth International Symposium*, Barcelona, Spain, 15-18 June 1997, pp. 56-66.

[Wellman, 1999] P.S. Wellman, R.D. Howe, N. Dewagan, M.A. Cundari, and others, "Tactile imaging: a method for documenting breast masses", *Proceedings of the First Joint BMES/EMBS Conference*, vol. 2, p. 1131, Atlanta, GA, October 13-16, 1999.

[Westling, 1987] G. Westling and R.S. Johansson, "Responses in glabrous skin mechanoreceptors during precision grip in humans," *Experimental Brain Research*, vol. 66, 1987, pp. 128-140.

Appendix A

Tactile sensor construction

Core preparation

Cut a 30 mm length of 25.4 mm diameter plexiglass rod. Using the lathe, drill a center hole with the #7 drill bit. Tap the hole for a 1/4”-20 thread. Cut a 90 mm length of 1/4”-20 threaded rod.

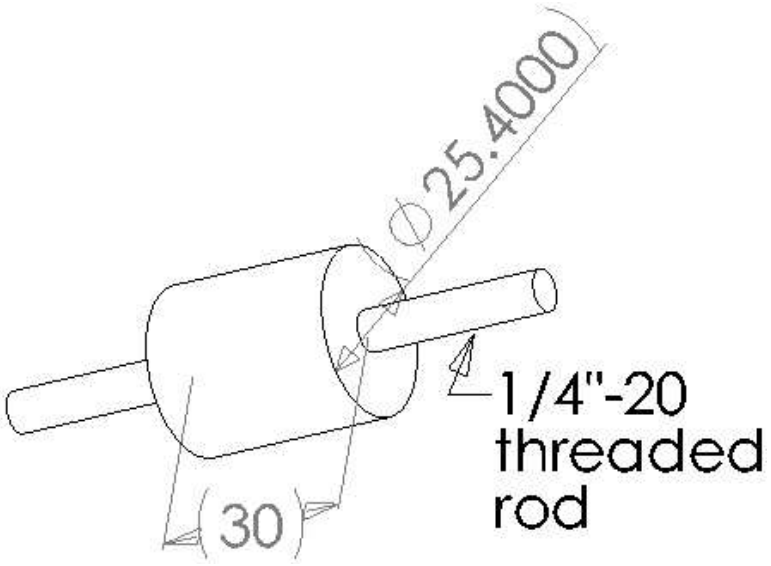

Copper lines preparation

Starting from a sheet of 10 copper lines with an adhesive plastic backing, cut out two 30 mm pieces with 10 lines each and two 30 mm pieces with 4 lines each. The 10 line pieces are the drive lines. The 4 line pieces are the sense lines.

Carefully cut out the plastic in between the copper strips in the 10 line pieces.

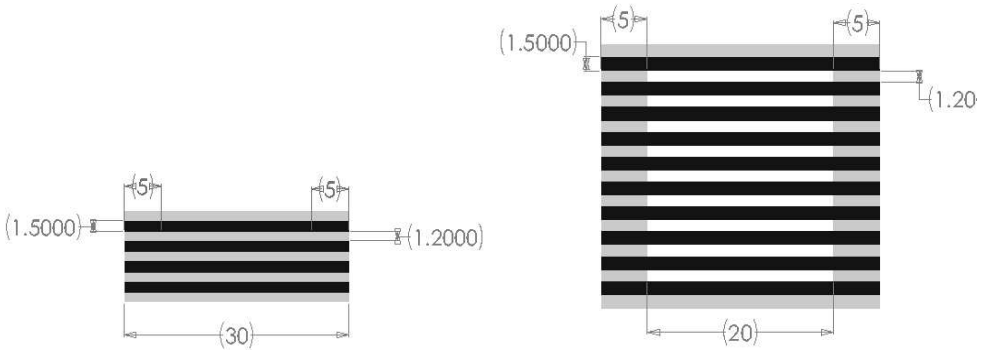

Dielectric preparation

Use the Thermaljet to make a dielectric mold. The dielectric is 30 mm × 30 mm × 0.5 mm. The bumps are 0.5 mm × 0.5 mm × 0.25 mm with 1 mm center-to-center spacing. Measure out Dow Corning HS II base and pink catalyst in a 10:1 ratio. Mash the catalyst into the base. Vacuum the mixture until there are no more big air bubbles coming from the mixture. Pour the HS II into the mold and cover with a plexiglass plate. Place weights on the plexiglass and let the HS II cure for 24 hours.

Cut the dielectric to 20 mm × 25 mm.

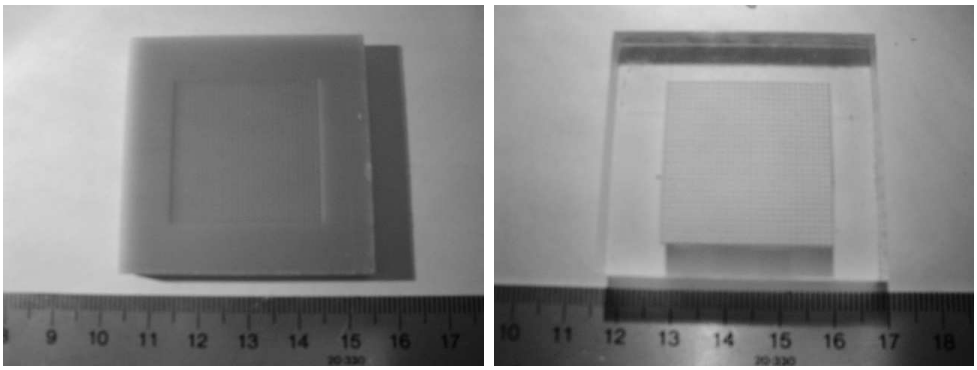

Wire and header preparation

Cut off four equal lengths of 8 conductor, 30 gauge, shielded Cooner wire (AS148). Two of the pieces are for drive lines and two are for sense lines. Cut, strip, and tin all 8 lines for the drive lines. Cut, strip, and tin 4 lines for the sense lines. Use black, brown, red, and orange for the first set of sense lines and yellow, green, blue, and white for the second set of sense lines.

Tin all the slots on the 18 pin header. Solder the drive and sense lines as shown below. There will be two drive lines coming from each drive pin.

Putting it all together

Remove the backing from the 4 line copper strips to reveal adhesive. Adhere the 4 line copper strip along the length of the core. Tin the 4 lines at one end of the copper strips. Solder one set of sense lines to the copper strips. Thread in an appropriate length of 1/4”-20 rod into the core. Test connections between the header pin and copper strip. Make sure there are no short circuits. Repeat for the other core.

Remove the backing from the 10 line copper strips to reveal adhesive. Spread a thin layer of silicone adhesive on the back of the dielectric. Attach the copper lines to the dielectric as shown below. Tin and solder the 8 drive lines to the middle 8 copper strips. Tin and solder the driven shield (the shielding from the SENSE lines) to the outer two lines and the 1/4"-20 center rod. Test connections between the header pin and copper strip. Make sure there are no short circuits.

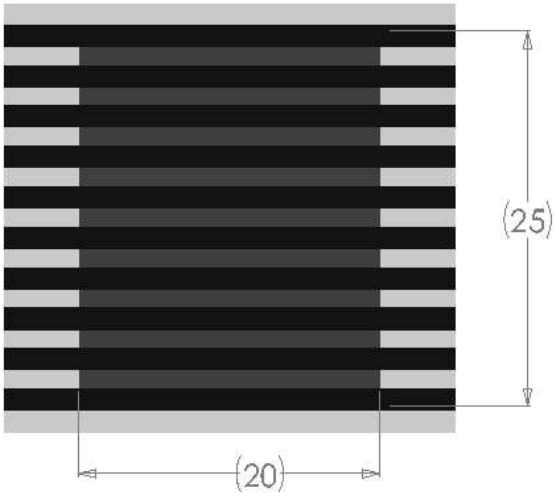

Attach the drive lines to the core with the adhesive backing. Mix up some HS II and apply a small amount along the edges and back of the dielectric. This step is to seal off the dielectric so that HS II will not fill up the dielectric in the final molding step. Use a Thermojet mold to ensure the drive lines and dielectric are firmly seated onto the core. Let the HS II cure for 24 hours. Repeat for second core.

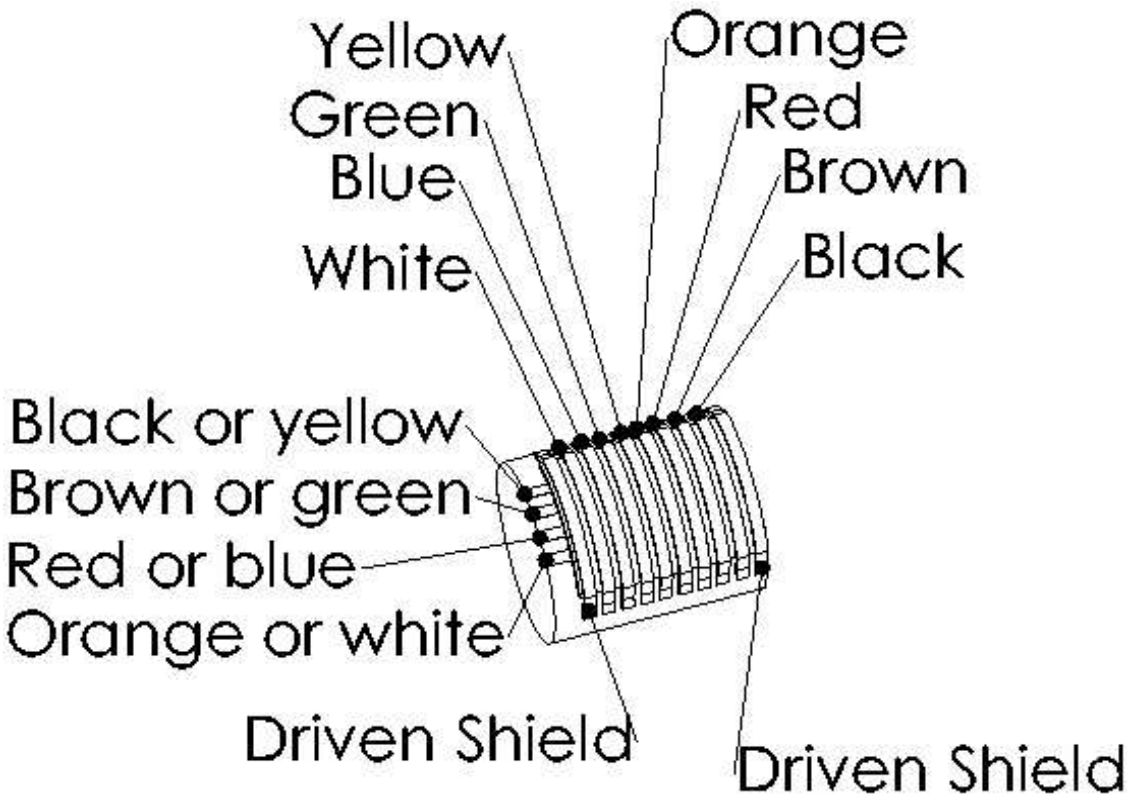

Use an X-Acto knife to separate the adhered edges of the drive lines from the core. The top drive lines are now floating. Use the final Thermojet molds to create a 2 mm rubber layer over the drive lines. Mix up a batch of HS II and fill the molds. Sandwich the molds around the sensor core. Let the HS II cure for 24 hours. Repeat for second core.

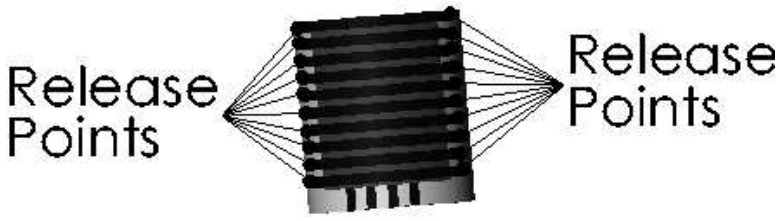

Pop the sensor out of the final molds.

Appendix B

Tactile display construction

Sacrificial mold design

Using Solidworks, we designed a sacrificial wax mold. Shown below are the dimensions we used to make the tactile displays for the bidigital teletaction system. The finger interface has a 14 mm diameter. The pin height determines the thickness of the rubber layer between the air chambers and finger. In our case, we used a 5.5 mm pin height to achieve a 0.5 mm membrane thickness. The pin spacing was 2 mm. The pins had a 1 mm diameter top section and a 1.75 mm bottom section. The bottom section allowed for the 2.2 mm silicone tubing to be inserted securely into the display. The 5 rows were spaced at 15^o intervals, also leading to a 2 mm spacing along the circumference of the finger/display interface.

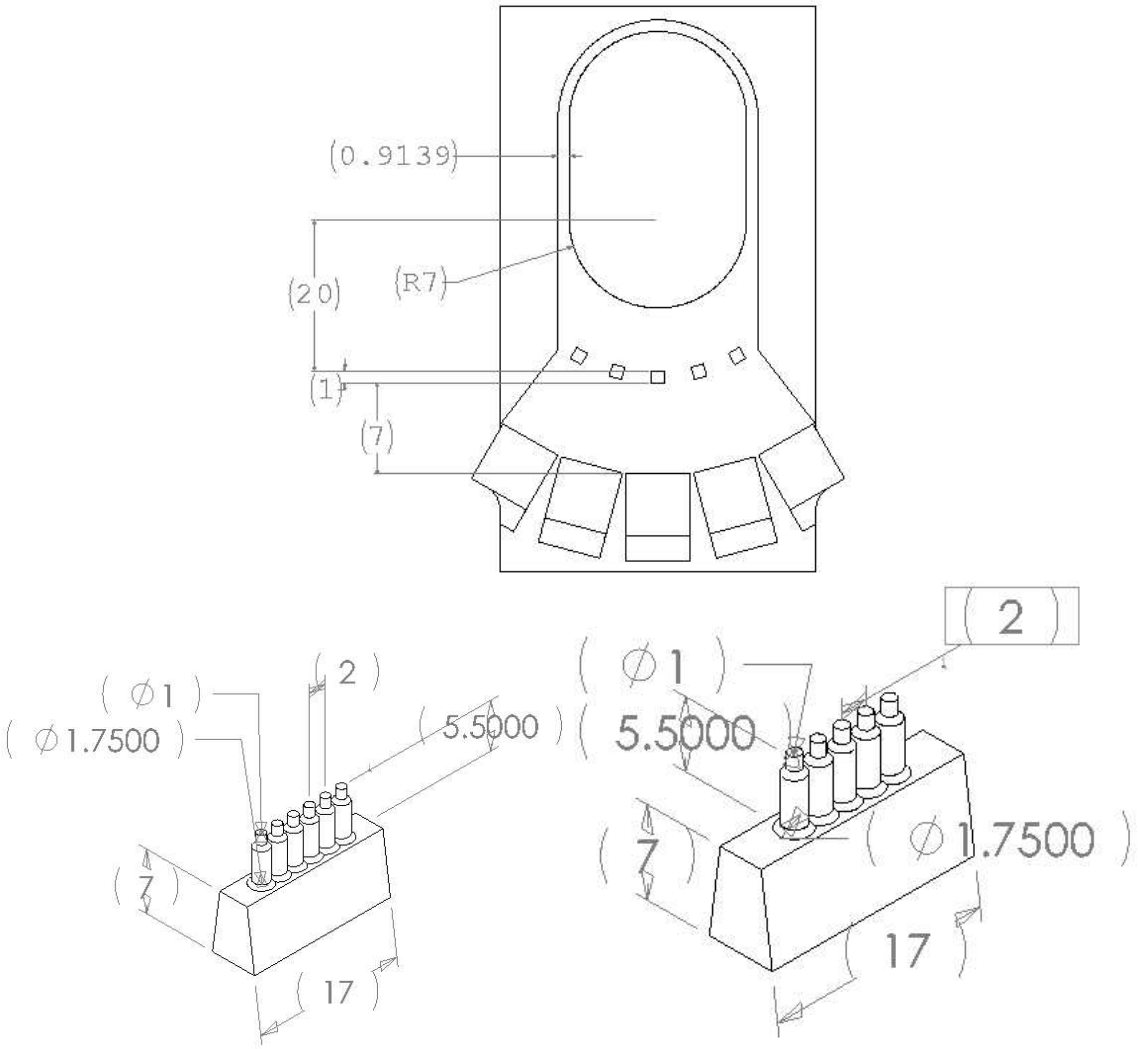

Mold preparation

Use the ThermalJet (3D Systems) to create the base and pin pieces for the tactile display mold. The base piece has slots for 5 rows of pins. The pieces shown below are for a 6-5-6-5-6 pin configuration for a 28 element display. The pin pieces have 2 mm center-to-center spacing. The base piece gives 2 mm center-to-center spacing between rows of elements. Carefully slide the pin pieces into the base piece.

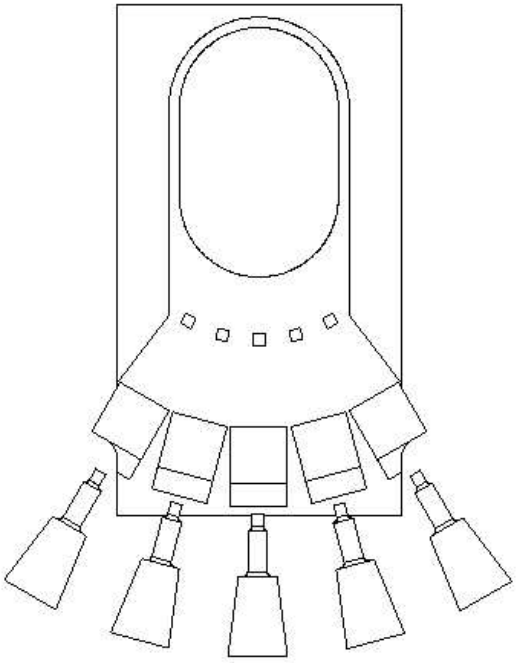

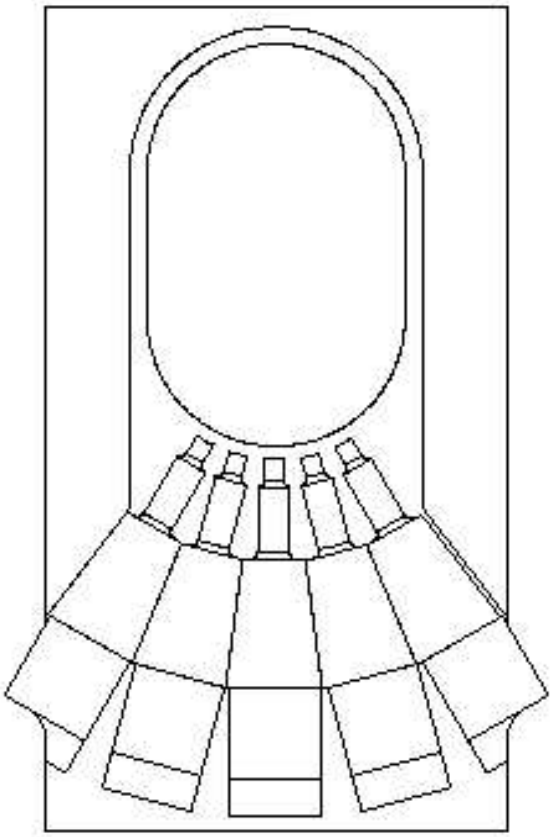

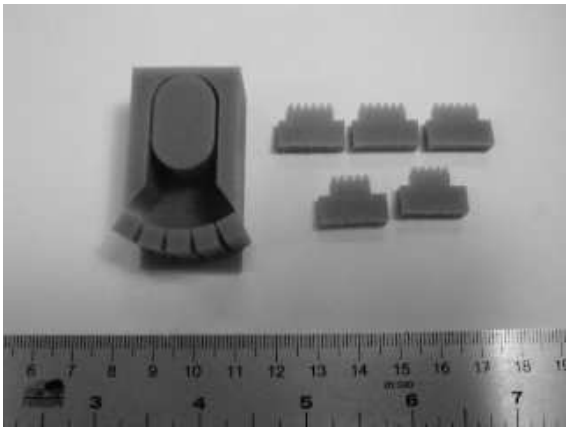

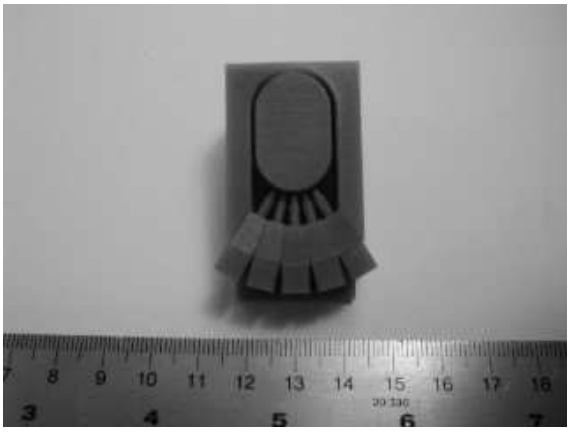

First molding step

Measure out Dow Corning HS II base and pink catalyst in a 10:1 ratio. Mash the catalyst into the base. Vacuum the mixture until there are no more big air bubbles coming from the mixture. Pour HS II into the mold until it overflows over the sides. Vacuum the mold until there are no more medium air bubbles coming from the mold. This vacuum step might take 20 minutes. Remove mold from the vacuum chamber and place a plexiglass plate on top of the mold. Place weights on top of the plexiglass and let the HS II cure for 24 hours.

Post-processing of first molding step

Remove weights and plexiglass plate.

Carefully break off the five support beams behind the pin piece molds. Slide out the 5 pin pieces. Remove broken pin piece structures left inside the mold with tweezers. Trim excess rubber with an X-Acto knife.

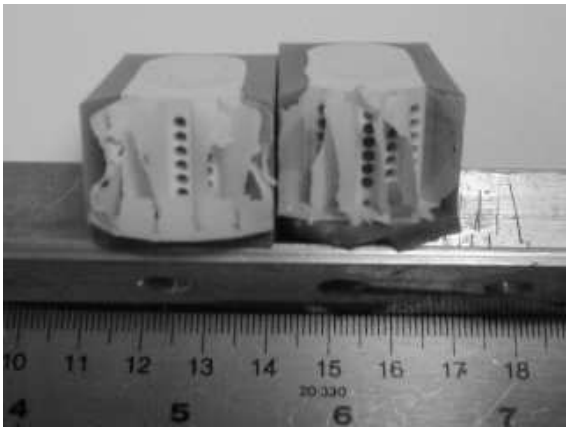

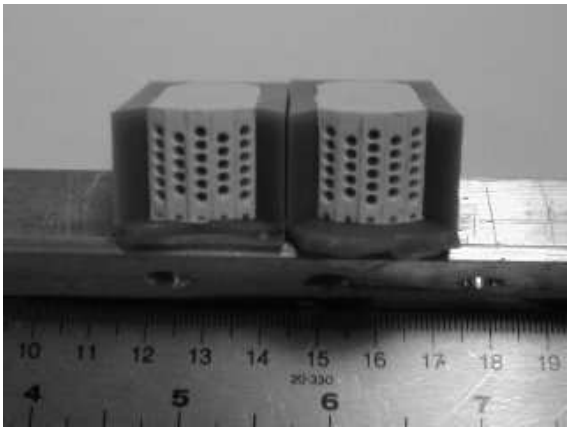

Tube insertion

Determine the number of elements for the tactile display. Cut silicone tubes with 1.106 mm ID and 2.159 mm OD (Product # 2810458 from New Age Tubing) to the desired length. Push the tubes into the mold. A 14 element display in a 5-4-5 configuration is shown below.

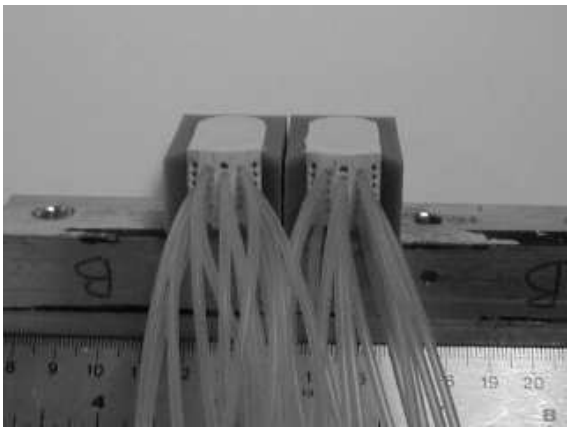

Final molding step

Determine the final mold shape and carefully place the display and tubes between two plexiglass plates. Use at least 2 mm of rubber to ensure that the tubes stay attached to the display. Use other base pieces as separators between the displays, if necessary. Mix some HS II and pour in between the tubes. Do not vacuum the workpieces as HS II might fill the air chambers. Separate the tubes with tongue depressors as shown below Let the HS II cure for 24 hours.

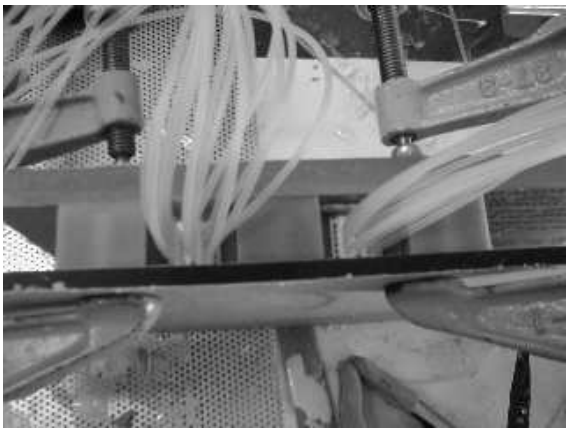

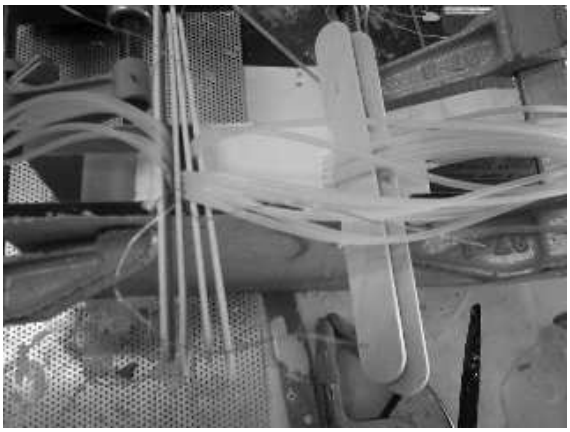

Post-processing

Remove the clamps and release the molds from the plexiglass. Remove the tactile display from the mold and trim excess rubber.

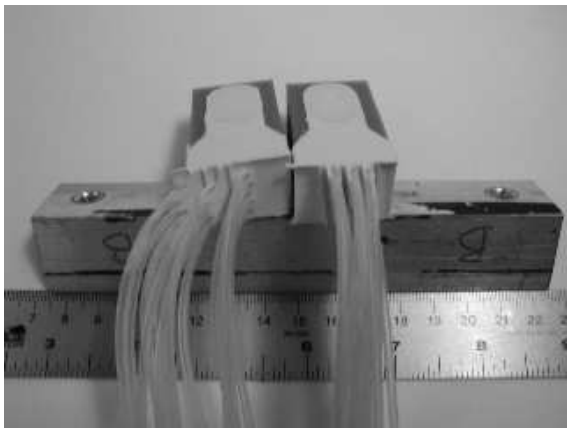

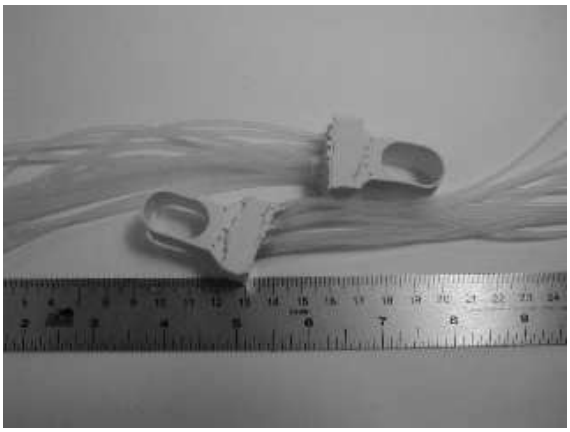

Appendix C

Stimulus construction

Using Solidworks, we design a wax mold for the stimulus. The essential dimensions are a 2 mm deep trench for the 2 mm OD silicone tube and silicone gel over a 50 mm $\times$ 50 mm area. The silicone tube should be long enough to reach the valve array. The mold with the silicone tube and gel is shown in Figure C.1 (left). We cover the mold and silicone with plastic wrap then a flat surface. After 24 hours, we break the wax mold, leaving the gel and tubing on the plastic wrap. We enclose the gel and tubing with another piece of plastic wrap to get the final stimulus shown in Figure C.1 (right).

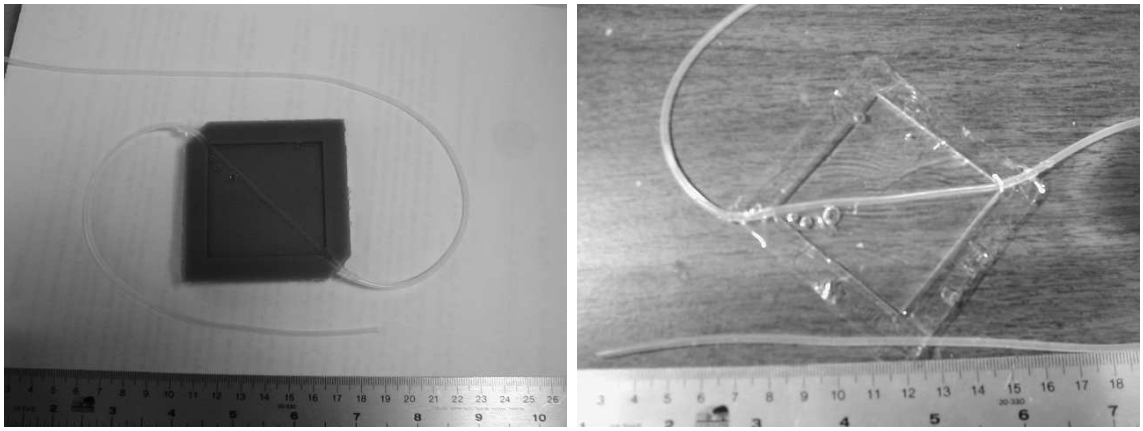

Figure C.1: Stimulus mold and final stimulus

Appendix D

Valve calibration curves

This appendix shows the raw data and PWM buzz of each valve used for the bidigital teletaction system. We sweep the PWM duty cycle in 0.4% steps and record 1000 points per duty cycle step. From the 250 swept duty cycles, we pick the 128 levels that most closely represents a linear valve. We use valves 0–27 for the tactile displays and valve 28 for the stimulus. The valves tend to have good pressure resolution at the upper end of duty cycles. We use a valve air supply pressure of 40 PSI and an orifice/chamber setup as the low pass filter. PWM buzz is less than 10% for duty cycles above 20%. Average peak-to-peak PWM buzz is 5.55 PSI with a standard deviation on 1.30 PSI.

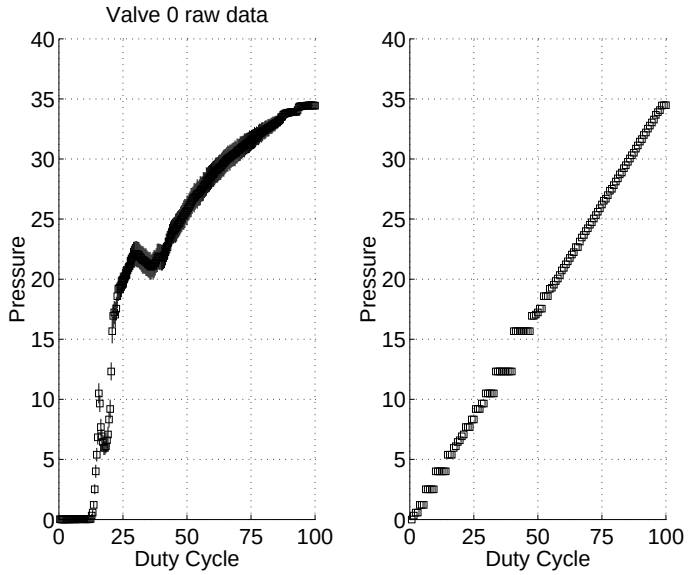

Figure D.1: Valve 0 calibration curve with PWM buzz and linearization

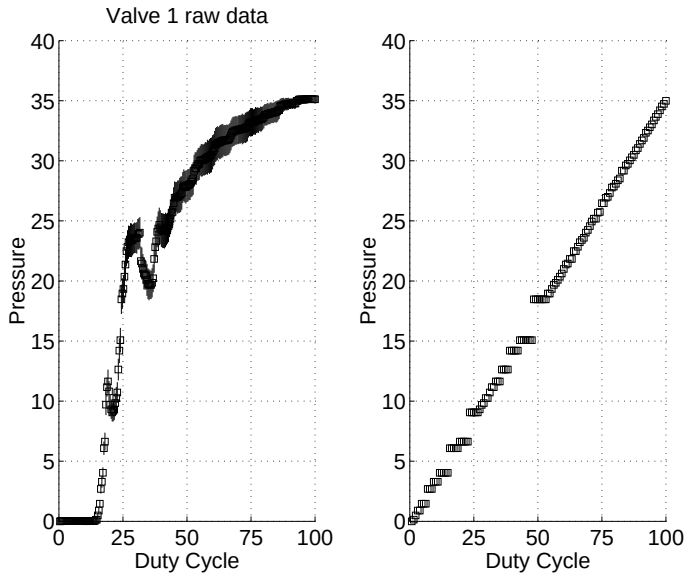

Figure D.2: Valve 1 calibration curve with PWM buzz and linearization

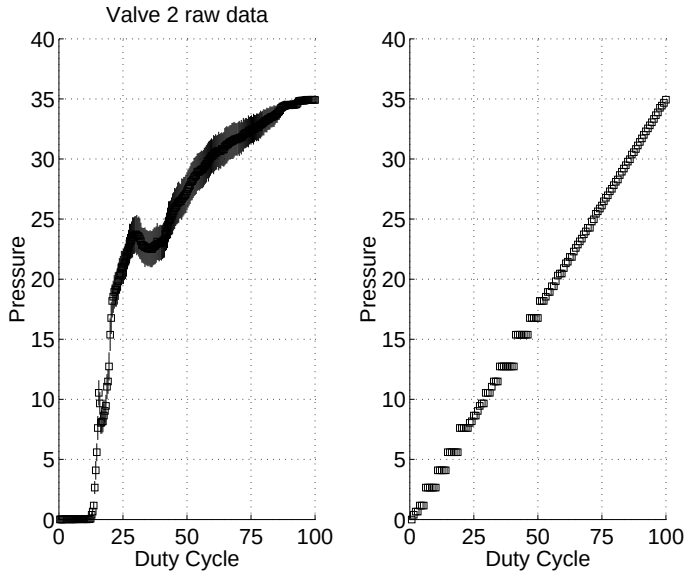

Figure D.3: Valve 2 calibration curve with PWM buzz and linearization

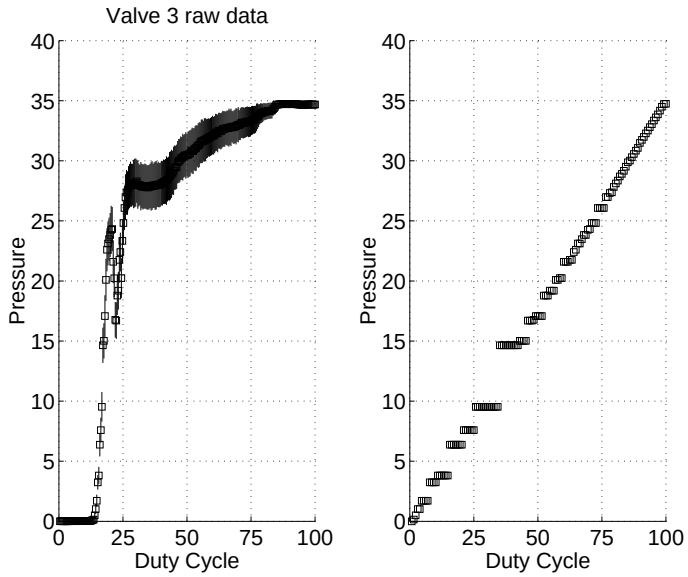

Figure D.4: Valve 3 calibration curve with PWM buzz and linearization

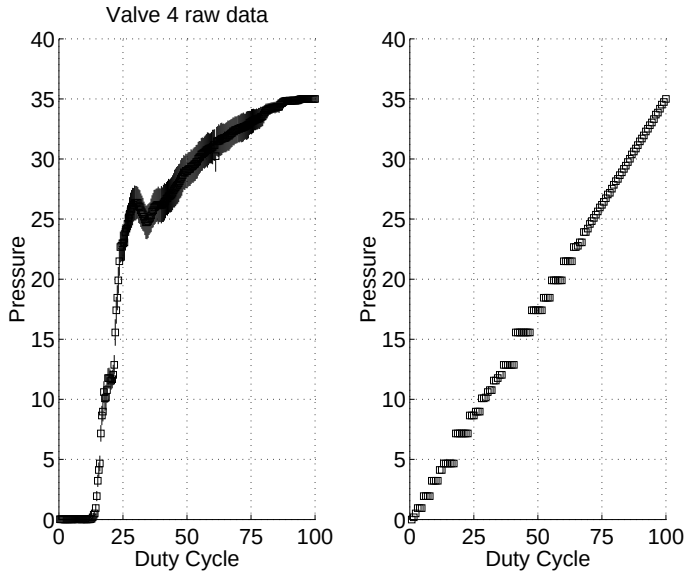

Figure D.5: Valve 4 calibration curve with PWM buzz and linearization

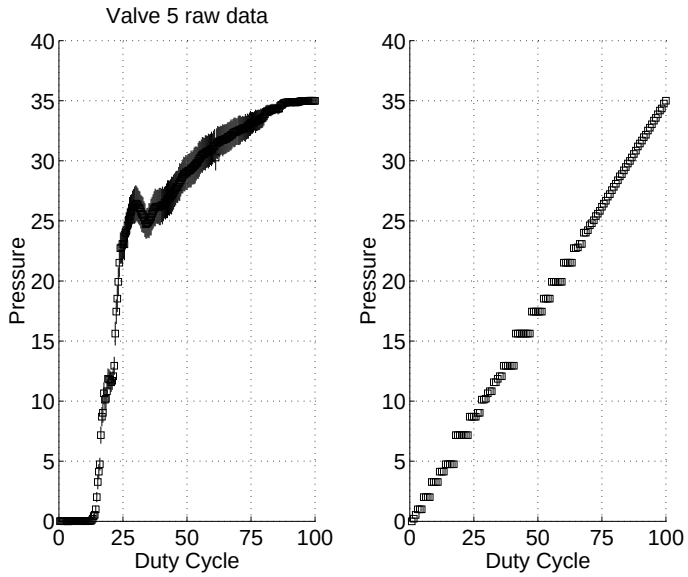

Figure D.6: Valve 5 calibration curve with PWM buzz and linearization

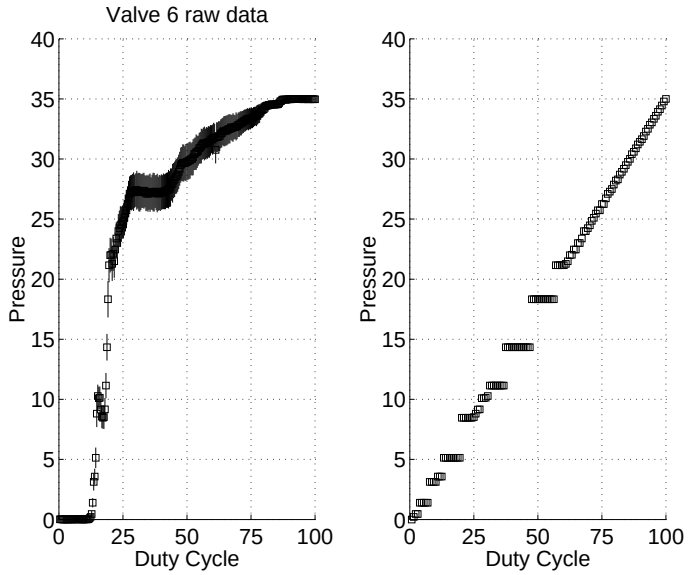

Figure D.7: Valve 6 calibration curve with PWM buzz and linearization

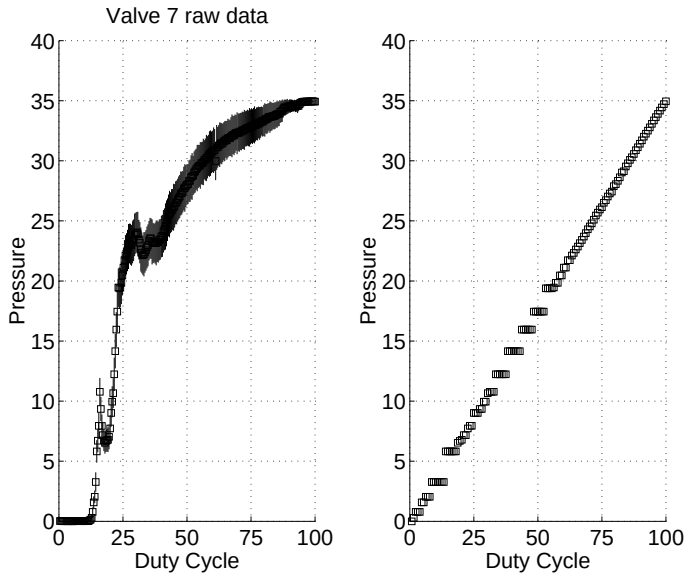

Figure D.8: Valve 7 calibration curve with PWM buzz and linearization

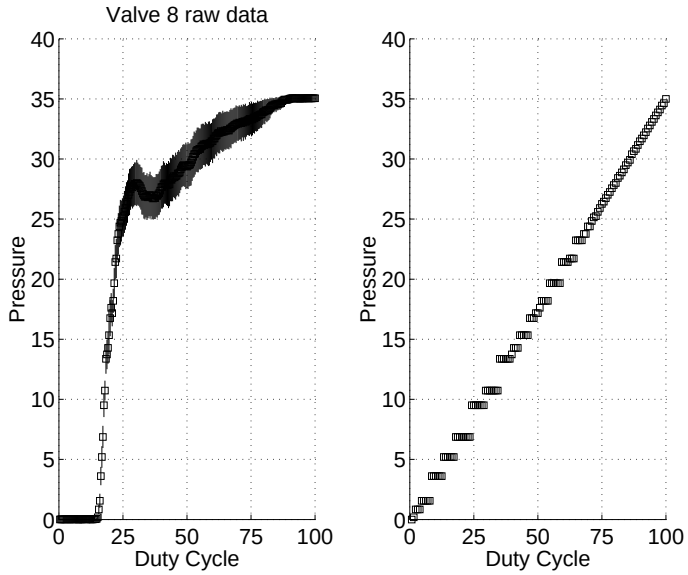

Figure D.9: Valve 8 calibration curve with PWM buzz and linearization

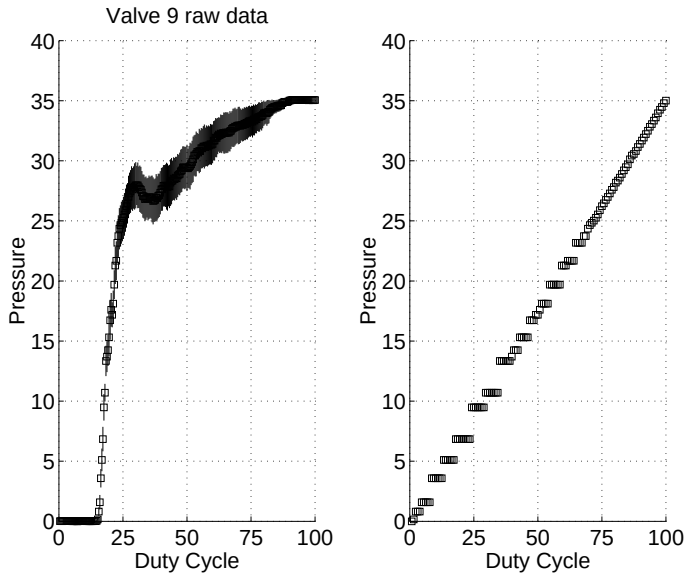

Figure D.10: Valve 9 calibration curve with PWM buzz and linearization

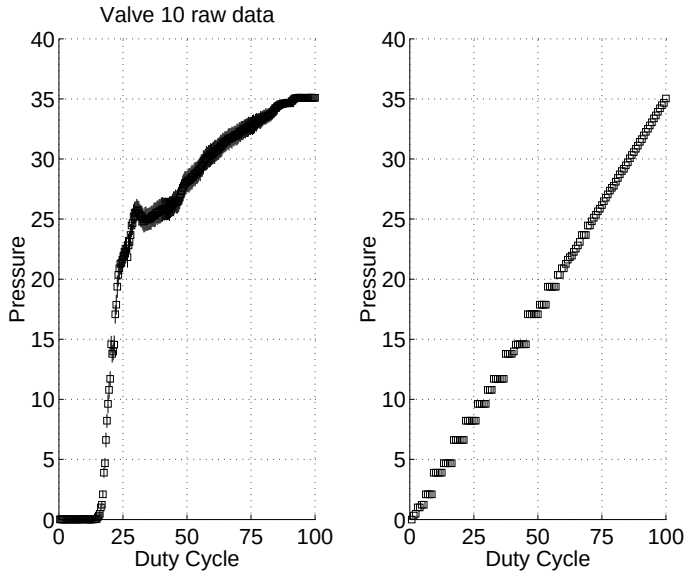

Figure D.11: Valve 10 calibration curve with PWM buzz and linearization

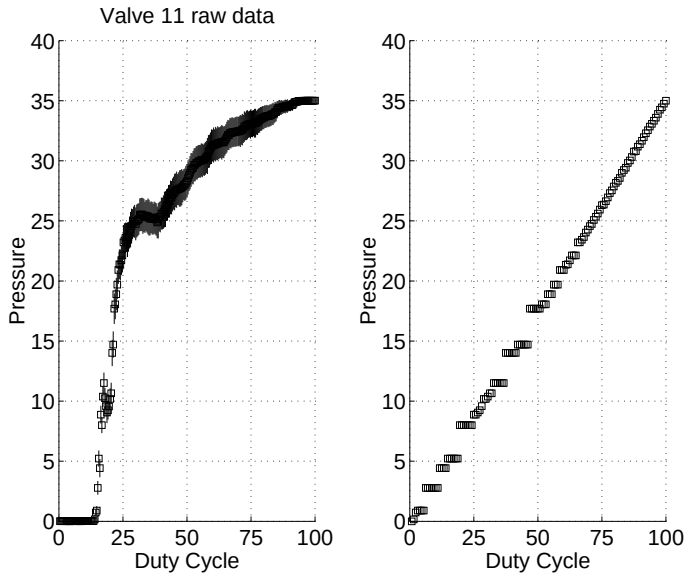

Figure D.12: Valve 11 calibration curve with PWM buzz and linearization

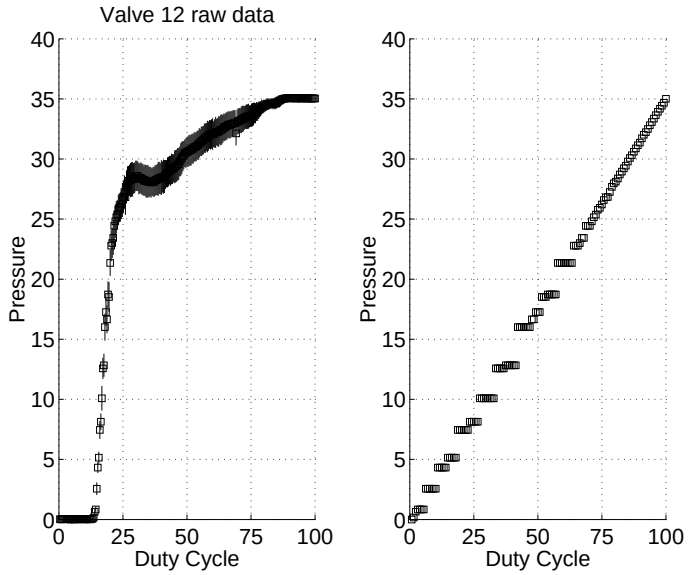

Figure D.13: Valve 12 calibration curve with PWM buzz and linearization

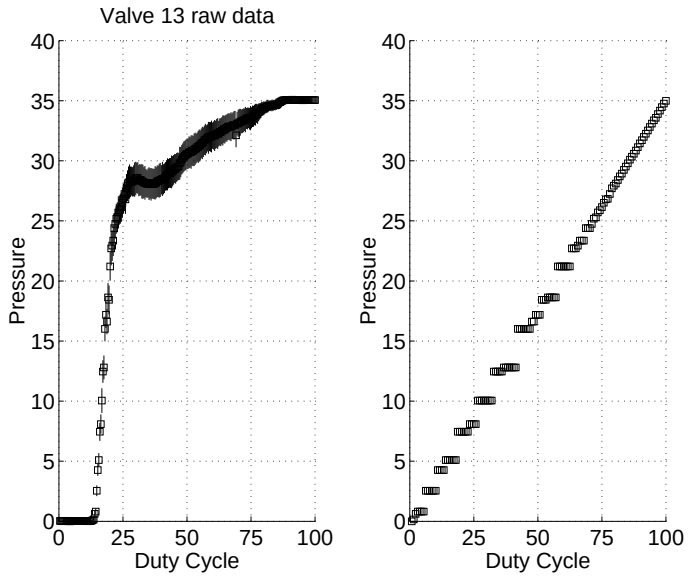

Figure D.14: Valve 13 calibration curve with PWM buzz and linearization

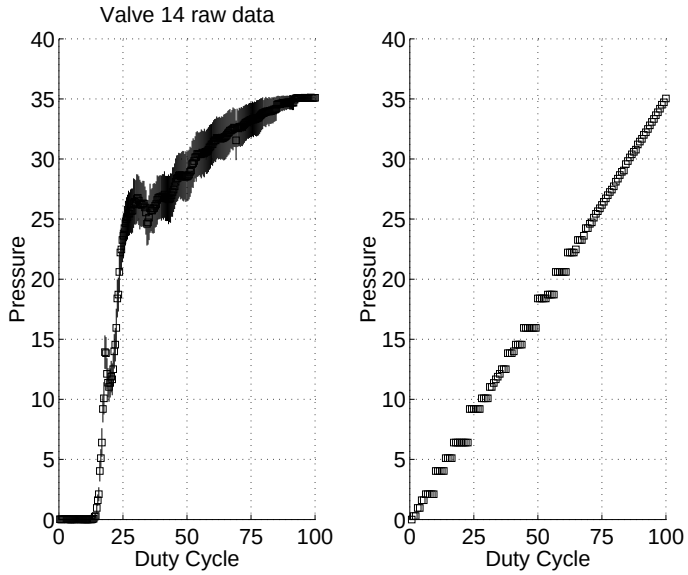

Figure D.15: Valve 14 calibration curve with PWM buzz and linearization

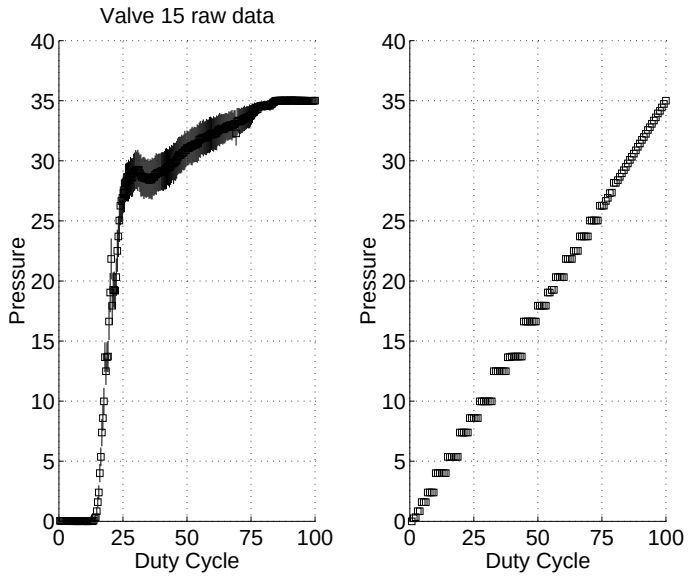

Figure D.16: Valve 15 calibration curve with PWM buzz and linearization

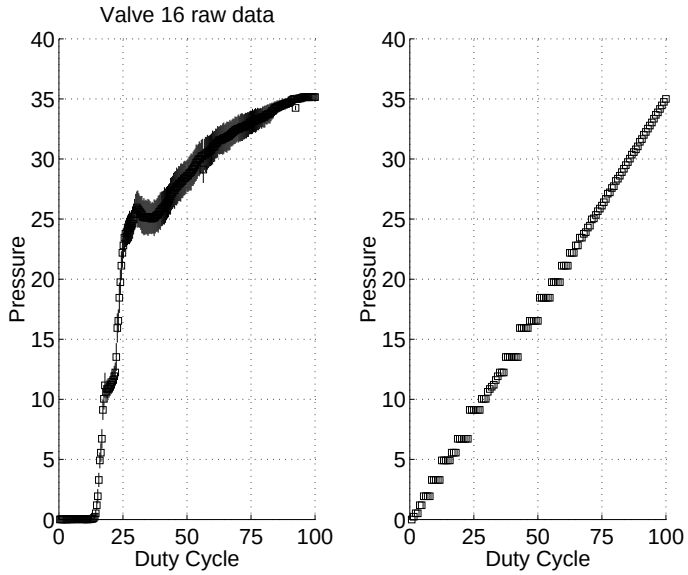

Figure D.17: Valve 16 calibration curve with PWM buzz and linearization

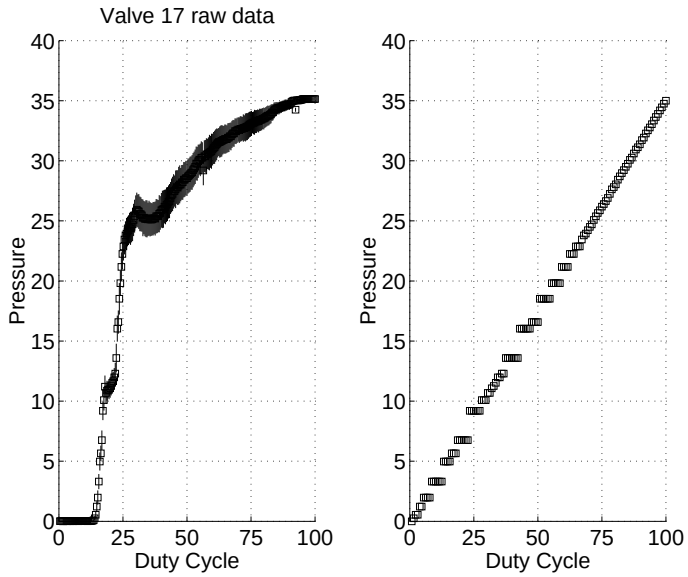

Figure D.18: Valve 17 calibration curve with PWM buzz and linearization

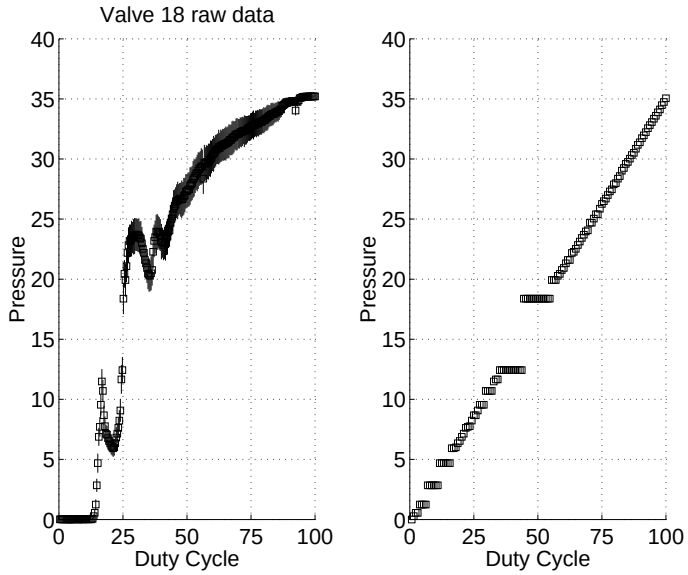

Figure D.19: Valve 18 calibration curve with PWM buzz and linearization

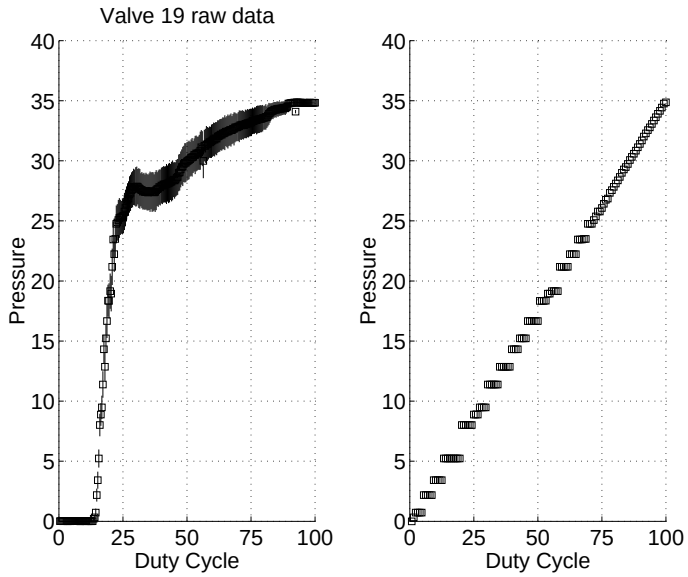

Figure D.20: Valve 19 calibration curve with PWM buzz and linearization

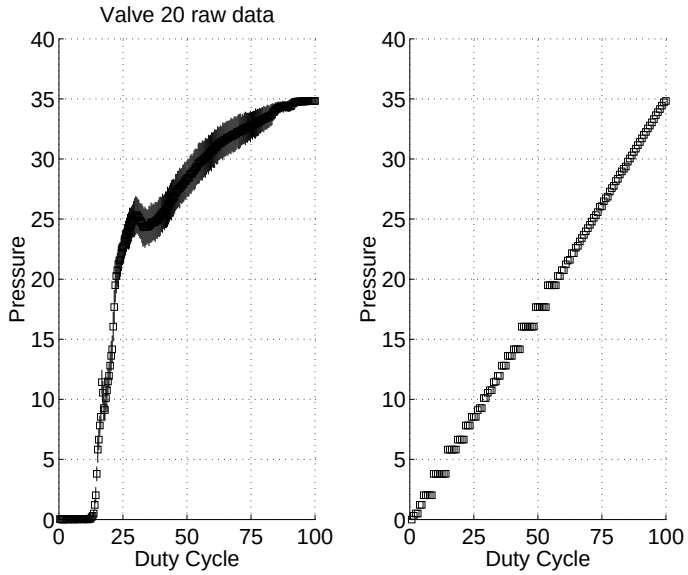

Figure D.21: Valve 20 calibration curve with PWM buzz and linearization

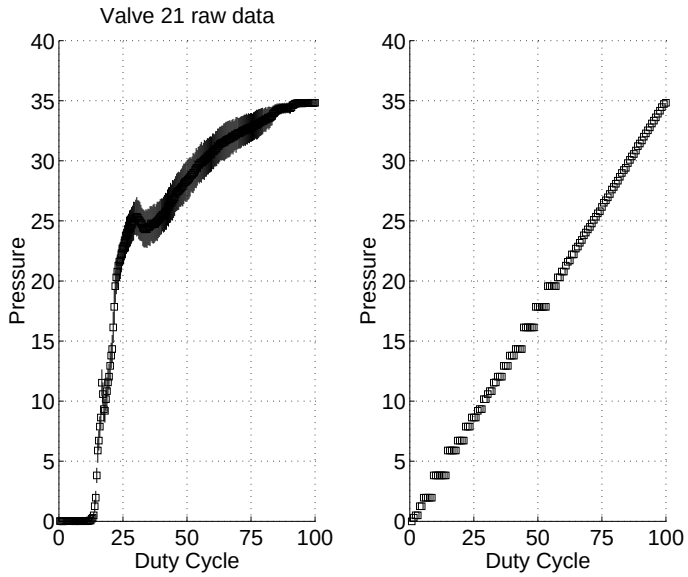

Figure D.22: Valve 21 calibration curve with PWM buzz and linearization

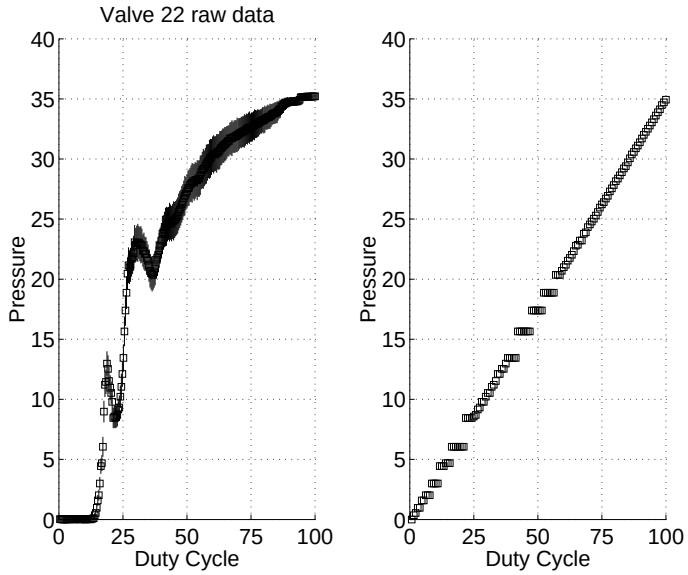

Figure D.23: Valve 22 calibration curve with PWM buzz and linearization

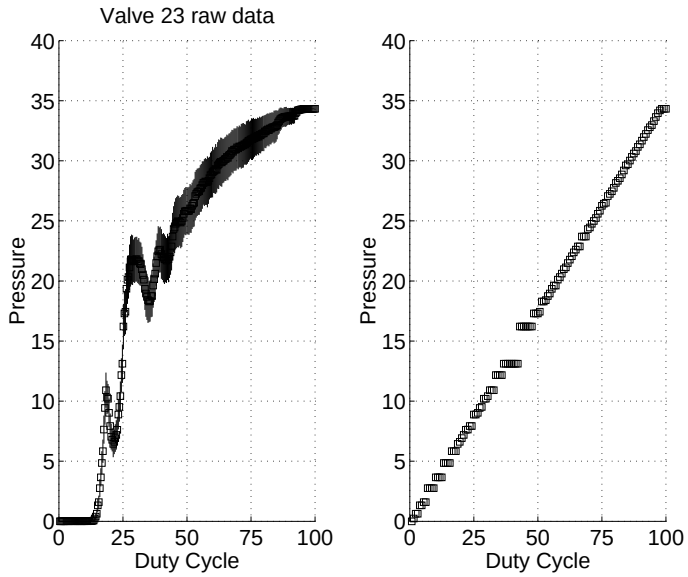

Figure D.24: Valve 23 calibration curve with PWM buzz and linearization

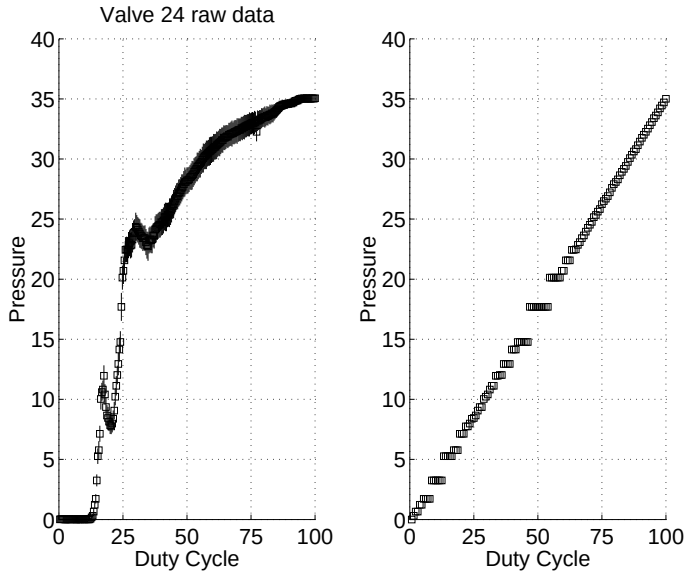

Figure D.25: Valve 24 calibration curve with PWM buzz and linearization

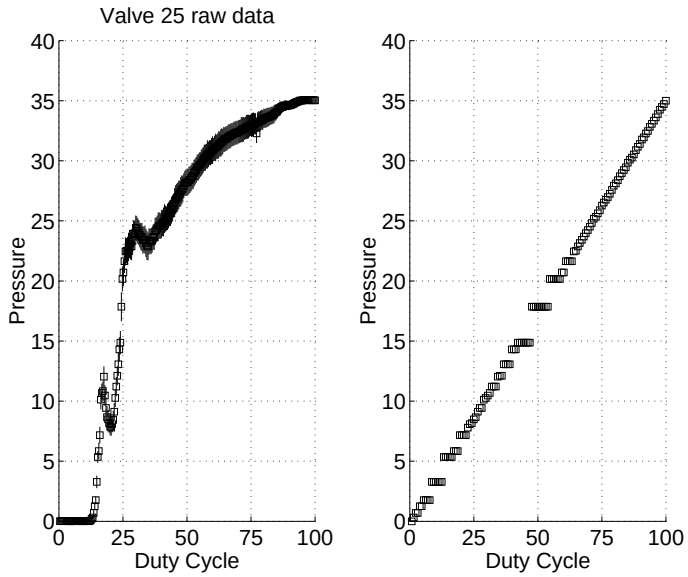

Figure D.26: Valve 25 calibration curve with PWM buzz and linearization

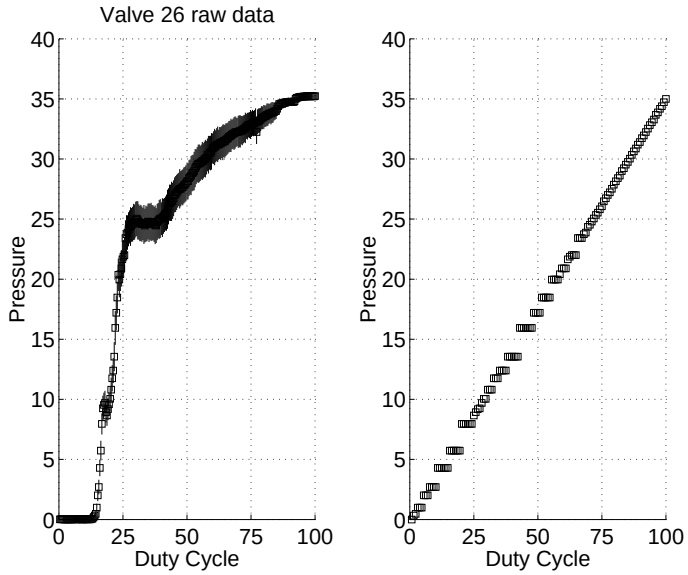

Figure D.27: Valve 26 calibration curve with PWM buzz and linearization

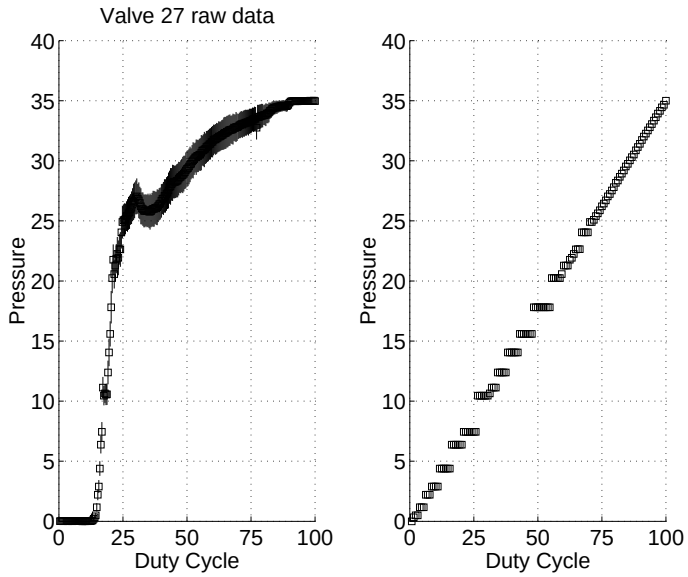

Figure D.28: Valve 27 calibration curve with PWM buzz and linearization

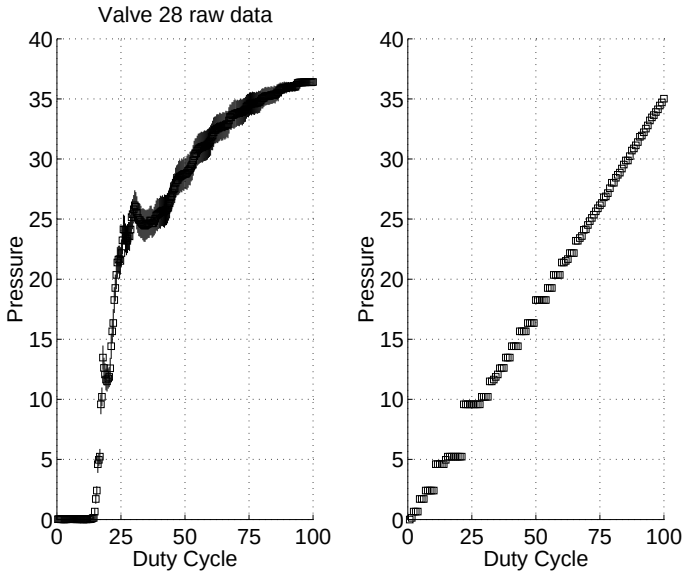

Figure D.29: Valve 28 calibration curve with PWM buzz and linearization

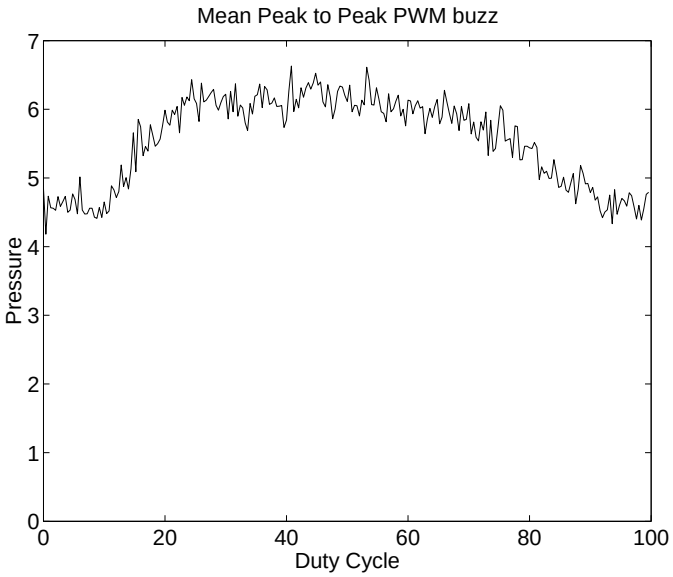

Figure D.30: Average PWM buzz vs. PWM duty cycle

Appendix E

Human subjects protocol and consent form

E.1 Protocol

Comparing Bidigital Teletaction System Performance and Direct Touch

#2001-8-92

Gabriel Moy
Graduate Student of EECS
333 Cory Hall
Berkeley, CA 94720
gmoy@eecs.berkeley.edu

Faculty Sponsor
Professor Ron Fearing
Department of EECS
265M Cory Hall
Berkeley, CA 94720
ronf@eecs.berkeley.edu

Summary

Humans can detect many details about an object grasped between their thumb and index finger. Using models of the finger and stimulus, we want to determine how well we can recreate the sense of touch with a bidigital tactile display system. With this data, we can design better teletaction systems which allow the sense of touch to be stored, transmitted, and played back like video and audio recordings are now.

The research proposed here will compare the performance of people to detect details of various stimuli either using direct touch or the bidigital teletaction system. We will test detection and orientation tasks of rigid and soft materials. Stimuli will consist of ball bearings, small rubber balls, small metal rods, and rubber tubing.

Subjects

For the experiments, ten (10) subjects will be recruited. The subjects for these experiments will be graduate and undergraduate students in the same field as the primary researcher. Subjects will be recruited through individual verbal solicitation by the primary researcher. The majority of these subjects will be naive subjects. In regard to gender and minority inclusion, we will use small numbers of subjects in our psychophysical experiments. All subjects will be between 18 and 50 years of age. No students in classes being taught by us will be used as subjects.

Procedures

The only research material obtained from the subjects will be their responses to the presented stimuli. The data will be obtained specifically for the purposes of the research and nothing else. The subject will participate in two sessions of 45 minutes each. Each session will consist of two 20 minute experiments with a 5 minute break between the experiments.

Subjects will grasp the stimuli between their thumb and index fingers. In a detection task, they will respond whether they feel the stimuli. In an orientation task, they will respond with the direction of the rod or tube. To test the bidigital teletaction system, the subject will wear tactile displays on their thumb and index finger. Data corresponding to the same stimuli will be presented to them and they will respond as described above.

The tactile displays are an array of small (1mm diameter) pressurized chambers molded from rubber. Subjects will place their fingers on the displays and have full control of how hard to push against the displays. The chambers will have a pressure range of 0 to 40 psi. The rubber does not tear.

Benefits

There are no direct benefits to the subjects from the proposed research. Possible benefits to society include greater understanding of the human tactile system. There might also be practical benefits, e.g. designing a teletaction system to aid surgeons in feeling inside the body without making large incisions.

Risks

There are no potential risks to the subjects. Participation involves subjects feeling rigid or soft stimuli through direct touch or the bidigital teletaction system and determining details about what they feel.

Confidentiality

We will not collect any personal data from the subjects. The experimental data collected will be stored on our computer disk and only identified by a code number. Any data published will also only be identified by this code number. Consent forms will be stored in a filing cabinet in a locked office (333 Cory). Consent forms will not be coded since they have the subject's signature and can be correlated with the data if they are coded.

Informed Consent

After the investigators thoroughly explain the experiments to the subjects, the subjects will be asked to read and sign a consent form before participating in the experiment. A sample form is included with this protocol. We will tell the subjects that they are under no obligation to complete the experimental session even after they have signed the consent form.

Financial Aspects

No costs to the subjects will result from this study. We will not pay the subjects to participate in the study.

Written Materials

No questionnaires, surveys, interview schedules, or newspaper advertisements will be used in the project.

Signature of Gabriel Moy, Primary Researcher _____ *Date* _____

Signature of Ron Fearing, Faculty Advisor _____ *Date* _____

Gabriel Moy's telephone numbers: 642–3248 (lab), 643–5794 (office), 848–0808 (home).

Ron Fearing's telephone number: 642–9193.

E.2 Consent form

My name is Gabriel Moy. I am a graduate student in Electrical Engineering and Computer Sciences at the University of California at Berkeley.

I would like you to take part in my research. It deals with how well people can detect details of various stimuli. The stimuli will be ball bearings, small rubber balls, small metal rods, and rubber tubing. You will be feeling these stimuli first with your fingers, then again with a teletaction system. A teletaction system consists of tactile sensors and tactile displays. Tactile sensors collect contact information with the stimulus while the tactile displays present the contact information to your fingers. While a video camera system records and displays video images, a teletaction system records and displays touch, or tactile, images.

If you agree to take part in the research, I will ask you to feel and make judgments about a number of stimuli. You will be provided with a hand rest for your comfort. The thumb and index finger will be used in these experiments. You will be asked questions about the stimuli, such as detection and orientation.

I will ask you to take part in two sessions, in which you will grasp the stimuli. Each session should take a total of about 45 minutes. The session will take place in 330 Cory Hall, here at the University of California at Berkeley.

There are no risks to participating in this research.

Data collected will help us in acquiring more insight on the limits of the human tactile system. Results will help in the design of future teletaction systems for use in areas such as telesurgery, and telerobotics.

I will keep all of the results obtained from you during this experiment confidential. Your responses to the questions you are asked will be kept in a file on a computer. The file will identify you only by a code number.

Your participation in this research is voluntary. You are free to refuse to take part, and you may stop taking part at any time. Whether or not you choose to participate in this research will have no bearing on your standing with the team or your grades at the University of California at Berkeley.

If you have any questions about your rights or treatment as a participant in this research project, please contact the University of California at Berkeley's Committee for Protection of Human Subjects at (510)642-7461, e-mail: subjects@uclink.berkeley.edu.

If you have any questions about the research, you may call me, Gabriel Moy, at 643-5794.

I have read this consent form and agree to take part in the research.

_____ _____

Signature *Date*